JOURNAL OF APPLIED PHYSICS

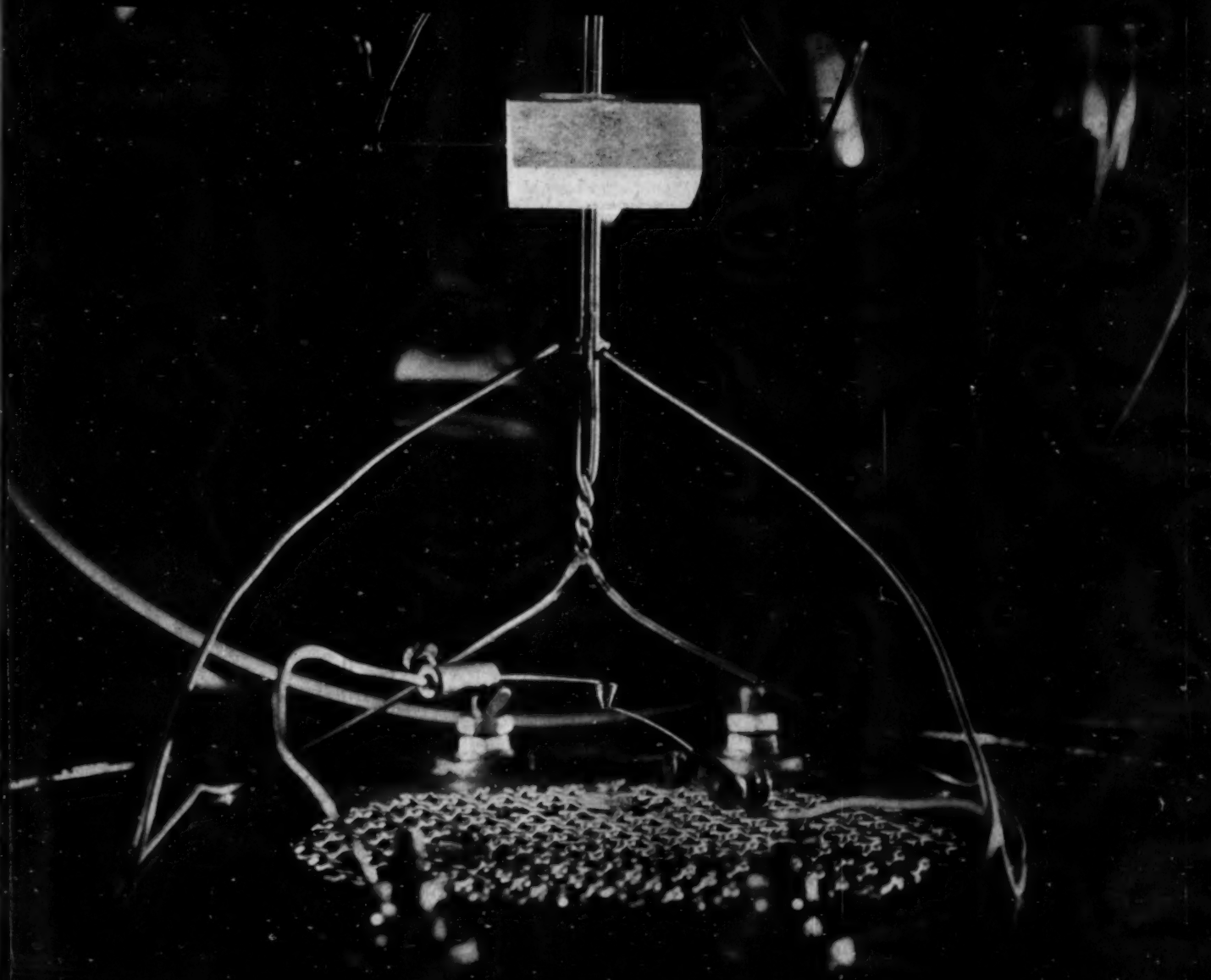

JOURNAL OF APPLIED PHYSICS

Vol. 18, No. 4 APRIL, 1947

In This Issue

	Page
Preparation and Uses of Silica Replicas in Electron Microscopy — Charles H. Gerould	333
X-Ray Storage Properties of the Infra-Red Storage Phosphor and Application to Radiography — O. E. Berg and H. F. Kaiser	343
Flux Plotting Method for Obtaining Fields Satisfying Maxwell's Equations, with Applications to the Magnetron — Prescott D. Crout	348
Magnetron Oscillator for Dielectric Heating — R. B. Nelson	356
Approximate Solution of the Differential Equation of the Ultracentrifuge — W. J. Archibald	362
Motion of a Conical Coil Spring — I. Epstein	368
Introduction to the Mathematical Theory of Plasticity — W. Prager	375
On the Theory of Noise in Radio Receivers with Square Law Detectors — Mark Kac and A. J. F. Siegert	383
Heating and Cooling of Bolometer Elements — J. N. Shive	398
Speed of Propagation and of Brittle Cracks in Steel — G. Hudson and M. Greenfield	405
Use of the Broadcast Band in Geologic Mapping — Larkin Kerwin	407
Note on a Paper by Faust and Beck — William M. Stone	414
Internal Friction of Zinc Single Crystals — Irvin H. Swift and John E. Richardson	417
Letters to the Editor:	
Measurement of Surface Tension — Robert Weil	426
Letter to the Editor — Francis J. Murray	426
In Every Issue	
Here and There	426
New Books	428
New Booklets	429
Calendar of Meetings	430
Index to Advertisers	xxx

BOARD OF EDITORS

Elmer Hutchisson, *Editor*

Associate Editors

R. Bowling Barnes
Otto Beeck
W. F. Busse
Selig Hecht
W. James Lyons
Philip Morrison
Paul E. Sabine
Frederick Seitz
J. R. Townsend
John Von Neumann

Publication of the American Institute of Physics

ADMINISTRATIVE STAFF

Henry A. Barton, *Director*

Margaret S. Griffin, *Publications Manager*

Theodore Vorburger, *Business Manager*

John T. Tate, *Adviser on Publications*

GOVERNING BOARD

G. R. Harrison, *Chairman*

Wallace Waterfall, *Secretary*

George B. Pegram, *Treasurer*

E. U. Condon
A. J. Dempster
W. F. Fair, Jr.
Floyd A. Firestone
Harvey Fletcher
R. C. Gibbs
K. S. Gibson
Paul E. Klopsteg
A. H. Pfund
John T. Tate
M. W. White
A. G. Worthing

The Journal of Applied Physics, published monthly at Prince and Lemon Sts., Lancaster, Pa., is devoted to physics in its role as the science basic to other natural sciences and to the arts and industries. Previous to 1937 this publication was known as Physics. The Journal of Applied Physics publishes editorials, news of physicists, and reviews, as well as technical papers of applied physics.

Manuscripts should be submitted to Elmer Hutchisson, Editor, Case School of Applied Science, Cleveland 6, Ohio.

Subscriptions and orders for back numbers should be addressed to Prince and Lemon Streets, Lancaster, Pa. or to the American Institute of Physics, 57 East 55 Street, New York 22, N. Y.

Subscription Price

	U.S. and Canada	Elsewhere
To members and associate members of the American Institute of Physics	$5.00	$5.70
To all others	7.00	7.70

Back Number Prices

Complete set: Vol. 1, July, 1931–Vol. 17, 1946—$124.00

Yearly back number rate: $10.00

Single copies: $1.00 each.

Changes of address and proofs should be addressed to the Publications Manager.

Advertising rates supplied on request. Orders, advertising copy, and cuts should be sent to the American Institute of Physics.

Entered as second class matter January 22, 1937, at the Post Office at Lancaster, Pennsylvania, under the Act of March 3, 1879.
Accepted for mailing at the special rate of postage provided for in the Act of February 28, 1925, authorized May 2, 1932.

Copyright 1947, by the American Institute of Physics

Journal
of
Applied Physics

Volume 18, Number 4 April, 1947

Preparation and Uses of Silica Replicas in Electron Microscopy

CHARLES H. GEROULD
The Dow Chemical Company, Midland, Michigan

(Received November 21, 1946)

A detailed description of the preparation of silica replicas and substrates and their many and varied uses is presented with photographs and electron micrographs. A method of preparing silica replicas of specimens which cannot be subjected to the temperatures and pressures of the ordinary technique is described. It consists of applying a polystyrene lacquer to the specimen surface in place of the conventional molding. The question of "up and down" in stereo pictures of silica replicas is definitely settled by adding a metal oxide smoke (MgO) to the polystyrene replica before the silica evaporation. A successful powder dispersing technique consists of dispersing the powder in an ethyl cellulose lacquer and depositing upon a silica substrate. Several other techniques are also included.

INTRODUCTION

WITHIN the last two years the field of electron microscopy has expanded many fold resulting in a great need for the development of new and improved electron microscopic techniques as well as the optimum use of those available. The great diversity of the recent entrants into the microscopic field has made an even greater need for literature on techniques which are of general application.

The polystyrene-silica replica technique of Heidenreich and Peck[1] is one which has succeeded in solidly establishing itself and is now being widely used on many and varied research problems involving the electron microscope. Among these we might mention the application of silica replicas to such metallurgical specimens as steels, copper alloys, and magnesium alloys.[2–5] We might mention also their application to nonmetallic materials such as teeth,[6] bones, minerals, glasses, ceramics, resins, woods, and textile fibers.[7] In addition, we must include the use of structureless silica substrates[8] as supports for many different types of electron microscope specimens such as bacteria, viruses, powders, emulsions, metallic oxide smokes, thin evaporated films, microtome sections, etc.

These many and varied uses of silica replicas have resulted in a demand for more explicit information on their preparation and uses. It is the purpose of this paper to fill this need and at the same time make available to the field some of the more recently developed, and as yet unpublished, microscope techniques in which silica replicas are an essential part.

These new techniques include a new method

[1] R. D. Heidenreich and V. G. Peck, J. App. Phys. **14**, 23 (1943).
[2] C. S. Barrett, J. App. Phys. **15**, 691 (1944).
[3] R. D. Heidenreich, SAE J. (trans) **53**, 588 (1945).
[4] R. D. Heidenreich, L. Sturkey, and H. L. Woods, J. App. Phys. **17**, 127 (1946).
[5] R. D. Heidenreich, C. H. Gerould, and R. E. McNulty, Tech. Pub. 1979, Metals Tech. **13** (April, 1946).
[6] C. H. Gerould, J. Dent. Res. **23**, 239 (1944).
[7] R. B. Barnes, C. J. Burton, and R. G. Scott, J. App. Phys. **16**, 730 (1945).
[8] R. D. Heidenreich, J. Opt. Soc. Am. **35**, 139 (1945).

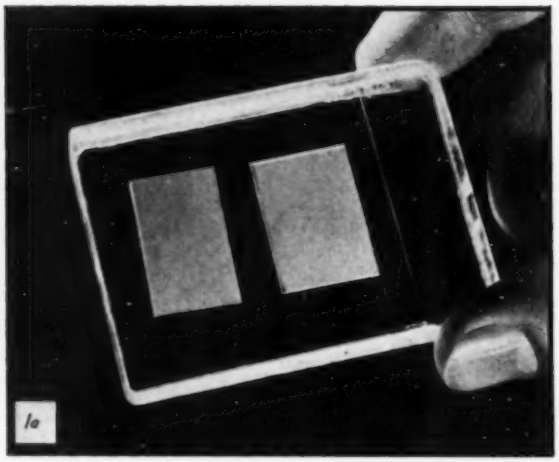

FIG. 1a. Block of clear polystyrene containing two specimens of a magnesium alloy sheet whose surfaces have been covered with a corrosion resistant coating. Silica replicas are to be prepared of this coating. The molding was formed from molding granules at a temperature of 160°C and a pressure of about 1500 lb./sq. in.

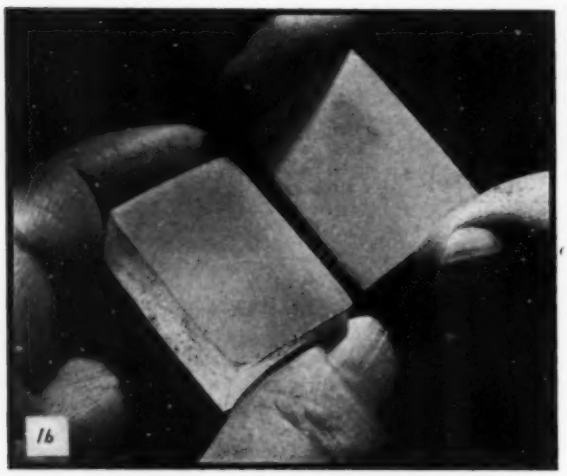

FIG. 1b. Polystyrene impression on left and coated metal specimen on right. Mechanical separation has been accomplished by sawing away the excess polystyrene from the edges of the specimen and then pulling the two surfaces apart. Specimens may be dissolved with acids or alkalies if necessary.

of preparing replicas for stereoscopy which makes it possible to settle definitely the question of "up and down" in stereo pictures, a procedure for preparing silica substrates, an ethyl cellulose lacquer particle dispersing technique for use with such substrates, a method of preparing silica replicas utilizing a room temperature produced polystyrene impression and several other miscellaneous techniques.

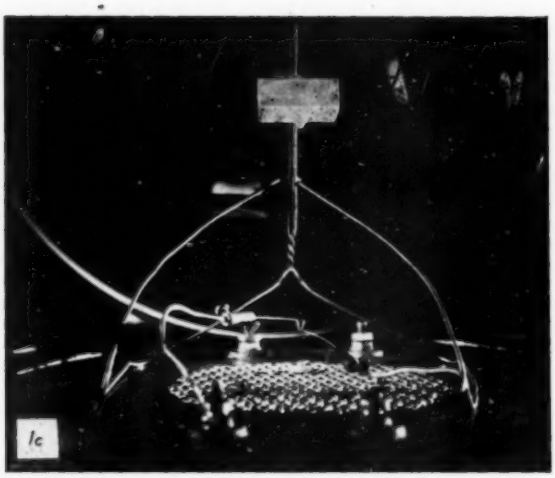

FIG. 1c. Polystyrene impression of specimen mounted 7 to 10 cm above conical tungsten filament containing approximately 1 mg of silica in the form of quartz.

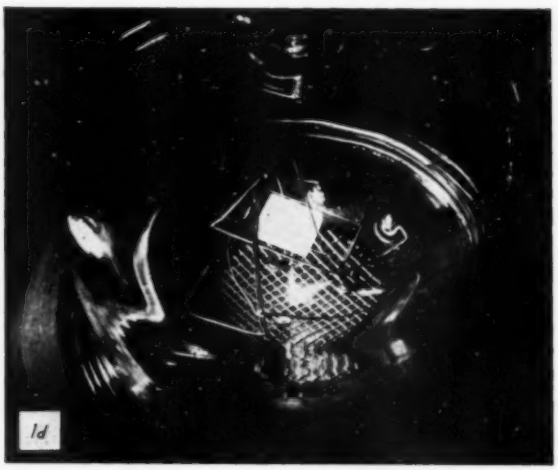

FIG. 1d. Actual evaporation of silica with filament incandescent under a vacuum of about 10^{-4} mm of Hg. Silica is completely evaporated in 5 to 15 seconds, part of which condenses on surface of polystyrene to give a continuous film of approximately 200Å thickness.

All micrographs were obtained with either the RCA type B or U electron microscope.

PREPARATION OF SILICA REPLICAS

The cleanliness of the specimen surface is one of the most important points to be considered in preparing silica replicas. In the case of an etched metal the prepared surface must be free of reaction products, grease, stains, oxide, or hydroxide films or any material which may either adhere to the replica or prevent it from repro-

ducing the true metal surface. When working with non-metallic specimens, the surface must likewise be free of any foreign material which would contaminate the replica. It is our belief that many of the difficulties met in preparing silica replicas by the polystyrene-silica technique arises from improperly prepared surfaces, mainly dirty surfaces.

The polystyrene-silica technique can best be illustrated by a series of photographs of the various steps involved in preparing the polystyrene impression, evaporating the silica upon the plastic, and removing the silica replica film. These various steps are described in detail in order that one may experimentally follow the technique and obtain good replicas with a minimum of difficulty.

The first step, after the specimen has been given a suitable surface preparation, is to mold polystyrene against the surface. This is accomplished quite simply by imbedding the specimen in polystyrene as illustrated in Fig. 1a. Polystyrene molding granules of medium viscosity or molecular weight* are best for this.

The molding may be accomplished in an ordinary electrically heated metallographic specimen mounting press or a steam-heated compression molding die. The specimen is placed in the molding die with the prepared surface upward and sufficient molding granules added to give a final clear molding at least $\frac{1}{4}$ inch thicker than the specimen. The actual molding is accomplished by heating the molding granules to a temperature of 160°C, care being taken that no pressure is applied until they are thoroughly softened. Otherwise they may be pressed against the specimen surface causing deformation. After the granules have had a chance to soften thoroughly (5 to 10 minutes usually is required), pressure is applied up to about 1500 lb./sq. in. and the cooling of the die commenced at once. The pressure is maintained until the molding has cooled below 80°C since release of the pressure at higher temperatures may result in the formation of bubbles in the molding.

The specimen is now separated from the plastic impression by first sawing away the excess material from the edges of the specimen and then separating the two, mechanically if possible. Figure 1b shows a magnesium alloy specimen which has just been mechanically separated or stripped from the polystyrene.

If mechanical separation is impossible without fracturing or otherwise distorting the polystyrene, chemical reagents may be used to dissolve the specimen. Mineral acids or strong caustic solutions may be used on most specimens without damage to the plastic impression.

Figures 1c and 1d show the next step in which silica is evaporated in vacuum upon the surface of the plastic impression. The molding is mounted 7 to 10 cm above a spiral tungsten filament (cone shaped of about 5-mm length with a 35° angle) containing about 1 mg of clear quartz in the form of small slivers weighing roughly 0.2 mg each. The filament of the type shown in the photographs is heated to incandescence for a period of 5 to 15 seconds, using 25 to 30 amp. at 10 to 15 volts. The silica is completely evaporated in a few seconds, providing the individual splinters of silica are not too large and the vacuum is 10^{-4} mm of Hg or better.

The tungsten filament used in this evaporation is prepared by winding 20-mil tungsten at a dull red heat on a tapered mandrel having about a 35° included angle. The quartz used may be prepared quite easily by breaking up a natural clear quartz crystal by means of mortar and pestle and then screening to obtain particles of the proper size. Other laboratories have successfully used cloudy quartz, fused silica, or Santocel.

The block of polystyrene supporting the silica film is now prepared for the removal of the film. The sides and bottom are first scraped thoroughly to remove all undesirable silica film and any dirt which may contaminate the solvents. The silica film is scored into slightly over $\frac{1}{8}$" squares and the polystyrene block lowered to the bottom of a dish of high purity ethyl bromide and benzene with the replica side up as shown in Fig. 2a. The block will stick to the bottom of the dish as the plastic softens. About 10 percent of benzene is added to the ethyl bromide to decrease its volatility and thus prevent moisture condensation upon the silica films as they are removed from the solvent. Such moisture condensation is invariably accompanied by precipitation of the polystyrene. Ethyl bromide is used for this step

* Such a material is available commercially as Styron No. 379-clear.

FIG. 2a. Silica film has been scored into squares and the whole polystyrene block is about to be immersed in ethyl bromide plus 10 percent benzene.

FIG. 2c. Silica films are being transferred on a piece of 200-mesh stainless steel screen to a rinse consisting of ethyl bromide plus a few percent of iso-amyl alcohol.

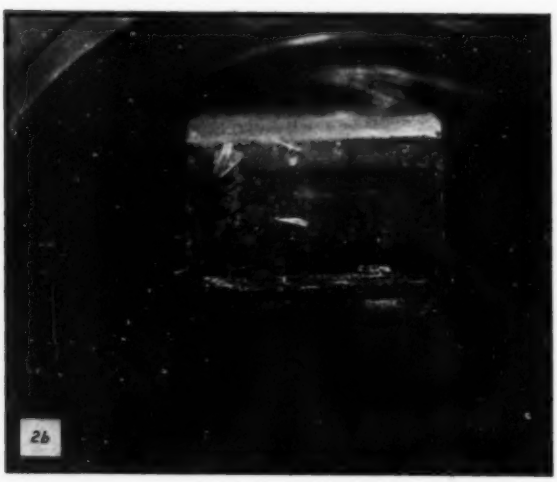

FIG. 2b. Silica films are seen as they start floating off from the polystyrene block stuck to the bottom of the dish of ethyl bromide and benzene. Silica films generally come free from the polystyrene 1 to 5 min. after immersion in the solvents.

FIG. 2d. Catching the silica films on a standard electron microscope specimen screen after they have washed in the solvent rinse for at least 5 min. After catching, the screens are blotted on a filter paper and viewed directly in the electron microscope.

in the replica technique for the following reasons: 1. It is an excellent solvent for polystyrene; 2. its density is sufficiently high to cause the films to float about in the solvent; 3. its great volatility tends to produce convection currents which aid in washing the films free from polystyrene; 4. its refractive index is such that the silica films are generally readily visible in the solvent.

The silica films will generally free themselves from the polystyrene 1 to 5 minutes after immersion. Side illumination with a dark red background is of great help in seeing them. Figure 2b shows the films as they come free from the polystyrene. They are transferred almost at once to a rinse containing ethyl bromide plus a few percent of iso-amyl alcohol added to reduce the solvent's volatility. Benzene is not used because an effective concentration is probably upwards of 10 percent. Transfer of the silica films to the rinse is easily accomplished by using a piece of 200-mesh stainless steel screen as shown in Fig.

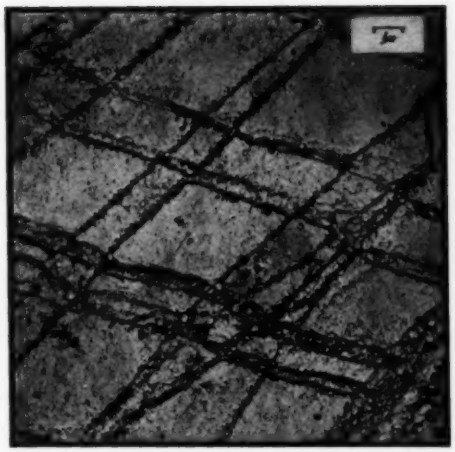

Courtesy A.I.M.E.

FIG. 3. Silica replica of magnesium alloy showing twinning and fine globular precipitation, 4000×.

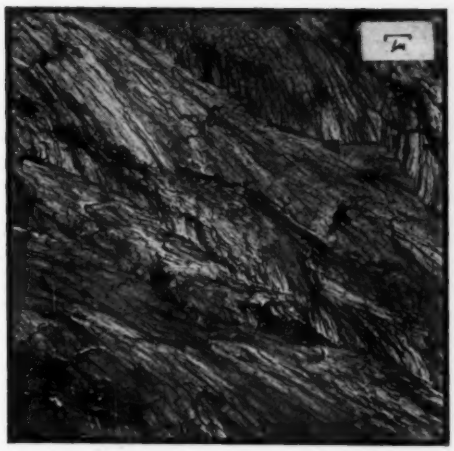

FIG. 6. Silica replica of cleaved enamel from human tooth, 3500×.

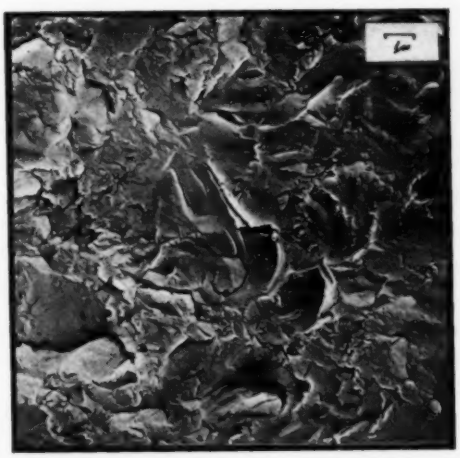

FIG. 4. Silica replica of ground surface of quartz crystal, 4000×.

FIG. 7. Silica replica of polished and acid-etched internal section of rabbit bone, 3000×.

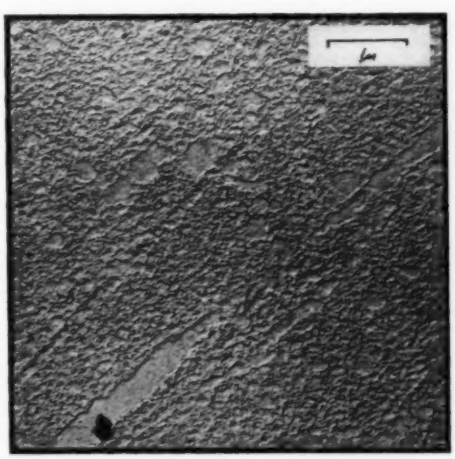

FIG. 5. Silica replica of glass etched with HF, 10,500×.

FIG. 8. Silica replica of maple wood cleavage, 4500×.

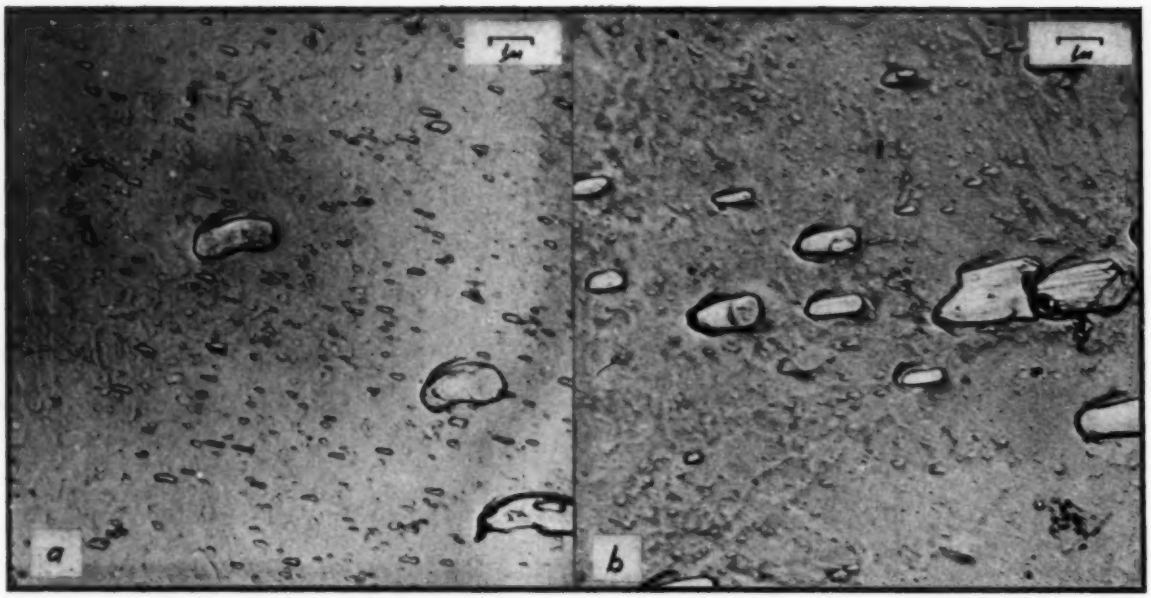

Courtesy A.I.M.E.

FIG. 9. Comparison between silica replicas of a magnesium alloy prepared by means of: (a) a polystyrene molding using both heat and pressure, 6000×. (b) a polystyrene lacquer film using no heat or pressure, 6000×.

2c. The films readily loose themselves from the screen when it is lowered into the rinse provided they are not allowed to dry during transfer.

The silica films are allowed to wash at least five minutes and then caught on the standard microscope specimen screens as shown in Fig. 2d. The screen with the films are dried by blotting on a filter paper. Such films are believed to have a thickness of about 200A.

Figures 3–8 show examples of silica replicas as applied to a magnesium alloy, quartz crystal, etched glass, tooth, bone, and wood.

One often finds in replica work a need for obtaining silica films from specific areas of a specimen. This is not difficult since the polystyrene molding with the silica film may be examined quite readily with the light microscope at magnifications up to 1000× using illumination through the specimen. Regions which are of particular interest may be outlined readily by scribing the surface with a needle point and then scraping off all the silica film except that of particular interest. This film may then be removed in the usual manner. Such a technique is often found very useful in studying interfaces between dissimilar materials.

As has been mentioned before, many of the difficulties experienced when preparing silica replicas arise from improperly prepared surfaces. Dirty surfaces often give silica replica films which tend to roll or fold up and which may refuse to straighten out by the customary method of "teasing" the films with a specimen screen as they float in the rinse. Another difficulty often experienced in preparing silica replicas is fragility of the films caused by lack of appreciable fine structure in the original specimen. It appears that fine detail in a specimen adds considerably to the mechanical strength of silica replicas.

On the other hand, silica replicas of single phase or electrolytically polished metals, glass, or other microscopically smooth surfaces are very often extremely fragile. Care must be taken to handle these films delicately and even then part of the film may break up on the specimen screen.

Occasionally one wishes to prepare replicas of surfaces which for some reason cannot be subjected to the temperatures and pressures necessary to obtain a polystyrene impression. In such cases an alternate method is used in which a polystyrene lacquer is applied to the specimen to give a heavy coating, stripped off and then used to prepare silica films in the ordinary manner. This technique has given quite reliable

results in practice using a 1 percent solution of polystyrene in benzene for the initial application and then backing this film up with several applications of a more viscous lacquer of 2 to 3 percent polystyrene in benzene. By means of the more concentrated solution one can build the original film up to the point where it may be mechanically stripped from the specimen or the specimen dissolved if it is felt to be advisable. Figures 9a and b show a comparison between the conventional method and this polystyrene lacquer technique.

The resolution possible with this technique appears to be very good though very likely not equal to that of the pressure molding technique whose resolution is apparently better than 100A. The resolution of this "cold" replica technique can probably be improved, as suggested by Matheson,* by vacuum boiling of the specimen in the lacquer as a means of outgassing the surface. The initial lacquer coating can then be built up as previously described.

STEREOSCOPY

The use of stereoscopy as an electron microscope technique has become of quite general application and is held to be invaluable in interpreting electron micrographs by many microscopists. The stereoscopic technique is especially well suited for use with silica replicas.[9] However, one of the difficulties experienced in such application has been the impossibility of definitely establishing the "up and down" of the stereo pictures unless something was known about the topography of the original specimen surface.

A very simple procedure is now being used to remove this uncertainty. This consists of adding a metal oxide smoke to a known side of the silica replica film and using this oxide smoke to determine the correct viewing arrangement. This is best accomplished by depositing the oxide smoke on the polystyrene impression of the specimen surface. Magnesium oxide smoke works very successfully, an even distribution being obtained by wafting the molding through the smoke of burning magnesium. Zinc oxide smoke can also be used but is much more difficult to distribute evenly.

Silica is evaporated upon the polystyrene impression and the films removed in the usual manner carrying the oxide smoke with them,

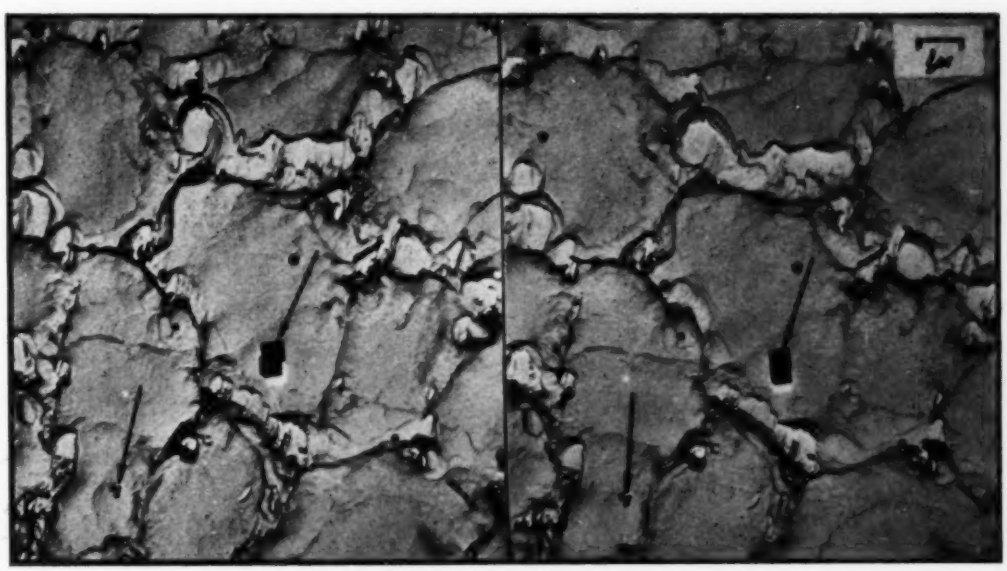

FIG. 10. Stereo pair from a fine grain magnesium alloy showing the addition of magnesium oxide smoke (indicated by arrows) to the replica film. The question of "up and down" is answered by viewing the stereo pair arranged so the oxide cubes appear below the surface. Compound precipitation can be observed projecting upward in relief from the grain boundaries. Magnification 6000×.

* L. A. Matheson and R. D. Heidenreich, "Magnification calibration of electron microscopes," Presented at Chicago meeting of E.M.S.A. (November, 1944).

[9] R. D. Heidenreich and L. A. Matheson, J. App. Phys. **15**, 423 (1944).

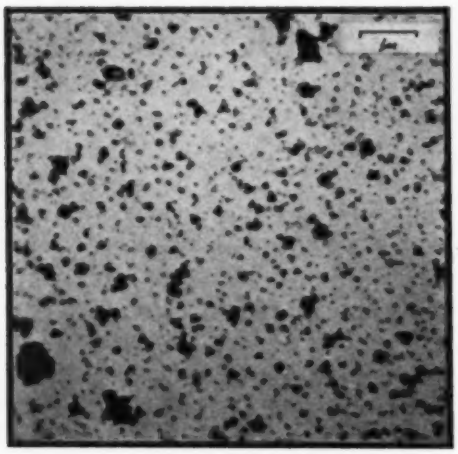

FIG. 11. Silica smoke dispersed in ethyl cellulose on a silica substrate, 7500×.

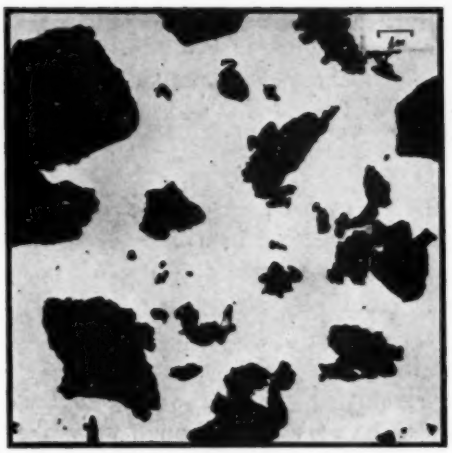

FIG. 12. $CaCO_3$ dispersed in ethyl cellulose on a silica substrate, 4500×.

attached to the side reproducing the specimen's surface structure. Electron micrograph stereo pairs of these films are then obtained and viewed through the stereoscope with the pictures arranged so the oxide smoke appears below the surface, the proper arrangement. By this method the question of "up and down" is definitely settled. Figure 10 shows a stereo pair of a magnesium surface with MgO smoke on the replica.

SILICA SUBSTRATES AND A POWDER DISPERSING TECHNIQUE

Structureless silica substrates have been found very useful as supports for a variety of electron microscope specimens. They can be prepared having a thickness of from <100 to 200A and are completely structureless and without holes or fibers. The films are structurally strong as compared to organic films, and may be subjected to very intense electron beams with a minimum of electron scattering, "charging up," and breakage. Microscope specimens may be heat treated at elevated temperatures for short periods of time while supported on silica substrates. They also can be successfully used as the support for specimens for electron diffraction transmission study.

These substrates are prepared by dipping a clean and dry microscope slide in a 2–5 percent solution of polystyrene in benzene and allowing to dry. The silica film is formed upon the lacquer film by the same technique as used for replicas except that 10 or 20 percent less silica is generally used. The films are removed in the same manner as other silica replica films and caught on standard electron microscope specimen screens. However, the silica films separate from the thin polystyrene film quite slowly, ½ hour to several hours usually being required.

Difficulties are occasionally met in preparing these films and they seem to be largely caused by improper thickness of the polystyrene film. For some inexplicable reason, if this film is too thick, the silica films are fragile, and if too thin, the silica films come loose from the lacquered slide with great difficulty or may not come loose at all.

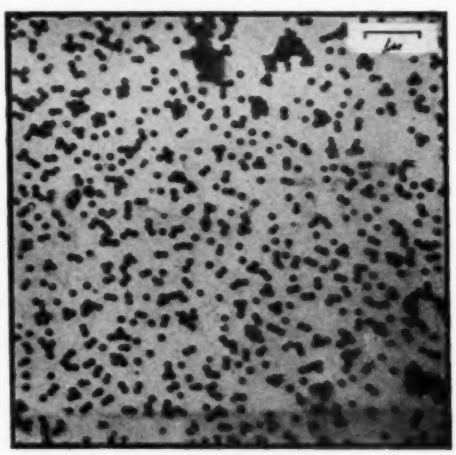

FIG. 13. Polystyrene emulsion dispersed on a silica substrate, 7500×.

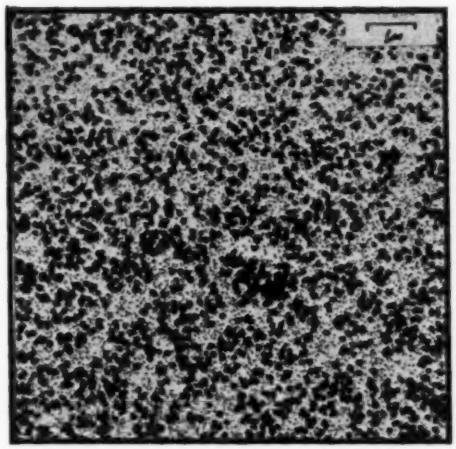

FIG. 14. Magnesium-aluminum alloy evaporated in vacuum and condensed on a silica substrate, 6500×.

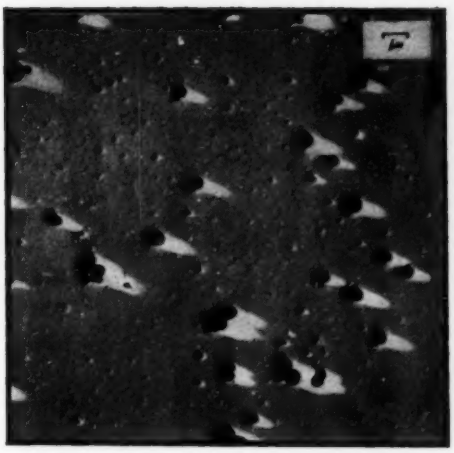

FIG. 16. Lampblack dispersed in ethyl cellulose on a silica substrate and shadowed with chromium, 3500×.

It appears that a 2–5 percent lacquer solution gives a film of optimum quality.

Precautions must also be taken to see that the lacquer is relatively moisture-free and the glass slide dry. Failure to observe these precautions may result in a cloudy lacquer film and substrates which show bubbles.

Many different particle dispersing techniques have been published[10,11] which make it possible to determine accurately particle size and shape. Most of these techniques can be successfully used with silica substrates with improved results. A powder dispersing technique has been in use here for several years which has given excellent results on a wide variety of powdered materials ranging in size from <0.01 micron to several microns. This technique consists of dispersing the powder in an ethyl cellulose lacquer as a thick slurry, diluting and adding to the silica substrate. This is accomplished in practice by placing a few milligrams of the powder in a mortar and adding a drop or two or an ethyl cellulose lacquer consisting of 2 percent ethyl cellulose in 70 percent amyl acetate and 30 percent ethyl alcohol. The mixture is lightly ground with mortar and pestle to a thick slurry or paste during which time the dispersion of the particles actually takes place. Amyl acetate is then added slowly at first and the concentrated dispersion diluted to the proper concentration for adding to the silica substrate on a specimen screen. Tests have indicated that the effect of the grinding action upon the particle size and shape is negligible in specimens having a particle size of less than 5 microns.

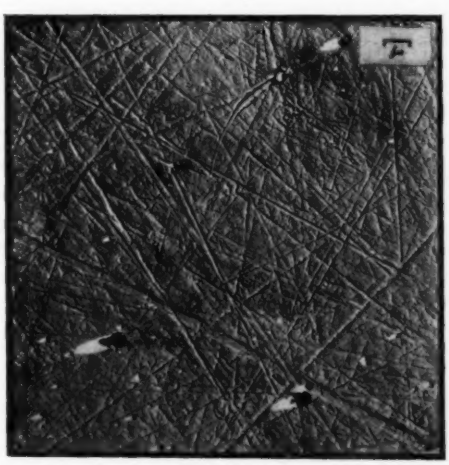

FIG. 15. Silica replica of a polished steel surface shadowed with chromium, 3500×.

Ability to judge the proper quantities and dilutions is readily obtained with a little experience. Generally the slurry dilution is about 1:50. Quantities should be varied so that the minimum thickness of dried ethyl cellulose is used, i.e., just sufficient to keep the particles firmly attached to the silica film. Figures 11 and 12 show typical particle dispersions obtained by this technique.

[10] M. L. Fuller, P. G. Brubaker, and R. W. Berger, J. App. Phys. **15**, 201 (1944).
[11] A. M. Cravath, A. E. Smith, J. R. Vinograd, and J. N. Wilson, J. App. Phys. **17**, 309 (1946).

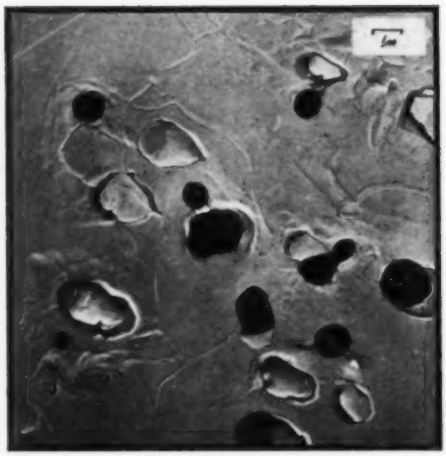

Courtesy A.I.M.E.

FIG. 17. Silica replica of a magnesium-nickel alloy showing not only a replica of the globular Mg_2Ni particles but also some of the actual particles themselves on the silica replica film. The faithfulness of the technique in reproducing the size and shape of the particles is evident. Figure 3 also shows this same phenomenon on a smaller scale. Magnification 4000×

Silica substrates may also be used for supporting a variety of other types of specimens as illustrated by Figs. 13 and 14 showing an emulsion and an evaporated magnesium alloy. Emulsions are readily dispersed by diluting to the proper concentration and then adding a drop of the liquid to the substrate on a specimen screen.

MISCELLANEOUS USES AND TECHNIQUES

Silica replicas and substrates have also been found to be useful in the field of heavy metal "shadow-casting."[12] This technique is probably not of great value on silica replicas for the purpose of improving contrast since silica replicas normally show considerable contrast. However, the technique has definite possibilities as a means of making elevation determinations without the use of stereoscopy.

Shadowing of silica replica films is probably best accomplished by evaporating the heavy metal upon the silica film while it is on the surface of the polystyrene molding. The films are then removed in the usual manner. Figure 15 shows an example of the "shadow-casting" of a polished steel specimen.

[12] R. C. Williams and R. W. G. Wyckoff, J. App. Phys. 15, 712 (1944).

Shadowing of various electron microscope specimens supported on silica substrates is of definite value both from the point of view of improving contrast and of making elevation determinations. This technique is probably best accomplished by applying the polystyrene lacquer film to a glass slide, evaporating the silica, adding the specimen, "shadow-casting," and then removing the silica film in the usual manner. It seems advisable to use such a procedure rather than attempt the shadowing of the substrate and specimen while supported by the specimen screen. In this case the silica film may be uneven, making it a very poor target for accurate "shadow-casting." Figure 16 shows a specimen of lampblack "shadow-cast" in this above recommended manner.

A very interesting and often valuable use of silica replicas lies in the isolating of impurities and certain second phase elements or compounds from some metals. This occurs occasionally in metals which contain one or more elements or compounds which are present as a second phase and which are relatively insoluble in the etchant used during the surface preparation. Such constituents of the metal are often either left lying on the metal surface after etching or are protruding from the surface and only loosely attached to the metal. When polystyrene is molded against the metal surface and separated, these particular constituents are imbedded in the polystyrene and removed with it. When the silica evaporation is completed and the polystyrene dissolved, as the silica films are removed, the particles are often transferred to the silica replica and attached to it. As a result we find that in the electron microscope we see not only a replica of certain second phase constituents in the metal but also some of these particular constituents actually attached to the replica film. Figures 3 and 17 show examples of this phenomenon. Such materials can often be identified by transmission electron diffraction.

Occasionally one finds an electron microscope specimen in particle form which tends to sublime when subjected to the high vacuum and heat of electron bombardment in the microscope. This sublimation may be appreciably decreased by supporting the specimen on a silica substrate

and then evaporating more silica over the surface of the specimen. Sulfur is a material which may be treated in this manner.

CONCLUSIONS

1. Silica replicas of a variety of bulk materials such as metals, minerals, glasses, ceramics, resins, woods, etc., can be successfully prepared using a heat and pressure molded polystyrene impression plus evaporated silica.

2. Silica replicas can be successfully prepared from bulk materials which cannot tolerate either the temperatures or pressures of (1), by applying a heavy polystyrene lacquer, removing and evaporating silica upon the lacquer impression.

3. The question of "up and down" in stereo pictures of silica replicas can definitely be established by depositing a metal oxide smoke on the polystyrene impression before evaporation of the silica.

4. Structureless silica substrates are well suited as the supporting membranes for specimens such as powders, emulsions, metallic oxide smokes, thin evaporated films, bacteria, viruses, microtome sections, etc.

5. Excellent dispersions of powders from <0.01 to several microns in diameter may be obtained on silica substrates using an ethyl cellulose lacquer dispersing technique.

6. Heavy metal "shadow-casting" can be effectively applied to both silica replicas and silica substrates.

7. Isolation of metallic phases directly on silica replicas of metal surfaces is often useful in minutely examining and identifying these constituents.

ACKNOWLEDGMENT

The author wishes to express his appreciation to R. D. Heidenreich of the Bell Telephone Laboratories and H. L. Woods of the Henry Ford Hospital who developed several of the techniques described in this paper while employed at The Dow Chemical Company.

The X-Ray Storage Properties of the Infra-Red Storage Phosphor and Application to Radiography

O. E. Berg and H. F. Kaiser

Naval Research Laboratory, Washington, D. C.

(Received November 4, 1946)

An application of the characteristics of infra-red storage phosphors to radiography is described, whereby the expense and trouble of x-ray film processing may be partially or completely eliminated. The properties of these materials to store x-ray energy for periods of time and release that energy upon exposure to infra-red radiation have proved practical for either temporary and permanent recording of the latent x-ray image. One distinct feature of this method is the complete removal of harmful x-radiation to the technician. The possibility of a new field of radiography in "flash fluoroscopy" is also suggested by the authors. Graphs and charts exhibiting the characteristic behavior of infra-red phosphors to x-ray energy are included as well as actual photographs and radiographs comparing radiography with phosphorography.

THE image storage phosphor was a research development required in war work as a practical and sensitive means for the detection of infra-red radiation. In the course of research[1] carried on to produce such phosphors it was found possible to produce phosphors which exhibited storage properties not only for visible light, but also for cathode rays, and x-rays. The optical characteristics of such materials have been described in papers of Roland Ward[2] and of N. F. Miller and C. E. Barnett.[3]

[1] Contract OEMSR 982, OSRD Report 16.5—119 (N5643).

[2] R. Ward, "Preparation and properties of infra-red sensitive strontium selenide and sulfide-selenide phosphor," J. Opt. Soc. Am. **36**, 351(A) (1946).

[3] N. F. Miller and C. E. Barnett, "Infra-red sensitive phosphors from zinc and cadmium sulfides," J. Opt. Soc. Am. **36**, 352(A) (1946).

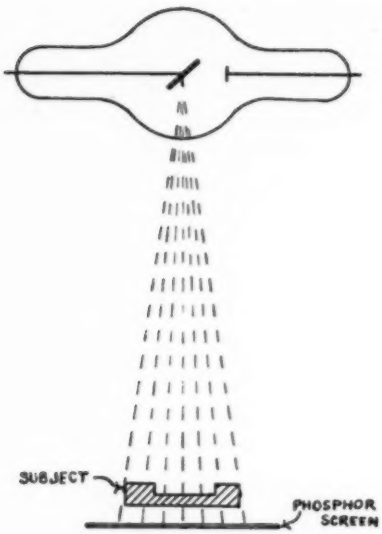

FIG. 1A.

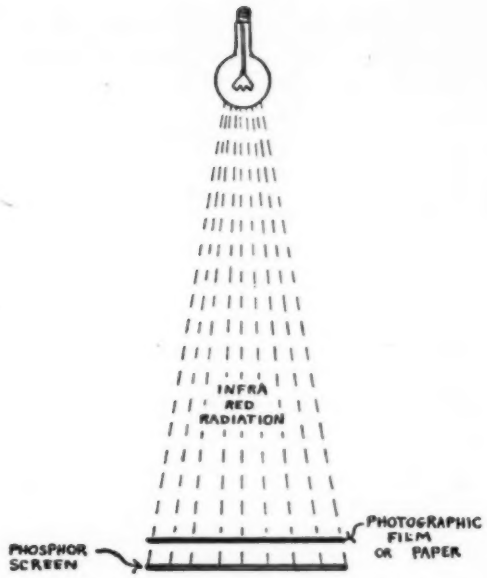

FIG. 1B.

Since no attempt had been made to study these materials for x-ray energy storage characteristics, the authors have carried out a series of experiments on materials kindly furnished by the Brooklyn Polytechnic for this purpose. The ability of these materials to save x-ray energy suggests their application to radiography as a possible substitute for the photographic emulsion for the retention of a latent image.

The ability of these materials to store radiant energy is not surprising in view of the fact that all phosphors exhibit such properties when cooled to liquid air temperature, exposed to an energy source to fill the electron traps and then warmed up, whereupon the freeing of electrons from the traps is indicated by bursts of light.[4]

Phosphors may be produced which store energy from x-rays, beta-rays, gamma-rays, and visible light and which hold this energy for indefinite periods of time. The energy is released, in the form of light varying from red to ultra-violet, by infra-red radiation with speed of release governed by intensity of the infra-red radiation. Figure 1A and B shows how these effects may be employed in radiography. The x-rays pass through the subject into the phosphor plate or screen, and by differential intensity record in detail thereon producing a latent image. This latent image is quite stable for many phosphors.

Then, in an adjoining room, away from harmful x-radiation, and at the convenience of the operator, the image is made visible to the eye by irradiating the plate with infra-red radiation. If a particular area of the image is of special interest to the technician, he may expose it separately with an infra-red spotlight (photographic masking technique is also applicable here). The length of viewing time of a phosphor plate may be determined from its energy decay rate graph shown in Fig. 2A which indicates the intensity of the released light as a function of time and intensity of the infra-red source.

When plotting light units against log time as in Fig. 2B, we get several linear portions indicating that the decay of luminescence is not of simple exponential character, but occurs in a set of several such processes. Light values are given as arbitrary light units measured by a 931A photo-cell multiplier with voltage regulators.

If a permanent record of the x-ray image is desired, it is an inexpensive and a simple task to expose the phosphor image directly to a sensitized paper (sensitive in the color region of the particular phosphor in use). Such a process eliminates the need for double emulsion x-ray film.

A 4″×5″ experimental phosphor viewing plate was prepared according to the following procedure:

[4] "Characteristics of luminescent materials for cathode-ray tubes," J. Inst. Elec. Eng. 92, Part III, No. 20, 300 (December, 1945).

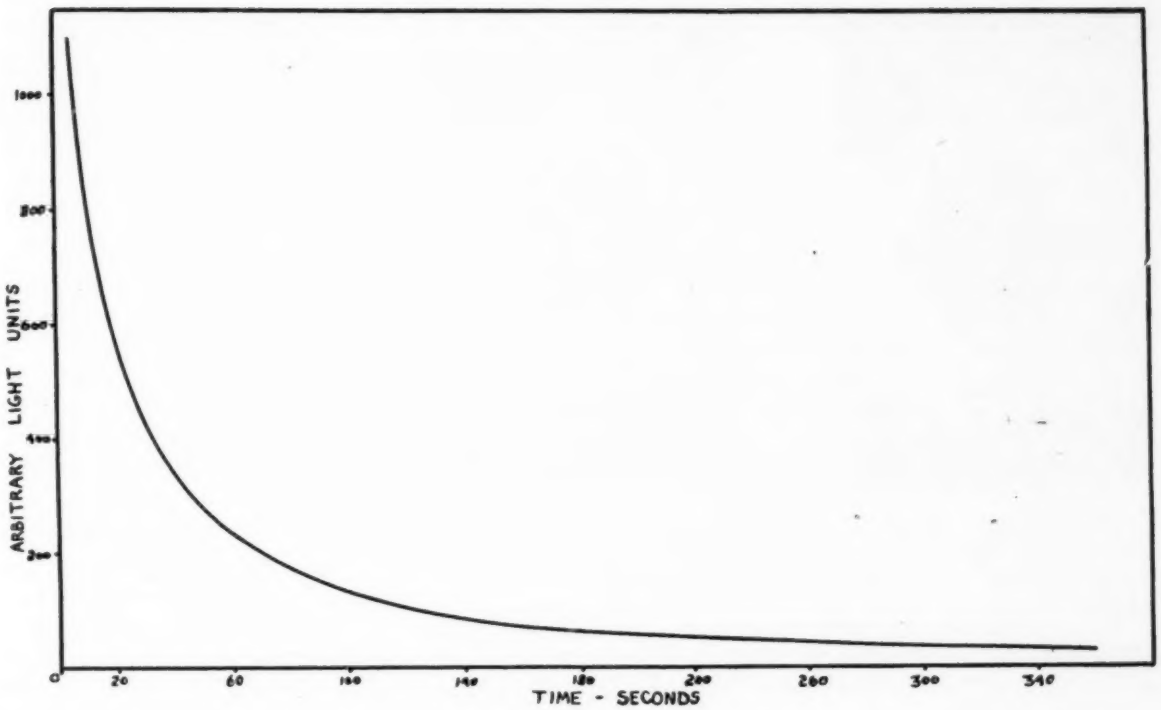

FIG. 2A.

While it might have been desirable to apply the phosphor to a thin cardboard base as for a fluorescent screen, because of the high processing temperatures involved, it was found necessary and advantageous to use a $\frac{1}{32}$" steel plate with a thick silver plating. This base plate was not affected by high temperatures and its silver coating prevented chipping or peeling of the phosphor during experimentation.

Furthermore, silver plated steel is preferable to a paper base in that it serves as an absorbing medium for transmitted x-radiation after the x-rays have transversed the subject and the phosphor, thereby reducing scatter.

An emulsified mixture of phosphor, ethylene dichloride, and jasonite (plastic binder) was applied with a small artist's spray gun, and dried at 850°C to remove excess binder and render the phosphor active.[5] After a few experiments, it was found that a .020-inch coating of the phosphor was sufficiently thick to produce peak luminescence.

Test exposures were made on the resultant plate at various kilovoltages and exposures.

[5] For further information on phosphor coating application see OSRD Report No. 5643.

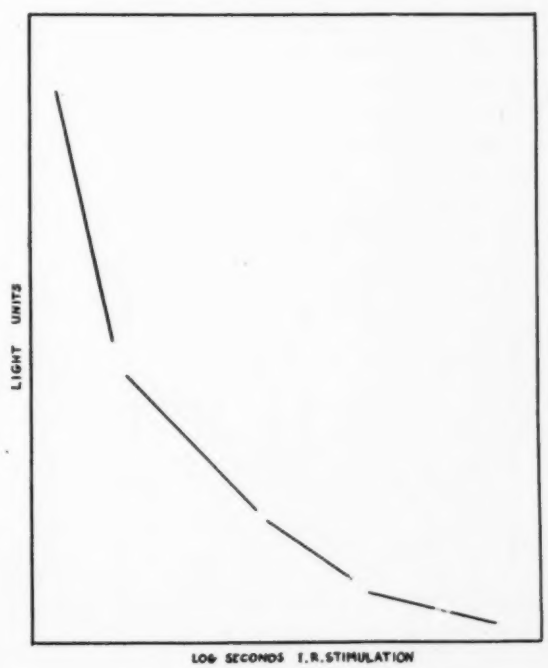

FIG. 2B.

Figures 3 and 4 are comparative results of an x-ray film image and a phosphor image, respectively, of a 3-inch ammeter. It is an indication

FIG. 3. Radiogram of 3 inch meter. X-ray exposure made on fine grain industrial x-ray film.

FIG. 4. Phosphorogram of 3-inch meter. Dark areas indicate uneven phosphor coating.

FIG. 5. Secondary film exposure to phosphor image of meter. Notice increased latitude and preservation of detail.

of the definition and latitude obtainable in a "phosphorogram."

An interesting and advantageous feature concerning latitude in this method of exposure is revealed in Fig. 5, another photograph of the same exposure after some diminution by previous

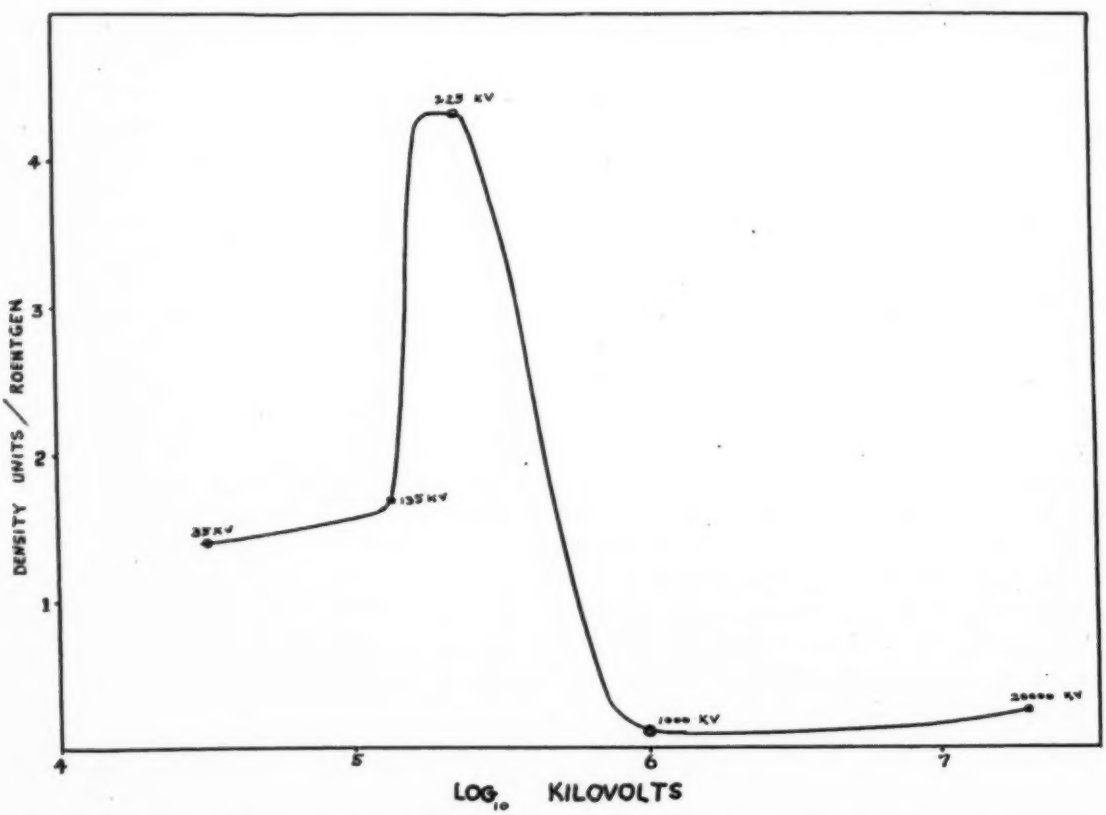

FIG. 6. The storage sensitivity curve in the x-ray region of the spectrum for one particular infra-red phosphor.

infra-red exposure. The definition is as sharp as before and areas that were overexposed (too brilliant) in the previous photographic exposure now appear in readable detail. The latitude of a phosphorogram is thus extensive and flexible. An overexposed plate can be irradiated with infra-red till it reaches a readable intensity. Likewise, an underexposed plate can be increased in intensity to a readable density by increasing the infra-red radiation.

Figure 6 shows the storage sensitivity curve in the x-ray region of the spectrum for a particular phosphor. Each type of storage phosphor has its own sensitivity curve and exhibits its own characteristic properties as well. Although a blue-green phosphor was used extensively in these experiments, it is now possible to obtain a phosphor for any color region in the visible spectrum. Blue-green is a comfortable color to the eye, but it is not the most efficient color for definition.

In general, the results of these experiments have revealed numerous possibilities of infra-red phosphors in radiography. Their properties, however, are not always advantageous.

Referring back to Figs. 3 and 4, we recognize the same undesirable characteristics of graininess and diffusion as in the fluorescent screen. This might be corrected to a large extent by more refined processing methods. Figure 2 shows another disadvantage—a reluctant release of stored energy, because of the exponential decay rate, which may handicap the speed of repeated exposures upon a given phosphor plate. For all practical purposes, however, the energy remaining in the phosphor after reasonable exposure to infra-red radiation is negligible and the contrast of the recorded image appears to diminish with time.

Phosphorography will not immediately replace the x-ray film nor the fluorescent screen. It will supplement these methods and be particularly valuable in special cases. For example: flash fluoroscopy will be possible with the high current condenser-discharge x-ray tubes, whereby an image made with a very short x-ray exposure of high intensity will be made immediately visible, and retained long enough for inspection or recording on paper or film.

Grateful acknowledgment is extended to Drs. R. E. Ward and R. T. Ellickson of the Polytechnic Institute of Brooklyn for their willing cooperation in supplying information and material for this work.

A Flux Plotting Method for Obtaining Fields Satisfying Maxwell's Equations, with Applications to the Magnetron

PRESCOTT D. CROUT
Radiation Laboratory, Massachusetts Institute of Technology, Cambridge, Massachusetts*
(Received September 13, 1946)

In this report the flux plotting methods which have previously been applied to fields satisfying Laplace's and Poisson's equations are extended to fields satisfying Maxwell's equations. Application is made to the hole and slot, and vane types of magnetron tubes.

1. INTRODUCTION

"FLUX plotting" is a procedure for drawing two mutually orthogonal families of curves in such a way that the rectangles so formed have a specified geometric shape at each point. This shape is so determined that the curves represent a field which satisfies a specified partial differential equation. This equation, which characterizes the field, is not used directly, but it or its equivalent is used only indirectly to determine the geometrical condition that is used in actually constructing the plot. Flux plotting procedures for obtaining fields satisfying Laplace's equation, Poisson's equation, and certain other equations have been devised and applied successfully to wide varieties of problems.[1] The purpose of this paper is to extend these methods to fields characterized by Maxwell's equations. In so doing we do not use these equations directly, but use Ampere's law and Faraday's law instead. These laws together with Stoke's theorem evidently give Maxwell's equations. Some familiarity with flux plotting methods is assumed.

For the sake of clarity the new method will be described in connection with the specific application which gave rise to it—that of an infinite, hole and slot type magnetron, a cross section of which is shown in Fig. 1, operating in its main mode (+ − + − or Π mode).[2] Later in Section 6 application is made to the vane type magnetron. All fields are sinusoidally alternating. The electric current which links each anode well (cavity) and passes across the gap between two adjacent anode segments produces the axial magnetic field in the well (Ampere's law); also the rate of change of this axial magnetic field produces the voltage which maintains the electric current (Faraday's law). Because of symmetry we need consider only the field which lies between two axial planes which bisect, respectively, an anode segment and an anode well, Fig. 2.

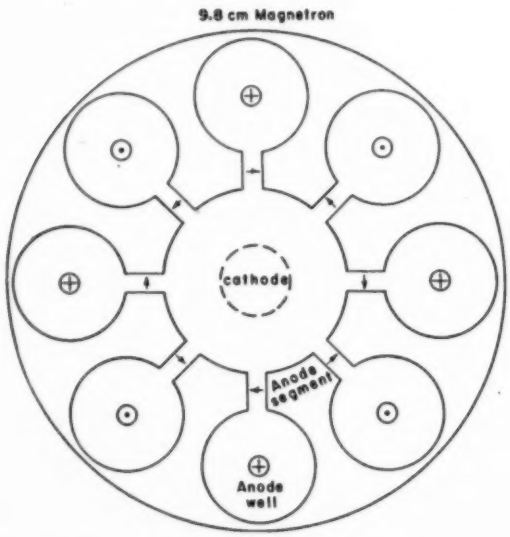

FIG. 1. Cross section of hole and slot type magnetron. Magnetic field is axial (perpendicular to the plane of the paper). Its directions in the anode wells at a certain instant are shown by the circles ⊕ and ⊙. Electric field is across the gaps between the anode segments. Its directions at a certain instant are shown by the arrows.

* This paper is based on work done for the Office of Scientific Research and Development under contract OEMsr-262 with the Massachusetts Institute of Technology.

[1] H. Poritsky, "Graphical field-plotting methods in engineering," Trans. A.I.E.E. **57**, 727 (1938). B. Hague, "Méthodes Analytiques, Graphiques et Expérimentales Utilisées Pour l'Étude des Champs Magnétiques et Électriques dans Les Machines et Appareils Électriques," Comptes rendus **4**, 47 (1932). (This reference contains an extensive bibliography.) A. D. Moore, *Fundamentals of Electrical Design*, p. 31. P. D. Crout, "The Determination of Fields Satisfying Laplace's, Poisson's, and Associated Equations by Flux Plotting," Radiation Lab. Rep. 1047.

[2] The field so obtained can be made the basis of calculations for determining the frequency spectrums of finite strapped or unstrapped magnetrons. See Crout and Bothwell, "A Method for Calculating Magnetron Resonant Frequencies and Modes," Radiation Lab. Rep. 1039.

2. NATURE AND CONSTRUCTION OF THE FLUX PLOT

The peak electric field is shown in Fig. 2 by means of a number of electric lines of force, which divide the region into corresponding tubes of flux; and a number of lines of no work, which are orthogonal to the lines of force, and which divide the region into corresponding strips. The peak magnetic field is perpendicular to the plane of the paper. Let the various tubes and strips be numbered consecutively as indicated, and let

L_{ij} = length of elementary rectangle common to ith tube and jth strip measured along a line of force through the center;
W_{ij} = width of elementary rectangle common to ith tube and jth strip measured along a line of no work through the center;
A_{ij} = area of elementary rectangle common to ith tube and jth strip;
$\sigma_i\phi$ = electric flux in the ith tube, ϕ being the arbitrarily chosen flux per unit tube; (1)
E = electric intensity = electric flux density since dielectric constant = 1;
H = magnetic intensity = magnetic flux density since permeability = 1;
ω = angular frequency;
c = velocity of light.

Gaussian units are used throughout

We shall first consider the equilibrium of an elementary rectangle, and shall leave till later the consideration of the elementary triangles which occur at the "kernel" or point of intersection of the lines of no work. The total peak displacement current flowing outside (on the cathode side) of the center of rectangle ij is[3]

$$\left(\tfrac{1}{2}\sigma_i+\sum_{k=1}^{i-1}\sigma_k\right)\frac{\phi\omega}{4\pi}; \tag{2}$$

hence, noting Ampere's law, we see that the value of H at this point is independent of j, and is given by

$$\left(\tfrac{1}{2}\sigma_i+\sum_{k=1}^{i-1}\sigma_k\right)\frac{\phi\omega}{c}. \tag{3}$$

The total magnetic flux in the jth strip between the center of rectangle ij and the kernel is therefore

$$\frac{\phi\omega}{2c}\left(\tfrac{1}{2}\sigma_i+\sum_{k=1}^{i-1}\sigma_k\right)A_{ij}+\frac{\phi\omega}{c}\sum_{l=i+1}^{n-1}\left(\tfrac{1}{2}\sigma_l+\sum_{k=1}^{l-1}\sigma_k\right)A_{lj}+\frac{\phi\omega}{c}\left(\alpha_j\sigma_n+\sum_{k=1}^{n-1}\sigma_k\right)A_{nj}, \tag{4}$$

where

$A_{ij}=L_{ij}W_{ij}$ for *rectangle* ij,
L_{nj} = base of triangle in jth strip,
W_{nj} = altitude of triangle in jth strip,
A_{nj} = area of triangle in jth strip =

$$(L_{nj})_{\text{average}}W_{nj}, \tag{5}$$

α_j = fraction of W_{nj} from the last line of force to the center of gravity of the last triangle (equals $\frac{1}{3}$ for triangles with straight sides).

By using the center of gravity as the point at which to evaluate B in an elementary rectangle or triangle, multiplication of this value of B by the elementary area gives the flux exactly if the surface which represents B is a plane, regardless of whether or not that plane is horizontal (B constant). The first term in (4) gives the peak magnetic flux in half of rectangle ij, whereas the last gives that in the triangle.

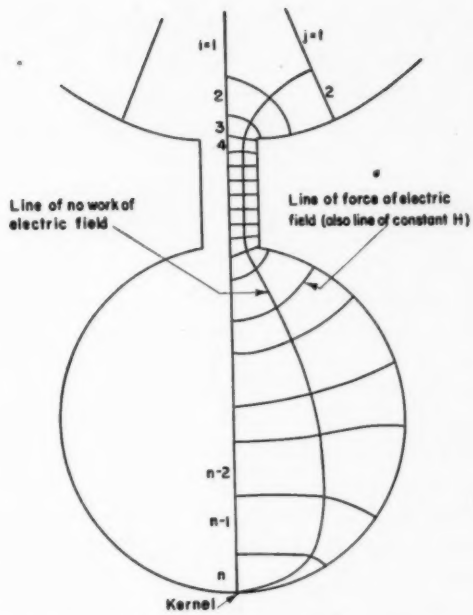

FIG. 2. Electric field in hole and slot type magnetron.

[3] From here on the word "peak" will be omitted, it being understood that all quantities are peak values of sinusoidally varying quantities. Complex notation can be used if desired, in which case the magnetic intensity will be purely imaginary.

Noting Faraday's law we see that the electric flux in the ith tube can be obtained from the rate of change of the magnetic flux given by (4), thus

$$\sigma_i\phi=\left\{\frac{\phi\omega}{c}\left[\tfrac{1}{2}\left(\tfrac{1}{2}\sigma_i+\sum_{k=1}^{i-1}\sigma_k\right)A_{ij}+\left(\alpha_j\sigma_n+\sum_{k=1}^{n-1}\sigma_k\right)A_{nj}+\sum_{l=i+1}^{n-1}\left(\tfrac{1}{2}\sigma_l+\sum_{k=1}^{l-1}\sigma_k\right)A_{lj}\right]\right\}\frac{\omega W_{ij}}{cL_{ij}}. \tag{6}$$

Here the brace is the magnetic flux given by (4), which with ω gives the rate of change of this flux, or the induced voltage in abvolts.[3] Division by cL_{ij} gives the electric intensity in statvolts/cm, and multiplication by W_{ij} gives the total electric flux in the rectangle, which must equal $\sigma_i\phi$. Cancelling ϕ and transposing, (6) becomes

$$\frac{L_{ij}\sigma_i}{W_{ij}}=\left(\frac{\omega}{c}\right)^2\left\{\tfrac{1}{2}\left(\tfrac{1}{2}\sigma_i+\sum_{k=1}^{i-1}\sigma_k\right)A_{ij}+\left(\alpha_j\sigma_n+\sum_{k=1}^{n-1}\sigma_k\right)A_{nj}+\sum_{l=i+1}^{n-1}\left(\tfrac{1}{2}\sigma_l+\sum_{k=1}^{l-1}\sigma_k\right)A_{lj}\right\}, \tag{7}$$

which is the desired equilibrium condition for the *rectangle.*

We shall next obtain the equilibrium condition for a triangular area at the kernel. Let the triangular area Fig. 3 be broken up into elementary bands of constant width dx by a suitable family of curves, x being measured along the orthogonal trajectory which passes through the center of gravity. We shall suppose that H is essentially constant over the triangle, its value H_0 being taken as that at the center of gravity; also we shall suppose that the length of the elementary band at x is given closely by

$$L=Kx^m, \tag{8}$$

where K and m are constants. The total magnetic flux in the triangle from the vertex to the elementary band is

$$\int_0^x H_0Kx^m dx=\frac{H_0Kx^{m+1}}{m+1};$$

hence the electric intensity at the band is

$$\left(\frac{1}{Kx^m}\right)\left(\frac{H_0Kx^{m+1}}{m+1}\right)\left(\frac{\omega}{c}\right), \tag{9}$$

in which the last two factors give the voltage across the band. Integrating (9) we obtain $\sigma_n\phi$, the total electric flux in the triangle, thus

$$\sigma_n\phi=\int_0^{W_{nj}}\frac{H_0\omega x}{c(m+1)}dx=\frac{H_0\omega W_{nj}^2}{2c(m+1)}. \tag{10}$$

Noting the last term of (4) we replace H_0 by its value

$$\frac{\phi\omega}{c}\left(\alpha_j\sigma_n+\sum_{k=1}^{n-1}\sigma_k\right), \tag{11}$$

and obtain, after cancelling ϕ and transposing,

$$W_{nj}^2=\frac{2(m+1)\sigma_n}{\left(\frac{\omega}{c}\right)^2\left(\alpha_j\sigma_n+\sum_{k=1}^{n-1}\sigma_k\right)}. \tag{12}$$

Dividing the left hand side by $L_{nj}W_{nj}$, and the right by its equal KW_{nj}^{m+1}, and noting that

$$A_{nj}=KW_{nj}^{m+1}/(m+1),$$

we finally obtain

$$\frac{L_{nj}\sigma_n}{W_{nj}}=\frac{1}{2}\left(\frac{\omega}{c}\right)^2\left(\alpha_j\sigma_n+\sum_{k=1}^{n-1}\sigma_k\right)A_{nj}, \tag{13}$$

which is the desired equilibrium condition for the *triangle.* We note that this expression contains neither K nor m; also, in comparing (13) with (7) we note the presence of the factor $\frac{1}{2}$ in (13).

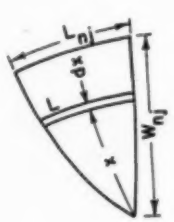

FIG. 3. Triangular area at kernel.

As usual with flux plotting methods, the actual process of making the plot is one of systematic trial and error. The choice of the σ_i's is a matter of convenience. If σ_i is put equal to one, the ith tube is a unit tube; however, at the edge of the plot and in the weaker parts of the field it is desirable to use fractional tubes so that more lines show on the plot.

In constructing the plot a step-by-step process can be used whereby the values of L_{ij}, W_{ij}, and σ_i taken from one approximate plot are placed in (7) and (13) to obtain improved values of L_{ij}/W_{ij} and σ_i, which are then made the basis of the plot which constitutes the next approximation. The first plot would be largely assumed from physical considerations. One step of the step-by-step process will now be described.

First we note that the σ_i's associated with a plot may be multiplied by any constant without altering the plot. This is evident from (7) and (13), and also from the fact that the effect is merely to magnify the field strength. Values of L_{ij}, W_{ij}, and σ_i taken from the given approximate plot are now placed in the right hand sides of (7) and (13) to give for each rectangle or triangle the value of $L_{ij}\sigma_i/W_{ij}$ to be used in constructing the next approximate plot.[4] In so doing the unknown factor $(\omega/c)^2$ is replaced by an arbitrary constant multiplier k; hence the values obtained are of the form $k\beta_{ij}$ where the β_{ij}'s are computed numbers. Dividing by the measured values of L_{ij}/W_{ij} we obtain a set of values of $k\beta_{ij}W_{ij}/L_{ij}$, which we denote by $\bar{\sigma}_{ij}$. If k can be chosen so that $\bar{\sigma}_{ij}=\sigma_i$ for all rectangles and triangles, then this value of k can be taken as $(\omega/c)^2$, all conditions are satisfied, and the given plot is final. Actually this cannot be done except with the final plot; hence in general we choose the new set of σ_i's so that σ_i approximates all the $\bar{\sigma}_{ij}$'s in the ith tube. Since σ_i is of the form $k\gamma_i$ this is equivalent to choosing γ_i so as to approximate all the values of $\beta_{ij}W_{ij}/L_{ij}$ in the ith tube. This can be done by choosing an average value or, perhaps better, a weighted average with the areas as weighting factors. Dividing the computed values of $L_{ij}\sigma_i/W_{ij}$, namely $k\beta_{ij}$, by these new values of σ_i we obtain the values β_{ij}/γ_{ij}, which we use as a new set of L_{ij}/W_{ij} values in constructing the new plot.[4] We note that these are independent of k, which may be given any convenient numerical value.

The step-by-step process ends when a value of k can be chosen for which $\bar{\sigma}_{ij}=\sigma_i$ for all rectangles and triangles, this value being $(\omega/c)^2$, as stated above.[5] The most accurate value of ω/c is probably given by equating the total electric energy to the total magnetic energy obtained from the final plot, as described in Section 4.[3]

[4] Each computed value of $L_{ij}\sigma_i/W_{ij}$ is associated with the center of its rectangle or the center of gravity of its triangle, respectively. If the center of a new rectangle differs appreciably from that of the old, interpolation in this field of values may be necessary. The same is true of triangles.

3. ALTERNATIVE PROCEDURE USING A PLANIMETER

Let

s_j = distance from the kernel measured along a line of no work at the center of the jth strip, (14)

$\Phi=\sigma\phi$ = total electric flux outside of the line of force at s_j. Here ϕ is again the arbitrarily chosen "normal" flux per tube.

A_j = area of jth strip from the kernel to s_j;

then proceeding as with (3), noting Ampere's law, the magnetic flux density for any s_j is

$$\Phi\omega/c=\sigma\phi\omega/c. \tag{15}$$

The total magnetic flux in A_j is therefore

$$\frac{\omega\phi}{c}\int_0^{A_j}\sigma dA_j,$$

it being permissible to consider σ a function of A_j since both σ and A_j are functions of s_j. Continuing as with (6), noting Faraday's law, we multiply by ω/c to obtain the voltage

$$\phi\left(\frac{\omega}{c}\right)^2\int_0^{A_j}\sigma dA_j \tag{16}$$

across the strip at s_j. Choosing for s_j the value at the center of the ith tube, dividing by L_{ij} to obtain the electric intensity, and multiplying by W_{ij} we obtain the flux $\sigma_i\phi$ of the tube, thus

$$\sigma_i\phi=\phi\left(\frac{\omega}{c}\right)^2\frac{W_{ij}}{L_{ij}}\int_0^{\bar{A}_{ij}}\sigma dA_j,$$

where $\bar{A}_{ij}$ is the strip area to the center of the ith tube. Cancelling ϕ and transposing we ob-

[5] From the derivation of (7) and (13) or, later, of (17) and (18) it is evident that the above method of successive substitutions is equivalent to using the first approximate electric field to determine the corresponding magnetic field, corresponding to which, in turn, is obtained an electric field, which is taken as the second approximation —and so on. A method of successive substitutions may not be desirable in some cases, in which the new set of L_{ij}/W_{ij} values may be chosen arbitrarily after comparing the new values computed as above with those of the preceding plots.

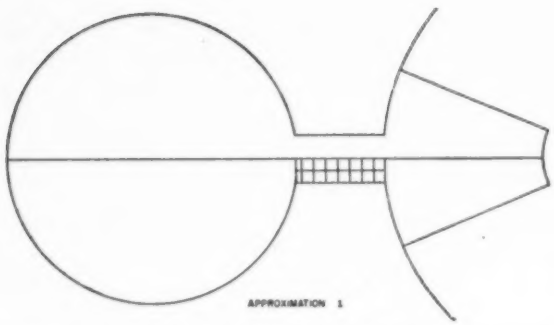

FIG. 4. Electric field in hole and slot type magnetron. Approximation 1.

tain finally

$$\frac{L_{ij}\sigma_i}{W_{ij}}=\left(\frac{\omega}{c}\right)^2\int_0^{\bar{A}ij}\sigma dA_j, \qquad (17)$$

which is the desired equilibrium condition for a *rectangle.*

We shall now derive a condition analogous to (17) which can be applied to the triangles at the kernel. Denoting by $\mathcal{E}_j$ the voltage, given by (16), across the strip at the base of the jth triangle, and noting from (9) that for any approximating function Kx^m for triangle width the field intensity varies linearly with x, we have for the total electric flux in the triangle

$$\sigma_n\phi=\frac{\mathcal{E}_j}{L_{nj}}\int_0^{W_{nj}}\frac{x}{W_{nj}}dx=\frac{\mathcal{E}_jW_{nj}}{2L_{nj}},$$

or, substituting from (16), cancelling ϕ, and transposing,

$$\frac{L_{nj}\sigma_n}{W_{nj}}=\frac{1}{2}\left(\frac{\omega}{c}\right)^2\int_0^{A_{nj}}\sigma dA_j, \qquad (18)$$

where the upper limit of the integral is the area of the triangle. This is the desired equilibrium condition for the *triangle.* In contrast to (17) we note the factor $\frac{1}{2}$ in (18), also the fact that L_{nj} and W_{nj} are the base and altitude of the triangle, respectively.

In applying (17) and (18) a convenient set of σ_i's for the various tubes is chosen, and A_j is obtained with a planimeter for values of s_j corresponding to lines of force on the plot. These values of A_j are then plotted against the corresponding known values of σ. This curve gives σ as a function of A_j; hence a planimeter or approximate integration can be used to give the integrals in (17) and (18). Such a curve is drawn for each strip.

The step-by-step process described at the end of Section 2 evidently applies here, (17) and (18) being used instead of (7) and (13). As before ω/c is not determined until the final plot has been made, after which ω/c is obtained by equating the total electric and magnetic energies as described in Section 4.

4. ELECTRIC AND MAGNETIC FIELD ENERGY. DETERMINATION OF ω/c

In any strip the electric flux passing through an elementary band bounded by two lines of force is $\phi d\sigma$. Dividing by ds_j we obtain the electric intensity. The total electric energy in the strip is therefore[6]

Electric energy in jth strip

$$=\frac{\phi^2}{8\pi}\int_0^{A_j}\left(\frac{d\sigma}{ds_j}\right)^2 dA_j. \qquad (19)$$

Noting (15) we also have

Magnetic energy in jth strip

$$=\frac{\phi^2}{8\pi}\left(\frac{\omega}{c}\right)^2\int_0^{A_j}\sigma^2 dA_j. \qquad (20)$$

Using the method of Section 3 a curve of σ as a function of s_j can be plotted, and $d\sigma/ds_j$ obtained by approximate differentiation; also a curve of σ as a function of A_j is already available.[7] The integrals in (19) and (20) can hence be obtained

---

[6] The expression for electric energy obtained by means of the magnetic field using (16) merely duplicates (20), as is shown by the following.

Electric energy in jth strip

$$=\frac{1}{2}\int_0^{\sigma}\left[\phi\left(\frac{\omega}{c}\right)^2\int_0^{A_j}\sigma dA_j\right]\frac{\phi d\sigma}{4\pi}$$

$$=-\frac{\phi^2}{8\pi}\left(\frac{\omega}{c}\right)^2\int_0^{A_j}\left[\int_0^{A_j}\sigma dA_j\right]\frac{d\sigma}{dA_j}dA_j.$$

Integrating by parts noting that $\sigma=0$ when A_j takes its greatest value, this becomes

Electric energy in jth strip

$$=-\frac{\phi^2}{8\pi}\left(\frac{\omega}{c}\right)^2\left\{\left[\sigma\int_0^{A_j}\sigma dA_j\right]_0^{A_j}-\int_0^{A_j}\sigma^2 dA_j\right\}$$

$$=\frac{\phi^2}{8\pi}\left(\frac{\omega}{c}\right)^2\int_0^{A_j}\sigma^2 dA_j,$$

which is (20).

[7] Tables for approximate differentiation are given in Crout, "An application of polynomial approximation to the solution of integral equations arising in physical problems," J. Math. and Phys. 19, 34 (1940).

using a planimeter or approximate integration. Adding the energies of the various strips the total electric energy and the total magnetic energy can be obtained, both being proportional to ϕ^2. Equating these, ϕ^2 cancels out, and we have

$$\frac{\omega}{c}=\left[\frac{\sum^{j}\int_0^{A_j}\left(\frac{d\sigma}{ds_j}\right)^2 dA_j}{\sum^{j}\int_0^{A_j}\sigma^2 dA_j}\right]^{\frac{1}{2}}, \tag{21}$$

the upper limits on the integrals being the strip areas, and the summations being over the strips. This method of determining ω/c reminds one of Raleigh's method in elastic vibration problems, and offers probably the most accurate way of using the flux plot to obtain the resonance frequency.

We shall finally obtain expressions for the electric and magnetic energies which are applicable if the individual rectangles and triangles are considered separately, as in Section 2. The electric energy in a rectangle is evidently

Electric energy in rectangle

$$=\frac{1}{2}\left(\frac{\sigma_i\phi}{4\pi}\right)\left(\frac{\sigma_i\phi L_{ij}}{W_{ij}}\right)=\frac{\sigma_i^2\phi^2 L_{ij}}{8\pi W_{ij}}; \tag{22}$$

also, noting (3), the magnetic energy of a rectangle is seen to be

Magnetic energy in rectangle

$$=\frac{\phi^2}{8\pi}\left(\frac{\omega}{c}\right)^2\left(\tfrac{1}{2}\sigma_i+\sum_{k=1}^{i-1}\sigma_k\right)^2 L_{ij}W_{ij}. \tag{23}$$

From (9) it follows that in a triangle the electric intensity is of the form K_1x where K_1 is a constant. K_1 can be determined by the relation

$$\sigma_n\phi=\int_0^{W_{nj}} K_1 x\,dx=\frac{K_1 W_{nj}^2}{2},$$

whence the electric intensity becomes

$$E_{nj}=\frac{2\sigma_n\phi x}{W_{nj}^2}.$$

The electric energy in the triangle is therefore, noting (8),

Electric energy in triangle

$$=\frac{1}{8\pi}\int_0^{W_{nj}}\left[\frac{2\sigma_n\phi x}{W_{nj}^2}\right]^2 Kx^m dx$$
$$=(\sigma_n\phi)^2 K W_{nj}^{m-1}/2\pi(m+3), \tag{24}$$

Electric energy in triangle

$$=(\sigma_n\phi)^2 L_{nj}/2\pi(m+3)W_{nj},$$

where L_{nj} and W_{nj} are the base and altitude of the triangle, respectively, and K and m are the values applicable to the jth triangle.

In the triangle the magnetic field is closely equal to the constant value (11); hence the magnetic energy is closely

Magnetic energy in triangle

$$=\frac{\phi^2}{8\pi}\left(\frac{\omega}{c}\right)^2\left(\alpha_j\sigma_n+\sum_{k=1}^{n-1}\sigma_k\right)^2\int_0^{W_{nj}} Kx^m dx \tag{25}$$

Magnetic energy in triangle

$$=\frac{\phi^2}{8\pi}\left(\frac{\omega}{c}\right)^2\left(\alpha_j\sigma_n+\sum_{k=1}^{n-1}\sigma_k\right)^2\frac{L_{nj}W_{nj}}{(m+1)}.$$

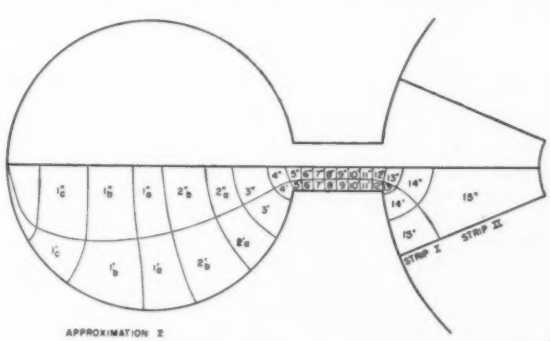

FIG. 5. Electric field in hole and slot type magnetron. Approximation 2.

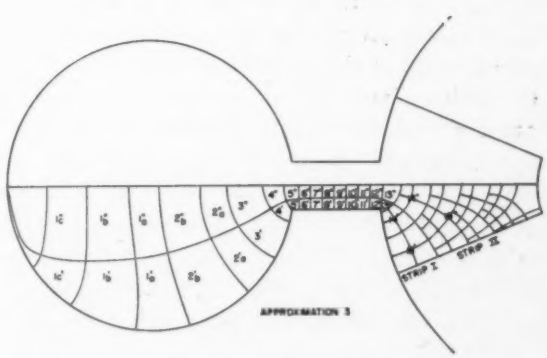

FIG. 6. Electric field in hole and slot type magnetron. Approximation 3.

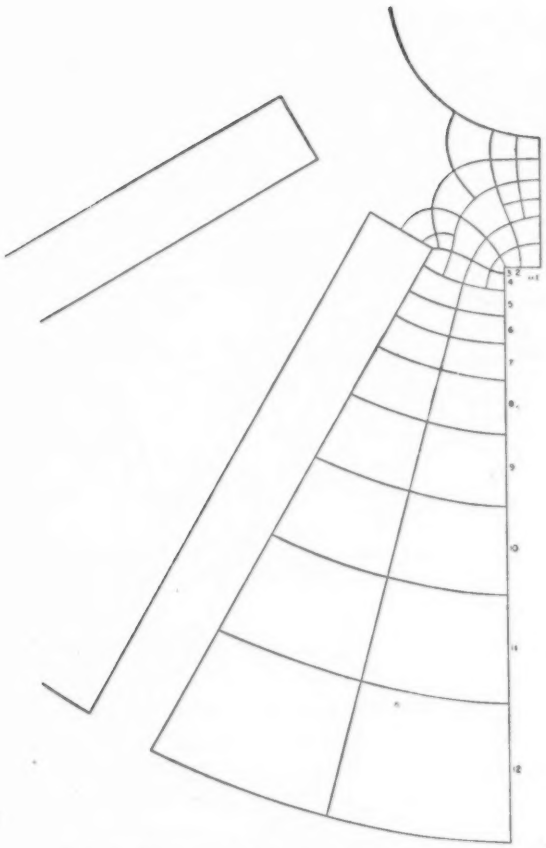

FIG. 7. Electric field in vane type magnetron.

5. APPLICATION TO A SPECIFIC PROBLEM. HOLE AND SLOT TYPE MAGNETRON

The procedure used to obtain the field in the cavity shown in Fig. 2 will now be outlined.[8] The approximation that was used for the electric field in order to get the step-by-step process started was a uniform electric field in the gap between two adjacent anode segments, the electric field being taken as zero everywhere else, Fig. 4. Data from this first approximation are now inserted in the right-hand sides of (17) and (18) as described in Section 3 to obtain corrected data for the plot which constitutes the second approximation. In so doing we note that σ is zero in the anode-cathode region, and increases linearly through the gap to a value which remains constant in the well. It follows that $\int_0^{\bar{A}_{ij}} \sigma dA_j$ and hence the computed values of $L_{ij}\sigma_i/W_{ij}$ are constant in the anode-cathode region, and that in the well $L_{ij}\sigma_i/W_{ij}$ and $L_{nj}\sigma_n/W_{nj}$ are proportional, respectively, to $\bar{A}_{ij}$ and $A_{nj}/2$. The flux plot which constitutes the second approximation was begun at the inner (cathode) side of the gap, the work being carried both inward and outward from this point. We note that in the anode-cathode region this plot can be a lattice of curvilinear squares, which gives a field satisfying Laplace's equation since $L_{ij}\sigma_i/W_{ij}$ is constant in this region; also we note that the choice of the σ_i's is a matter of convenience. The second approximation is shown in Fig. 5.[9]

Continuing the step-by-step process, data from this second approximation are now inserted in (17) and (18) to obtain data for a third approximation. In so doing each new value of σ_i is taken as the average of the $\bar{\sigma}_{ij}$'s of the elementary areas in the ith tube. After the third approximation, Fig. 6, was obtained, it was found that the ratio of σ_i to $W_{ij}\beta_{ij}/L_{ij}$ was constant for all the elementary areas to within the accuracy expected of the graphical process. This third approximation, Fig. 6, was therefore taken as the final result, the constant ratio being $(\omega/c)^2$. The frequency corresponding to the value so obtained for ω/c is $2.818 \cdot 10^9$ c.p.s.; that obtained by equating electric and magnetic energies using (21) was $2.825 \cdot 10^9$ c.p.s. The various tube dimensions were

Cathode radius	0.1182″
Anode radius	0.3175″
Gap width	0.066″
Radius to center of well	0.640″
Well diameter	0.398″.

The values of the σ_i's for the final plot, Fig. 6, are shown in Table I.

6. APPLICATION TO A SPECIFIC PROBLEM. VANE TYPE MAGNETRON

If the shape of the electric field is known approximately, the work required to obtain a plot can be greatly reduced.[10] For example in the

[8] The work outlined in this section including that involved in constructing the flux plots shown in Figs. 5 and 6 was done by Mr. F. S. Holt.

[9] The labels shown in Figs. 5 and 6 are those that were used in making the plot. The strips are indicated by primes, the tubes are numbered, and subdivisions are indicated by letters or, if obvious, are not indicated. This notation differs from that used in the derivation of (7), (13), (17), and (18); but is convenient for actual construction.

[10] The work outlined in this section including that involved in constructing the flux plot Fig. 7 was done by Mr. F. E. Bothwell.

TABLE I. Values of σ_i.

Tube	σ_i	Tube	σ_i	Tube	σ_i
Triangle	.0625	4	.999	11	.999
1c	.125	5	.999	12	1.00
1b	.250	6	.999	13	1.00
1a	.250	7	.985	14	1.00
2b	.499	8	.989	15	.836
2a	.499	9	.994		
3	.997	10	.997		

vane type magnetron, Fig. 7, the electric lines of force in most of the region between the vanes evidently approximate arcs of circles centered at the cathode; also in the anode cathode region, where the magnetic field is weak, the electric field approximates a solution of Laplace's equation. With these facts in mind Fig. 7 was drawn for the case where the cathode and all vanes but one are at the same voltage, no attempt being made to satisfy (7). Omitting the line of no work let us temporarily consider the field as occupying a single strip; then Eqs. (7) form a set of twelve homogeneous, linear, algebraic equations for the σ_i's. These can be conveniently solved by successive substitutions by first placing all σ_i's on the right-hand side of (7) equal to unity. The σ_i's so obtained are inserted in the right-hand sides of (7) to give the next approximation, and so on. In each step the k which replaces $(\omega/c)^2$ was given that value which would make the average of the computed σ_i's equal to unity. This method of successive substitutions has the physical significance described in footnote 5; its convergence was rapid, and the results obtained are shown in Table II. When put equal to $(\omega/c)^2$ the last obtained value of k corresponds

TABLE II.

	Values of σ_i				
i \ step	1	2	3	4	5
1	1.00000	.97989	.97990	.97998	.97999
2	1.00000	.97444	.97484	.97489	.97491
3	1.00000	.96696	.96786	.96792	.96793
4	1.00000	.96162	.96293	.96302	.96300
5	1.00000	1.14617	1.14824	1.14833	1.14835
6	1.00000	1.00887	1.01120	1.01130	1.01127
7	1.00000	1.06811	1.07140	1.07148	1.07150
8	1.00000	1.24744	1.25118	1.25127	1.25128
9	1.00000	1.32741	1.33002	1.33001	1.33002
10	1.00000	1.14551	1.14404	1.14388	1.14386
11	1.00000	.83281	.82418	.82390	.82388
12	1.00000	.34074	.33420	.33401	.33400

Table of values of k

step	1	2	3	4	5
k		6.0374	5.7562	5.7517	5.7516

to a wave-length of 2.6200 cm. The (probably) more exact value obtained by equating total electric and magnetic energies as described in Section 4 is 2.6456 cm.

Let us finally try to improve the accuracy of the plot by subdividing and proceeding as in Section 5. We therefore draw the line of no work that was omitted above; and, placing the σ_i's of Step 5 in the right-hand side of (7), determine a new set of values L_{ij}/W_{ij}. These new values, however, duplicate the old values in all tubes except the first four, in which there is a discrepancy of one percent. Since L_{ij} and W_{ij} cannot be measured to within one percent, no alteration of the plot is indicated, and it is therefore taken as final. It is probable that the procedure used in this section on the vane type magnetron can be used to advantage on the hole and slot type magnetron considered in Section 5.

A Magnetron Oscillator for Dielectric Heating

R. B. NELSON
Research Laboratory, General Electric Company, Schenectady, New York
(Received January 31, 1947)

Magnetron oscillators can provide very high frequency power for dielectric heating. Factors determining the choice of frequency for particular jobs are discussed. The design of a magnetron having 5 kw continuous output at 1050 megacycles is described, and performance data on the tube are given.

INTRODUCTION

THE method of heating non-conducting materials by dielectric loss in a high frequency electric field is becoming an important industrial process. Many of the materials heated by this method, such as plastics, are of such low loss that it is hard to heat them as rapidly as desired. The rate of heating increases with the electric field strength and, in practically all materials, with the frequency. Since the usable field is definitely limited by arcing between the electrodes, the only remaining way to speed up the heating process is to increase the frequency.

Commercial dielectric heaters have been restricted to frequencies below about 40 megacycles by the limitations of available vacuum tubes. However, the recent development of magnetron oscillators has made available considerable power at frequencies up to some 10,000 megacycles. Using magnetrons for heating thus allows the choice of almost any desired frequency.

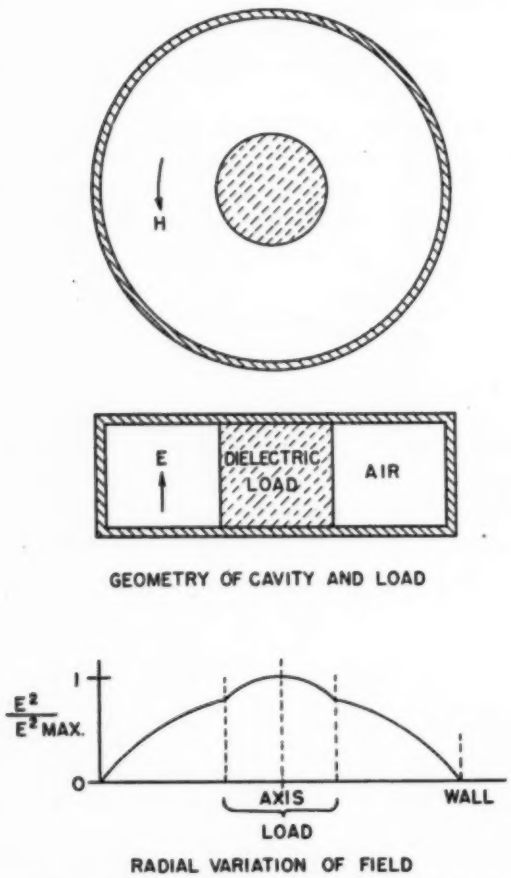

FIG. 1. Distribution of heating in cylindrical load. In a simple cylindrical cavity where the electric field is produced by radial currents in the walls, the r.m.s. field is a maximum at the center and decreases radially as a Bessel function. The rate of decrease depends upon the wave-length in the dielectric, giving the discontinuity in slope of the curve of E^2 plotted against radial distance. Rate of production of heat per unit volume is proportional to E^2.

CHOICE OF FREQUENCY

It must not be assumed that the highest frequencies are always best. While heating rates go up with frequency, a point is reached where non-uniformity of heating limits the usable frequency. Two effects contribute to non-uniformity. First, in the case of high loss materials such as most foods, there is the decreased heating toward the center of large objects because the power is absorbed by the surface layers before it can penetrate. Second, in the case of low loss materials such as plastics, the wave-length of the heating power limits the volume of material that may be heated uniformly. To apply power efficiently to low loss material, it is necessary to surround the material with reflecting walls so that the electromagnetic wave passing through it is not radiated and lost after one passage. The reflecting walls set up a standing wave in and around the load material. This wave has in general a three-dimensional space variation of electric field, with periodic maxima and minima.

Since the dielectric heating at any point is proportional to the square of the electric field strength, widely varying temperatures will be produced in the material if its dimensions are comparable with a wave-length. As an example of how the standing-wave pattern limits the usable frequency, consider a cylinder of load material located axially in a cylindrical resonant cavity, as shown in Fig. 1. Exciting the cavity in its lowest mode with axial electric field, the field is a maximum at the center and falls off radially as

$$E = E_{\max} J_0(6.28r/\lambda),$$

where E is the electric field strength at radius r from the axis, $E_{\max}$ is the field on the axis, and λ is the wave-length in the material. If it is required to heat the edges of the load 90 percent as much as the center,

$$E^2/E_{\max}^2 = J_0^2(6.28r/\lambda) \geqq .90 \text{ at the edges,}$$

and solving the above equation for a load of radius a

$$a \leqq .0725\lambda.$$

If, for example, the load is a piece of phenolic plastic with dielectric constant 4.0 and radius 1.0 cm,

$$\lambda = \lambda_0/4.0^{\frac{1}{2}},$$

where λ_0 is the free space wave-length corresponding to the frequency used. Solving for λ_0

$$\lambda_0 \geqq 27.6 \text{ cm.}$$

Thus, the maximum frequency allowed in this case would be 1087 megacycles.

OSCILLATOR DESIGN CONSIDERATIONS

On the basis of considerations such as the above example, it appeared that many dielectric heating processes could be done well at a frequency of about 1000 mc. Therefore, a magnetron oscillator was developed in the General Electric Research Laboratory to give 5 kw output at 1050 mc. In designing this oscillator, consideration had to be given to several special requirements of heating apparatus which differ from other uses of magnetrons.

The most important specific requirement is that the heating oscillator must be capable of operating into any load impedance, including the completely unloaded condition. This is caused by the non-uniformity of successive charges of load material, to the certainty of bad adjustment of matching transformers by unskilled operators, and the possibility of accidentally running the oscillator with no load at all. To meet these conditions, the anode should be capable of dissipating the entire input power to the tube. The output seal and transmission line to the load must stand very high voltages and currents associated with high standing wave ratios. The cathode should not be damaged by the excessive power it receives from back-bombardment by electrons, which is a function of the load impedance as well as the plate voltage and current.

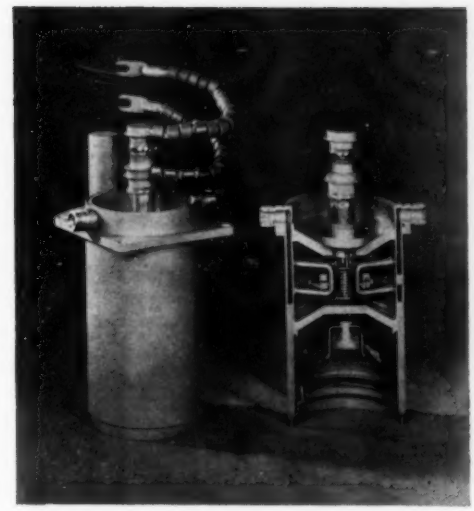

FIG. 2. Photograph of the 5-kw magnetron, showing the external appearance and also an axial section.

Although the multiple-cavity magnetron has many resonant modes, efficient oscillation occurs only in the "π" mode where each anode is 180° out of phase with those adjoining it. When this mode is overloaded, as may occur by poor load matching, the oscillator will tend to jump to another mode, which is usually completely unloaded, and may continue in the spurious mode, even if the mismatch is corrected, until it is turned off and restarted. The accepted cure for mode jumping is to strap the anodes together in two alternate sets with low impedance conductors. This raises the frequency of all modes except the "π" mode to a point where the oscillator does not readily excite them. The

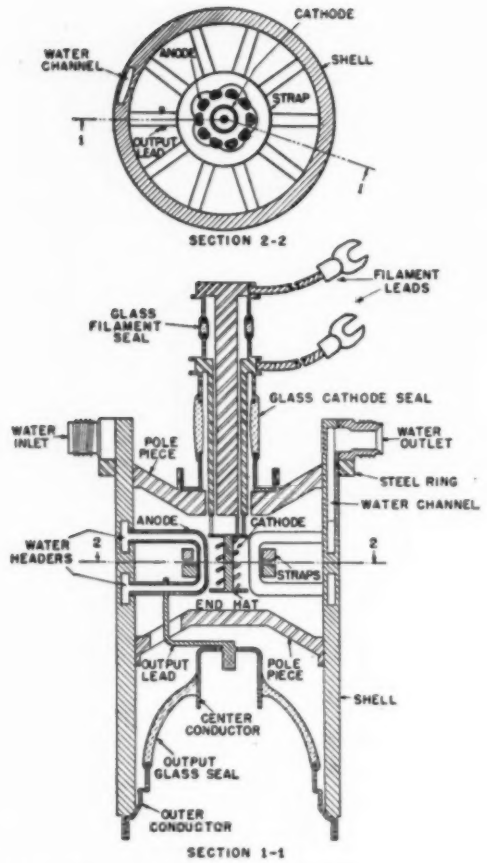

FIG. 3. Construction of water cooled magnetron. Sectional views showing the tubular anodes and water circulating channels. The O.D. of the copper shell is 3½".

heating magnetron, as distinguished from the radar transmitter, runs continuously, so once it has jumped modes it does not have a chance to restart properly. Also the wide range of load impedances favors mode jumps. These factors necessitate very tight strapping. It is desirable that the next higher frequency mode be at least twice the frequency of the operating mode. In the oscillator to be described, this separation was attained by a new method of strapping.

A 5-KW, 1050-MC MAGNETRON

The magnetron is shown in the photograph, Fig. 2, and constructional details in Fig. 3. It has 10 anodes, and so may be run at relatively low voltage and magnetic field. Rated operating conditions for the full 5 kw output are: plate voltage 5.0 kv, plate current 1.5 amp., magnetic field 1500 gauss. Water cooling was adopted for the anodes, and this allowed making the anodes of U-shaped pieces of copper tubing through which the water flows. Channels in the copper tube shell form headers for water distribution.

In addition to providing excellent cooling, the tubular anodes have a minimum of inter-anode capacity, thus allowing a large fraction of the capacitance of the resonant circuits to be provided by low impedance straps. The resulting tight strapping gives a frequency ratio of 1:2 between the operating mode and the next higher mode. The double ring straps are looped inside the anode U's. This allows the straps to be attached near the centers of the anode faces, eliminating unbalanced r-f voltages on the anodes. Also, the anodes shield the cathode and the rest of the tube from the fundamentally unbalanced double ring straps. The ten resonant circuits formed by the anode loops extending radially inward from the tube shell are electrically similar to conventional vane resonators.

The over-all size of the magnetron is determined by the output seal, which must be large to

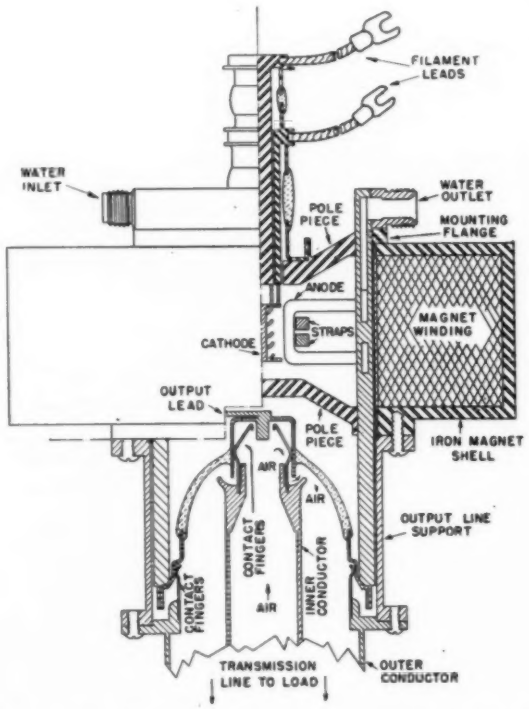

FIG. 4. Magnetron mounting and connections. The tube is slid downward into the cylindrical magnet, simultaneously plugging in to the coaxial output transmission line which is rigidly mounted on the magnet. The iron magnetic circuit is shown in heavy cross-hatching.

handle the power. In this cylindrical structure the seal occupies the entire diameter of the tube shell. The coaxial arrangement of the seal with the cathode and magnetic pole pieces allows the tube to be plugged into its magnet and output transmission line simultaneously. Figure 4 shows the method of mounting the tube. An electromagnet is used, consisting of a solenoidal coil with an iron shell whose ends line up with the iron pole pieces inside the tube. Air is blown through the center conductor of the output line to cool the seal, the inverted cup shape of the seal giving a good distribution of the cooling air as well as protecting the seal from breakage.

The power output is obtained by attaching a flat strap from the center conductor of the seal to one of the anodes. The exact point of attachment is selected to provide proper loading of the oscillator when the 52.5-ohm transmission line on the output has no standing wave.

The cathode is a simple spiral of pure tungsten wire with molybdenum end hats. It requires 600 watts heating power. In a magnetron having considerable electron bombardment of the cathode, it is desirable to use a very inefficient high wattage cathode, so that the back heating becomes a small fraction of the total heating power.

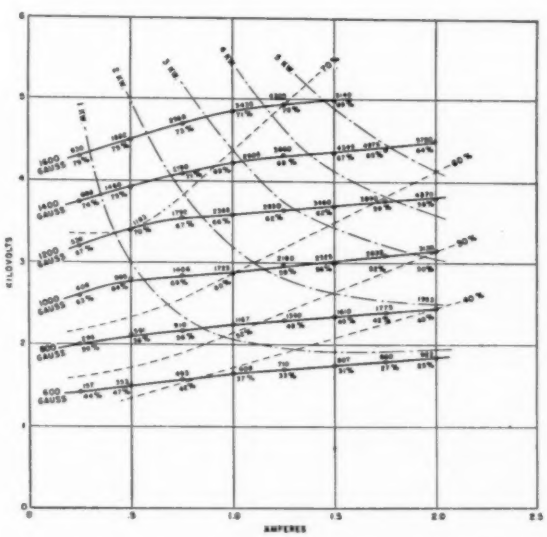

FIG. 5. Performance chart. Solid lines are contours of constant magnetic field, dashed lines are constant power, and dotted lines constant efficiency. Power, in watts, and efficiency measured are indicated on the experimental points. This chart is taken with a load matched to the transmission line.

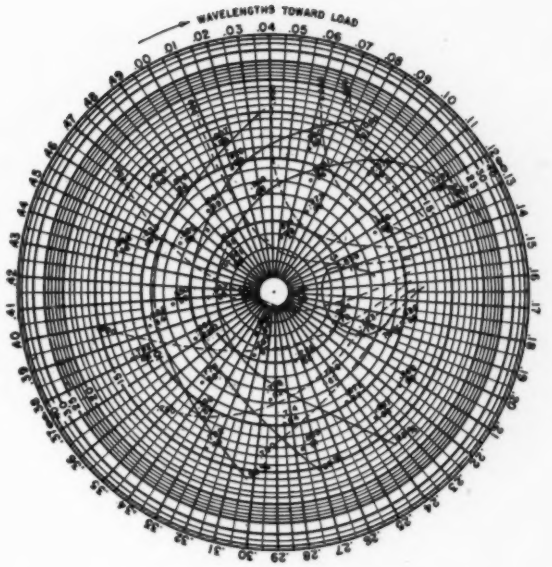

FIG. 6. Rieke diagram. The effect of load impedance on the efficiency and wave-length of the oscillator is best shown by this chart. The data were taken at fixed conditions of 1.0 amp. plate current and 1200 gauss magnetic field. Upper figures are wave-length (add 29.000 cm) and lower figures percentage efficiency. Constant efficiency and constant wave-length contours are shown by solid and dotted lines, respectively. The radial coordinate is voltage reflection coefficient, with the scale marked in standing wave ratio in decibels. The azimuthal coordinate is the phase angle of the reflection coefficient, with the scale marked in wave-lengths displacement of the standing wave minimum from an arbitrary zero.

MAGNETRON OPERATING CHARACTERISTICS

The performance of the magnetron as an oscillator is graphically presented by several charts. Shown in Fig. 5 is the "performance chart" in which power output (upper numbers) and efficiency (lower numbers) are plotted against plate voltage and current. Lines of constant magnetic field are also shown.

Another important oscillator characteristic is shown in Fig. 6, the "Rieke diagram," in which efficiency and wave-length are plotted as a function of load impedance for constant current and magnetic field. The radial coordinate is standing wave ratio in the output line (in voltage) plotted on a scale proportional to reflection coefficient. The angular coordinate is the phase angle of the standing wave minimum. Thus the position of a point on the chart represents a complex load impedance, which might be transformed into resistance and reactance components by superposition of a Smith chart.

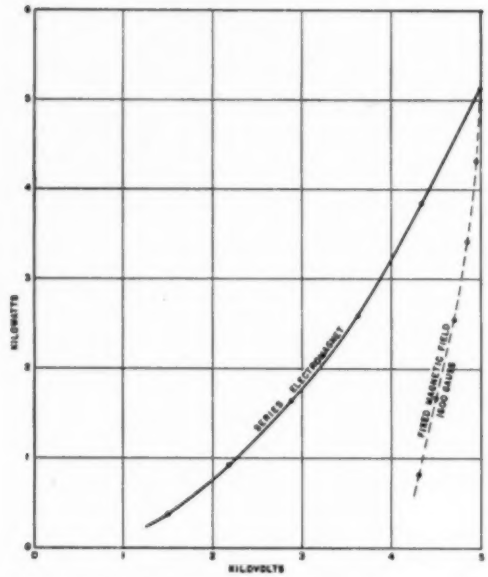

FIG. 7. Effect of plate voltage on output power. With a constant magnetic field as obtained from a permanent magnet, power output varies rapidly with plate voltage, following the dotted curve. An electromagnet excited by the magnetron plate current reduces this variation.

It is apparent from Fig. 5 that the plate current changes very rapidly with plate voltage at constant magnetic field. That is, the variational resistance for plate modulation is around 250 ohms. This is a good situation if one desires to use amplitude modulation, as the modulating power is low. However, in dielectric heating, a constant r-f output is desired, and account must be taken of variations in line voltage. It is obvious from the curves that a small variation in line voltage and hence in plate voltage will produce a large change in plate current and in output power. Figure 7 shows this relation, neglecting the regulation of the plate supply rectifier.

A method of greatly reducing the effect of line voltage fluctuations and, incidentally, plate supply ripple, is to run the tube's electromagnet in series with the low voltage end of the plate supply. This gives a magnetic field directly proportional to the plate current. Since the plate voltage is almost directly proportional to the magnetic field, the plate current will in turn be proportional to plate voltage. The resultant ohmic plate resistance characteristic produces the variation of r-f power with plate supply voltage shown by the solid curve in Fig. 7.

The relationship between d.c. plate current, plate voltage, and magnetic field also affects the way in which the magnetron output depends on the load impedance. The data plotted in Fig. 6 were taken under the easily reproducible conditions of constant current and magnetic field, letting the voltage find its own value. The voltage varies much less at constant current than the current would at constant voltage.

In practical operation we do not have either a constant current or constant voltage power supply, and the regulation characteristics of the supply affect the relationship of magnetron power output and load impedance. It is obvious that this is a very important relationship for heating applications.

With the magnetic field supplied by a series electromagnet, some of the effects of power supply regulation are simulated, and r-f power output tends to be stabilized. For a constant voltage power supply and series magnet, the variation of output power with load for a pure resistive load is plotted in Fig. 8. For comparison, there is also shown the relations obtained with constant voltage power supply, and with constant current.

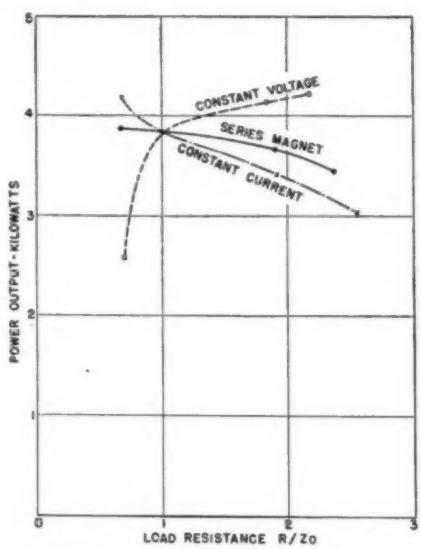

FIG. 8. Effect on output power of varying pure resistance loads. For loads which present a pure resistive impedance to the magnetron, the power delivered is plotted as a function of the ratio of load resistance R to the characteristic impedance Z_0 of the transmission line. At constant magnetic field, the power increases with load resistance if the magnetron plate voltage is held constant, but decreases if the current is constant. Using a series electromagnet with constant voltage supply, the better characteristic shown by the solid line is obtained.

It has been found that if plate voltage is applied to the magnetron with no magnetic field but with the magnet in series, the tube will start in a very high frequency mode of oscillation, drawing plate current so that the voltage never rises enough to start the desired mode of circuit oscillation. To prevent this, it is necessary to have a field of at least 600 gauss present before plate voltage is applied. A rectifier across the magnet as shown in Fig. 9 supplies this starting current, and normally stops supplying current when the magnetron current builds up a voltage drop across the magnet coil greater than the output voltage of the rectifier.

The magnet supply rectifier can be made to do another useful job as a fine control for plate current and output power. In the plate supply rectifier, continuous voltage control is expensive, but a few taps for step control are cheap. Now at any given plate voltage, the magnetron is approximately a constant-magnetic-field device, independent of plate current. If the plate current supplies part of the magnetic field and the rest comes from the magnet rectifier, any increase in rectifier current will tend to increase the magnetic field and thus will cause a corresponding decrease in magnetron current. In this way continuous adjustment of output power is obtained by regulating the 100-watt magnet rectifier. Figure 9 shows the Variac connection used for control.

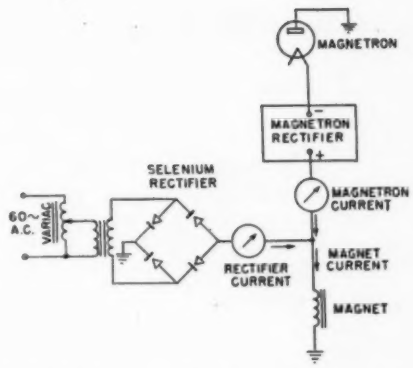

FIG. 9. Current supply for electromagnet. An auxiliary d.c. supply for the magnet is necessary to assure proper starting. This variable-voltage rectifier may be used to control the magnetron power output.

R-F LOADING EQUIPMENT

The problem of carrying the 1050 mc power from the magnetron and coupling it into a load is one which has almost as many answers as there are varieties of material to be heated. The power is taken from the oscillator on a stub-supported coaxial line, the start of which is shown in Fig. 4. A line size of $3\frac{1}{8}''$ O.D. with $1\frac{1}{4}''$ center conductor has been adopted as adequate for this power level and frequency. For most loads, a large step-up in impedance is necessary to match the line to the load. This usually takes the form of a resonant cavity tuned to the operating frequency and coupled to the transmission line by a loop or antenna.

ACKNOWLEDGMENTS

The author wishes to thank Dr. A. W. Hull for his continued interest and advice in carrying out this development. Mr. T. C. Swartz, Miss H. C. Hertha, and Mr. P. J. Scavullo have contributed largely to its progress.

REFERENCES

So much of the literature on modern magnetron developments is unpublished that no attempt has been made at references to original sources. For a general discussion of magnetron principles and a pre-war bibliography, refer to J. B. Fisk, H. D. Hagstrum, and P. L. Hartman, "The magnetron as a generator of centimeter waves," Bell Sys. Tech. J. **25**, 167 (April 1946).

An Approximate Solution of the Differential Equation of the Ultracentrifuge

W. J. Archibald
Dalhousie University, Halifax, Nova Scotia
(Received November 13, 1946)

In determining molecular weights with the ultracentrifuge by the equilibrium method, it is necessary to drive the rotor at relatively high speeds for very long periods of time. It would be a real advantage to be able to deduce molecular weights from the distribution of concentration within a cell placed in a rotor without waiting for equilibrium. The solution of a certain differential equation gives the theoretical distribution within the cell at any time, and a comparison of the experimentally determined concentrations with those deduced from theory should yield molecular weights without waiting for equilibrium. The exact solution of this differential equation is known, but it is not suitable for numerical work. The present paper presents an approximate solution from which numerical results can be obtained with ease.

ONE of the most important methods of measuring high molecular weights is by the use of the ultracentrifuge as developed by Svedberg and Beams. A dilute solution of the substance whose molecular weight is to be determined is placed in a small cell, with radial sides and cylindrical ends, near the periphery of the rotor, and under the influence of the centrifugal force the distribution of concentration changes from an initial uniform distribution to an exponential one. When this final equilibrium state has been reached the concentration "c," at any point in the cell, is given by the expression

$$c = c_0 \exp\left[\frac{M(1-V\rho)\omega^2(r^2-r_0^2)}{2RT}\right], \qquad (1)$$

where "M" is the molecular weight of the dissolved substance, "V" its partial specific volume, ρ the density of the solvent, ω the angular velocity of rotation, and "r" the distance of any point in the cell from the axis of rotation. "C_0" is the concentration at the point "r_0." "R" is the gas constant per mole and "T" the absolute temperature. The equilibrium state is reached when the tendency for solute particles to settle to the outer part of the cell because of the centrifugal force is exactly equal to the tendency for them to diffuse inwards because of the concentration gradient. It is obvious that Eq. (1) gives "M" in terms of quantities that can be measured, although the experiment is one that can only be performed successfully with faultless optical and mechanical equipment.

The time required for the attainment of the equilibrium state is often very long—sometimes the centrifuge must run for many days, or even weeks, at constant speed and at a constant temperature. If the time of a run could be shortened this method of molecular weight determination would be much more useful. The experimental difficulties would be greatly reduced and the number of runs made with any centrifuge would be increased. This latter consideration is an important one in view of the many substances that could be studied by this method. If the distribution of concentration within the cell at any time after the start of an experiment could be deduced theoretically, a comparison of the measured and computed distribution might enable "M" to be found without waiting for equilibrium. The function $c(r, t)$, which gives the concentration at any point at any time, would be required for this purpose and this is obtained by solving the following differential equation:

$$\frac{1}{r}\frac{\partial}{\partial r}\left\{\left(D\frac{\partial c}{\partial r}-\omega^2 rsc\right)r\right\}=\frac{\partial c}{\partial t}. \qquad (2)$$

In (2), "D" is the diffusion constant of the solute and "s" the sedimentation constant, i.e., the velocity of settling of the dissolved substance in unit gravitational field. The quantities "D" and "s" are related to each other. It is possible to show that

$$D/s = RT/M(1-V\rho). \qquad (3)$$

A proof of this relation is given in a previous paper by the author.[1] The differential Eq. (2) was

[1] W. J. Archibald, Phys. Rev. **53**, 746 (1938).

first derived by Lamm.[2] A simple derivation is to be found in reference 1.

A treatment of Eq. (2) which is free of any mathematical approximations has been given and is to be found in two places in the literature.[3,4] While the solution given is exact and can be employed for purposes of computation, yet the cost in time of getting numerical results is so great that little use has been found for it. The expression obtained for $c(r, t)$ is simple in form and would be most serviceable if the mathematical functions which it contains could be looked up in tables. However such tables are not available and the task of compiling them would be a major project in applied mathematics. It is the purpose of this paper to derive another expression for $c(r, t)$ which, while not exact, is felt to be good enough for many purposes, and which contains functions that are tabulated.

In dealing with Eq. (2) it is more convenient to use "z" and "τ" rather than "r" and "t" as the independent variables, where

$$z=\frac{\omega^2 s}{2D}r^2=\frac{M(1-V\rho)\omega^2}{2RT}r^2 \quad \text{and} \quad \tau=2\omega^2 st. \tag{4}$$

As $r_1 \leq r \leq r_2$ where r_1 and r_2 are the inner and outer limits of the cell, respectively, then $a \leq z \leq b$ where

$$\begin{Bmatrix} a \\ b \end{Bmatrix}=\frac{M(1-V\rho)\omega^2}{2RT}\begin{Bmatrix} r_1^2 \\ r_2^2 \end{Bmatrix}.$$

In terms of these variables we find

$$\frac{c(z,\tau)}{c_0}=\frac{b-a}{e^b-e^a}e^z+\sum_{n=1}^{\infty}\frac{\int_a^b e^{-z}M(\alpha_n, 1, z)dz}{\int_a^b e^{-z}\{M(\alpha_n, 1, z)\}^2 dz} \times M(\alpha_n, 1, z)e^{(\alpha_n-1)\tau}, \tag{5}$$

where $M(\alpha, \gamma, z)$ is a solution of the differential equation

$$\frac{d^2M}{dz^2}+\left(\frac{\gamma}{z}-1\right)\frac{dM}{dz}-\frac{\alpha}{z}M=0 \tag{6}$$

and the α_n's are the "eigenvalues" of the parameter α. The α_n's are those particular values of α which give the functions $M(\alpha_n, 1, z)$ the property that

$$\frac{d}{dz}M(\alpha_n, 1, z)=M(\alpha_n, 1, z) \tag{7}$$

for $z=a$ and $z=b$. "c_0" is the initial uniform concentration. (The reader is asked to consult reference 3 or 4 for a detailed proof of (5) and a full explanation of the results stated here.) $M(\alpha_n, 1, z)$ is an abbreviation for

$$F(\alpha_n, 1, z)-\frac{F(\alpha_n, 2, a)}{W(\alpha_n, 2, a)}W(\alpha_n, 1, z), \tag{8}$$

where $F(\alpha_n, \gamma, z)$ and $W(\alpha_n, \gamma, z)$ are the two independent solutions of (6) which are to be found written out in full.[3,4] It is the difficulty of obtaining numerical values for the F and W functions which limits the usefulness of Eq. (5).

It will be our purpose to see if it is possible to derive some expression for the functions $M(\alpha_n, 1, z)$, other than that given in (8), and which contains only well-known functions. This alternative expression will of necessity be an approximation and a careful study of the magnitude of the different quantities involved will be required to make the approximation a good one. A further purpose will be to discover a simple method for determining the eigenvalues α_n.

In (5) the first term, in e^z, gives c/c_0 for the equilibrium state. In an actual experiment it is not desirable to have the final concentration vary too widely throughout the cell. If one were to accept as a reasonable set of conditions that finally the concentration at r_2 be three times that at r_1 then

$$e^b/e^a \simeq 3, \quad \text{or} \quad (b-a)\simeq 1.1.$$

This serves to show the narrow limits within which the variable "z" is confined. Furthermore, since

$$b/a=r_1^2/r_2^2,$$

we have

$$a=(b-a)\frac{r_1^2}{r_2^2-r_1^2}\simeq 1.1\frac{r_1^2}{r_2^2-r_1^2}.$$

The cells used are usually small and one might

[2] Lamm, Ark. Mat. Astron. Fysik. **21B**, No. 2 (1929).
[3] W. J. Archibald, Phys. Rev. **54**, 371 (1938).
[4] W. J. Archibald, Ann. N. Y. Acad. Sc. **43**, 211 (1942).

choose as typical values the following: $r_2=5.0$ cm and $r_1=4.5$ cm. This gives $a\simeq 4.7$. As a result of these considerations we are entitled to treat the variable "z" as being moderately large (of the order of 5.0) and as being confined within a short range of values. The results of a computation on a typical experiment[3,4] show that $5.0\leqq z\leqq 6.2$ and these figures are probably typical of most cases in which the equilibrium method is used.

A further point of interest has to do with the quantities α_n. The exact theory gives $\alpha=1$ as one of the eigenvalues. This α, of course, gives rise to the first term in (5). All the other α's have large negative values. In the computations referred to above it was found that $\alpha_1=-38.7$. α_2 was not determined, but the indications were that it was less than -100.

The first term in (5) presents no difficulty: but the terms in the summation part of the expression are bothersome. Thus we will confine our attention to these terms. This means that we must study Eq. (6) (with $\gamma=1$), remembering that α is very large and negative and that "z" is moderately large and of restricted variation. In (6) let

$$M=e^{z/2}z^{-\frac{1}{2}}V. \tag{9}$$

The equation for "V" then becomes

$$\frac{d^2V}{dz^2}+\left\{-\frac{1}{4}+\frac{1}{4z^2}-\frac{(\alpha-\frac{1}{2})}{z}\right\}V=0. \tag{10}$$

The considerations given above suggest that it is permissible to drop the term $1/4z^2$. This term is very small in comparison with $-(\alpha-\frac{1}{2})/z$ and is even quite small in comparison with $\frac{1}{4}$. Then (10) becomes

$$\frac{d^2V}{dz^2}+\left\{-\frac{1}{4}-\frac{(\alpha-\frac{1}{2})}{z}\right\}V=0.$$

This is still an inconvenient equation to deal with but it can be further simplified by replacing the term in braces by

$$\left\{-\frac{1}{4}\frac{(a+b)}{2}-(\alpha-\tfrac{1}{2})\right\}\frac{1}{z}=\frac{\sigma^2}{z}. \tag{11}$$

This term is a very close approximation to $-\frac{1}{4}-(\alpha-\frac{1}{2})/z$ when $z\simeq 5$, α is large and $b-a$ is of the order of unity. As an example we may use the numerical data from reference 3 or 4. Putting $\alpha=-38.7$, $a=5$, and $b=6.2$ with $5.0\leq z\leq 6.2$ we obtain the results given in Table I. It will be observed that the maximum difference between the two quantities is less than 0.5 percent.

TABLE I.

z	$f(z)$	$f(z)$ approx.
5.0	7.59	7.56
5.2	7.29	7.27
5.4	7.01	7.00
5.6	6.75	6.75
5.8	6.51	6.52
6.0	6.28	6.30
6.2	6.07	6.10

$$f(z)=-\tfrac{1}{4}-\frac{(\alpha-\frac{1}{2})}{z}$$

$$f(z)\text{ approx.}=\left\{-\tfrac{1}{4}\frac{(a+b)}{2}-(\alpha-\tfrac{1}{2})\right\}\frac{1}{z}$$

With $\alpha=-38.7$, $a=5.0$, and $b=6.2$.

Thus if one uses

$$\frac{d^2V}{dz^2}+\frac{\sigma^2}{z}V=0, \tag{12}$$

as the differential equation for the function "V" it seems reasonable to suppose that (9) will give a close representation of the function "M" for "z" between "a" and "b."

Now Eq. (12) has for its most general solution

$$V(z)=z^{\frac{1}{2}}\{AJ_1(2\sigma z^{\frac{1}{2}})+BN_1(2\sigma z^{\frac{1}{2}})\}, \tag{13}$$

where J_1 and N_1 are Bessel functions of the first and second kind, respectively, and A and B are arbitrary constants to be determined by the conditions of the problem. Combining (9) and (13) we have

$$M(\alpha,z)=e^{z/2}\{AJ_1(2\sigma z^{\frac{1}{2}})+BN_1(2\sigma z^{\frac{1}{2}})\}. \tag{14}$$

It must be emphasized that this expression can only be made to approximate $M(\alpha, 1, z)$ (by the proper choice of A and B) for large values of α and for z between a and b. For any other range of variables it will undoubtedly be wide of the mark. Even subject to these restrictions there is no reason to suppose that $e^{z/2}J_1(2\sigma z^{\frac{1}{2}})$ is an approximation to $F(\alpha, 1, z)$ or $e^{z/2}N_1(2\sigma z^{\frac{1}{2}})$ to $W(\alpha, 1, z)$. All we are entitled to expect is that a linear combination of $F(\alpha, 1, z)$ and $W(\alpha, 1, z)$ can be replaced by some linear combination of the functions $e^{z/2}J_1(2\sigma z^{\frac{1}{2}})$ and $e^{z/2}N_1(2\sigma z^{\frac{1}{2}})$.

We will now adopt for the function $M(\alpha_n, 1, z)$, which occurs in Eq. (5), the form given in (14). However it is still necessary to discover what values of α_n to use. (It must be remembered that α is contained in the quantity σ.) It will be recalled that the function $M(\alpha, z)$ must be such that

$$dM/dz = M \tag{15}$$

for $z=a$ and $z=b$. This equation will be found to hold only when the α's are properly chosen. Let

$$Z_1(2\sigma z^{\frac{1}{2}}) = AJ_1(2\sigma z^{\frac{1}{2}}) + BN_1(2\sigma z^{\frac{1}{2}})$$

and in order to be specific let $N_1(2\sigma z^{\frac{1}{2}})$ be the Neumann function whose properties are well known. Then

$$M(\alpha, z) = e^{z/2} Z_1(2\sigma z^{\frac{1}{2}}). \tag{16}$$

Substituting (16) in (15) one gets

$$\frac{dZ_1}{d(2\sigma z^{\frac{1}{2}})} - \frac{z^{\frac{1}{2}}}{2\sigma} Z_1 = 0. \tag{17}$$

(In the following the argument of Z, J, and N will be omitted.) But

$$\frac{dZ_1}{d(2\sigma z^{\frac{1}{2}})} = Z_0 - \frac{1}{2\sigma z^{\frac{1}{2}}} Z_1.$$

Therefore, (17) becomes

$$Z_0 - Z_1 \tan\zeta = 0, \tag{18}$$

where

$$\tan\zeta = \frac{1}{2\sigma}\left(\frac{1}{z^{\frac{1}{2}}} + z^{\frac{1}{2}}\right). \tag{19}$$

In terms of the J and N functions (18) becomes

$$A(J_0 - J_1 \tan\zeta) + B(N_0 - N_1 \tan\zeta) = 0. \tag{20}$$

At this point it is useful to make a further approximation. We have carried the Bessel and Neumann functions as far as it is convenient—to carry them further leads to complicated expressions. However the argument $2\sigma z^{\frac{1}{2}}$ is so large that they may be replaced by their asymptotic representations. The quantity $2\sigma z^{\frac{1}{2}}$ will usually have values in excess of 20 and in this range we may use the following:

$$\left.\begin{aligned} J_0 &= (\pi\sigma z^{\frac{1}{2}})^{-\frac{1}{2}} \cos(2\sigma z^{\frac{1}{2}} - \pi/4), \\ N_0 &= (\pi\sigma z^{\frac{1}{2}})^{-\frac{1}{2}} \sin(2\sigma z^{\frac{1}{2}} - \pi/4), \\ J_1 &= (\pi\sigma z^{\frac{1}{2}})^{-\frac{1}{2}} \cos(2\sigma z^{\frac{1}{2}} - 3\pi/4), \\ N_1 &= (\pi\sigma z^{\frac{1}{2}})^{-\frac{1}{2}} \sin(2\sigma z^{\frac{1}{2}} - 3\pi/4). \end{aligned}\right\} \tag{21}$$

Substituting these expressions in (20), and simplifying, one obtains

$$A(\cos\epsilon - \tan\zeta \sin\epsilon) + B(\sin\epsilon + \tan\zeta \cos\epsilon) = 0,$$

where $\epsilon = 2\sigma z^{\frac{1}{2}} - \pi/4$. Dividing through by $\cos\epsilon$ this becomes

$$A(1 - \tan\zeta \tan\epsilon) + B(\tan\zeta + \tan\epsilon) = 0$$

or

$$A + B\tan(\zeta + \epsilon) = 0. \tag{22}$$

Now ζ and ϵ are both functions of z and equation (22) must hold for $z=a$ and $z=b$. Therefore, we get the two equations

$$\left.\begin{aligned} A + B\tan\{\zeta(a) + \epsilon(a)\} &= 0 \\ A + B\tan\{\zeta(b) + \epsilon(b)\} &= 0 \end{aligned}\right\}. \tag{23}$$

These equations can only have roots other than the trivial ones $A=B=0$ if

$$\tan\{\zeta(a) + \epsilon(a)\} = \tan\{\zeta(b) + \epsilon(b)\}. \tag{24}$$

Equation (24) can be satisfied if

$$\{\zeta(b) + \epsilon(b)\} - \{\zeta(a) + \epsilon(a)\} = n\pi, \quad n = 0, 1, 2, \cdots \tag{25}$$

Introducing the functions ζ and ϵ explicitly (25) becomes

$$x = n\pi + \tan^{-1}\left\{\frac{(b^{\frac{1}{2}} - a^{\frac{1}{2}})}{x}\left(\frac{1+a}{a^{\frac{1}{2}}}\right)\right\} - \tan^{-1}\left\{\frac{(b^{\frac{1}{2}} - a^{\frac{1}{2}})}{x}\left(\frac{1+b}{b^{\frac{1}{2}}}\right)\right\}. \tag{26}$$

where $x = 2\sigma(b^{\frac{1}{2}} - a^{\frac{1}{2}})$. The permissible values of α are determined by finding the values of x for which this equation is satisfied (x is a function of α). Before looking at (26) in detail it is obvious that when $n=0$ its solution is $x=0$. This means $\sigma = 0$ or

$$\alpha = \tfrac{1}{2} - \tfrac{1}{8}(a+b).$$

This will give a small negative value for α. Remembering that out treatment cannot be expected to be correct when α has a small absolute value it will be realized that this is the approximation to the eigenvalue $\alpha=1$. However the term in (5) arising from this eigenvalue (*viz.*, the term in e^z) is simple and there is no point in doing otherwise than taking it as it stands.

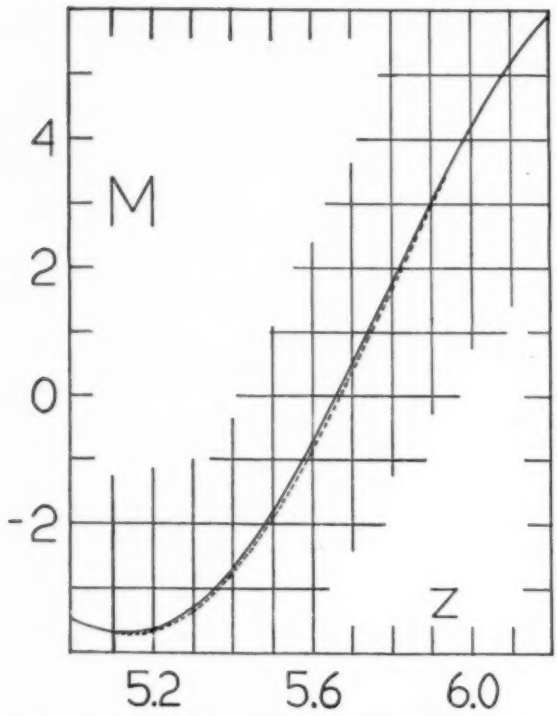

FIG. 1. The full line is the function $M(-38.7, 1, z)$ and the dotted line the function $-0.4205M(-38.77, z)$.

Since $b-a\simeq 1$, we have

$$(b^{\frac{1}{2}}-a^{\frac{1}{2}})\simeq\frac{1}{b^{\frac{1}{2}}+a^{\frac{1}{2}}}\simeq\frac{1}{2b^{\frac{1}{2}}}.$$

Therefore,

$$\frac{(b^{\frac{1}{2}}-a^{\frac{1}{2}})}{x}\frac{(1+b)}{b^{\frac{1}{2}}}\simeq\left(\frac{0.5}{x}\right)\frac{1+b}{b}\simeq\frac{0.5}{x}.$$

When $n=1, 2, \cdots$ in (26) an actual computation using representative figures shows that $x\simeq n\pi$. Thus the arguments of the inverse tan functions will be small, and these terms will be very small in comparison with $n\pi$. This being the case we will replace x by $n\pi$ in the inverse tan functions and expand them retaining only the first term of the expansions. This gives

$$x=n\pi+\frac{(b^{\frac{1}{2}}-a^{\frac{1}{2}})}{n\pi}\left\{\frac{1+a}{a^{\frac{1}{2}}}-\frac{1+b}{b^{\frac{1}{2}}}\right\}$$

or

$$\sigma_n=\frac{n\pi}{2(b^{\frac{1}{2}}-a^{\frac{1}{2}})}+\frac{1}{2n\pi}\left\{\frac{1+a}{a^{\frac{1}{2}}}-\frac{1+b}{b^{\frac{1}{2}}}\right\}. \quad (27)$$

It is interesting to see how accurately this formula gives α_1 (i.e., $n=1$) for the problem referred to above in which $a=5.0$ and $b=6.2$. A simple computation gives $\sigma_1=6.154$ or $\alpha_1=-38.77$. The correct value is $\alpha_1=-38.70$. Thus it is seen that for large absolute values of α the approximation is a very good one. Using the exact theory, several weeks of computing were required to get α_1 and the labor involved in getting α_2 seemed prohibitive. Formula (27) gives a result, correct to within 0.2 percent in this case, with only a few minutes required for the computation. When $n=2$, we have $\sigma_2=12.36$ and $\alpha_2=-154.6$. This checks with the exact theory as to order of magnitude and is probably quite accurate because for such large values of α the approximations are especially valid. This eigenvalue and the ones which follow it are so large that rapid convergence of the summation in (5) is assured even for small values of τ.

Returning to a consideration of Eq. (14) we see that it should now be written

$$M(\alpha_n, z)=A_n e^{z/2}\{J_1(2\sigma_n z^{\frac{1}{2}})+K_n N_1(2\sigma_n z^{\frac{1}{2}})\}, \quad (28)$$

where

$$K_n=B_n/A_n=-\cot\{\zeta_n(a)+\epsilon_n(a)\}. \quad (29)$$

Since it is not usual to find the J_1 and N_1 functions tabulated for such large values of the argument as occur in this problem it seems best to replace them by their asymptotic representations in $M(\alpha_n, z)$. Then (28) becomes

$$M(\alpha_n, z)=e^{z/2}z^{-\frac{1}{4}}\{\cos(2\sigma_n z^{\frac{1}{2}}-3\pi/4)+K_n\sin(2\sigma_n z^{\frac{1}{2}}-3\pi/4)\}. \quad (30)$$

It will be noted that the A_n as well as some other constants which occur as multiplying factors have been dropped. That this is permissible is at once evident from Eq. (5). $M(\alpha_n, 1, z)$, or its approximation $M(\alpha_n, z)$, is found twice in the numerator and twice in the denominator and any constant multiplying factor will cancel. Hence $M(\alpha_n, z)$ as written in (30) will replace $M(\alpha_n, 1, z)$ as given by the exact theory, and the α_n's will be given by (27) and (11).

A noteworthy feature of the function $M(\alpha_n, z)$ is its simplicity and the ease with which numerical results can be obtained from it. Its validity is best illustrated by comparing the curve obtained from it with that obtained from

the exact function $M(\alpha_n, 1, z)$. This latter function is tabulated for $5.0 \leq z \leq 6.2$ and $\alpha = -38.7$.[4] In Fig. (1) the two functions $M(-38.7, 1, z)$ and $-0.4205M(-38.77, z)$ are plotted for purposes of comparison. (It is to be observed that the two M functions are not identical—one is a multiple of the other.) No attempt has been made to find the best multiplying factor: the factor -0.4205 is the one that makes the two functions identical at $z = 5.0$, the extreme end of the range. The usefulness of the approximation seems well attested within the range of values for which it was devised.

The evaluation of the integrals which occur in Eq. (5) does not seem of importance. Since $M(\alpha_n, z)$ must be computed in any case the simplest procedure is to evaluate these integrals by numerical integration.

Two sets of values of c/c_0 for several values of τ are to be found in Table II. In the first column of each group are the results given by the approximate functions and in the second column those given by the exact functions. These latter values are obtained from reference 4, for the problem considered there. In computing the values of c/c_0 from the exact solution the terms in $\alpha_2, \alpha_3, \cdots$ etc., were not used. This did not seem to introduce a serious error into the results because it was felt that these higher terms were insignificant even for such a small value of τ as .015. However, no proof of this could be given and it is reassuring to discover from the approximate solution that this omission is justified. If the term in α_2 is included the numerical values most seriously affected are only changed by a few units in the third figure beyond the decimal. (It should be stated that the values given in Table II for the approximate solution do not include the terms in $\alpha_2, \alpha_3, \cdots$. They were omitted purposely in order to have the same conditions in both sets of calculations.) The greatest differences between the two sets of figures occur in the section headed $\tau = .015$. (This corresponds to a time equal to about 1/7 of that required to reach full equilibrium.) But even here the approximation is within 1.2 percent of being correct over most of the range of z. For larger values of τ the differences are much less.

To obtain a set of curves from the exact solution would take an experienced computer several weeks: using the functions derived in this paper the same curves could be obtained in six or eight hours.

TABLE II. $c(z, \tau)/c_0$.

z	$\tau = .015$		$\tau = .03$		$\tau = .05$		$\tau = .10$	
	A	B	A	B	A	B	A	B
5.0	.726	.717	.632	.627	.569	.567	.524	.524
5.1	.795	.784	.695	.689	.627	.625		
5.2	.853	.841	.754	.747	.687	.684	.640	.639
5.3	.900	.889	.809	.804	.748	.746		
5.4	.938	.926	.863	.857	.813	.810	.778	.777
5.5	.968	.956	.916	.910	.882	.879		
5.6	.994	.983	.971	.965	.955	.953	.944	.944
5.7	1.021	1.013	1.030	1.026	1.037	1.035		
5.8	1.051	1.050	1.096	1.095	1.126	1.126	1.148	1.148
5.9	1.094	1.099	1.174	1.177	1.228	1.229		
6.0	1.157	1.165	1.269	1.273	1.344	1.346	1.398	1.398
6.1	1.241	1.254	1.382	1.389	1.476	1.479		
6.2	1.358	1.374	1.519	1.528	1.628	1.632	1.705	1.705

Columns A contain the approximate values and columns B the exact values of the function $c(z, \tau)/c_0$.

The Motion of a Conical Coil Spring

I. EPSTEIN*
Department of Physics, University of Cincinnati, Cincinnati, Ohio
(Received November 22, 1946)

The elongations and natural frequencies of conically-shaped coil springs are derived theoretically for several dynamic boundary conditions. Frequencies are verified experimentally on nickel and piano wire springs, attesting the reliability of the computations.

1. EQUATION OF MOTION

THE dissimilarities in the analytic expressions for the oscillatory motions of conically-shaped springs on one hand and cylindrical ones on the other, arise as results of the variability of mass per unit length in the direction of motion and of the inconstancy of the spring "constant" in the case of the conical type. If a constant mass per unit length of wire, m, is assumed, the total mass of a single complete turn of wire can be stated as a function of the diameter of the turn, or as a function of the diameter of the largest turn and the linear distance from it. Let it be required to find the mass of a complete turn of wire at an average distance x from a coil of diameter D_0 (Fig. 1). The circumference of the turn in question is $\pi(D_0-2ax)$, where a is the tangent of the half-angle at the vertex of the cone. Hence, its mass is m times this value. The "inertial force" (mass times acceleration) of a single turn of wire is then, $\pi(D_0-2ax)m\partial^2E/\partial t^2$, where E is the displacement of the turn (elongation of the spring), measured from its unstretched position. The inertial force of an element dx must be equated to the net force necessary to give the element displacement E. The formula for the deflection of a single turn of wire (as measured by one 360° revolution of the coil around the longitudinal axis of the cone) of loop diameter D and wire thickness d, under a load of P pounds, is $f=8D^3P/Gd^4$, where f is the deflection in inches, D and d are measured in inches, and G is the torsional modulus of elasticity of the wire used.[1] Since the spring constant K is defined as the force per unit deflection, the conical spring "constant" is $K=Gd^4/8D^3$, and the force on an element of wire due to spring tension is:

$$F=\frac{\partial}{\partial x}\left[K\frac{\partial E}{\partial x}\right]dx=\frac{\partial}{\partial x}\left[\frac{Gd^4}{8D^3}\frac{\partial E}{\partial x}\right]dx.$$

It is advantageous to use as independent variable the diameter of a turn of wire, defined by the equation $Z=D=D_0-2ax$. Thus, equating the inertial force to the tension force, the equation takes the form:

$$\frac{2\pi mZ^4}{a^2Gd^4}\frac{\partial^2E}{\partial t^2}=\frac{\partial^2E}{\partial Z^2}-\frac{3}{Z}\frac{\partial E}{\partial Z}. \tag{1}$$

A solution of the form $E(Z,t)=w(Z)\cdot T(t)$ is assumed, and substitutions are made back into Eq. (1). The variables Z and t may be separated and two ordinary differential equations arise. For the equation in t we get:

$$d^2T/dt^2+\lambda^2T=0. \tag{2}$$

The general solution of this equation is $T=T_0\cos(\lambda t+\delta)$, where $\lambda=2\pi f$, where f_j are the natural frequencies of the oscillatory system to be determined by boundary conditions operating on the ordinary differential equation in Z. For the equation in Z we get:

$$\frac{-2\pi m\lambda^2}{a^2Gd^4}=\frac{1}{Z^4w}\frac{d^2w}{dZ^2}-\frac{3}{Z^5w}\frac{dw}{dZ}. \tag{3}$$

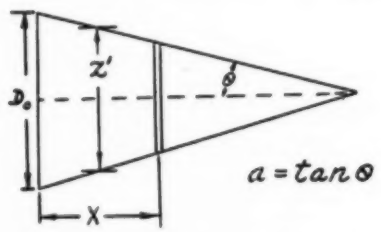

FIG. 1. Schematic diagram of spring (longitudinal section).

* Graduate student.

[1] *National Metals Handbook* (American Society for Steel Training, Cleveland, 1933), p. 990.

For ease in computation to be done later, the following changes are made at this point. Z is changed so that $z=Z/D_0$. Thus, the range of the independent variable, rather than being from 0 to D_0, will now be from 0 to 1. Further, let $a^2Gd^4/2\pi mD_0^6$ be denoted by a single bulk constant c. Equation (3) then reduces to:

$$\frac{d^2w}{dz^2}-\frac{3}{z}\frac{dw}{dz}+\frac{\lambda^2z^4w}{c}=0. \tag{4}$$

Series solutions of Eq. (4) may be identified with solutions in Bessel functions of orders $\frac{2}{3}$ and $-\frac{2}{3}$ of the form:

$$W(y)=(y/2)^{\frac{1}{2}}\{AJ_{-2/3}(y)+BJ_{2/3}(y)\}, \tag{5}$$

where $y=\lambda z^3/3\sqrt{c}$. Finally, the general solution of Eq. (1), in terms of the independent variable z, is:

$$E(z,t)=(\Lambda/2)^{\frac{1}{2}}z^2\{AJ_{-2/3}(\Lambda z^3)+BJ_{2/3}(\Lambda z^3)\}\cos(\lambda t+\delta), \tag{6}$$

where $\lambda/3\sqrt{c}$ has been replaced by Λ. An investigation will now be conducted into the particular solutions of this equation to be used to satisfy specific boundary conditions.

2. SPECIAL BOUNDARY CONDITIONS

I. Both Extremities Fixed

The particular solutions of Eq. (6) which satisfy the boundary conditions $E(0,t)=E(1,t)=0$, are:

$$E(z,t)=(\Lambda/2)^{\frac{1}{2}}z^2BJ_{2/3}(\Lambda z_3)\cos(\lambda t+\delta). \tag{7}$$

By taking $\delta=0$, we assume that the motion starts from rest, that is, $\partial E/\partial t=0$ at $t=0$. In order to satisfy the boundary condition at the base, it is necessary that $E(1,t)$ in Eq. (7) be zero for all t. This can be accomplished by limiting the values of Λ to those which are roots of the equation $J_{2/3}(\Lambda)=0$. The first two roots of this equation are $\Lambda_1=3.38$ and $\Lambda_2=6.53$, while other roots may be deduced by adding π successively to each former root.[2] Since $\Lambda_j=\lambda_j/3c^{\frac{1}{2}}$, and $\lambda_j=2\pi f_j$, then f_j (the natural frequencies of the system under assigned boundary conditions) will be $f_j=3c^{\frac{1}{2}}\Lambda_j/2\pi$, where the Λ_j are roots of $J_{2/3}(\Lambda)=0$. The constant c may be determined in one of three ways. First, by the defining formula for c: $c=a^2Gd^4/2\pi mD_0^6$, using quantities which are deemed reliable for a, G, d, and m. Another method is to analyze the static case for an experimental determination of Gd^4 and using values for the other quantities to the best of one's knowledge. A third method is to solve for $\sqrt{c}$ using one experimentally determined natural frequency. Once determined in this manner, c will retain the same value regardless of boundary conditions or initial distortions. It is best to arrive at a suitable value of c by using all three methods simultaneously, and arriving at consistent values for all of the constants included in c.

[2] Dinnik, Archiv d. Math. und Phys. [3], 18, 337–338 (1911).

TABLE I.

	Root	Λ_j	f_j(c/sec.)	f_j(experimentally)
Ni	1st	3.38	2.59	2.58
	2nd	6.53	5.21	
Piano wire	1st	3.38	2.53	2.55
	2nd	6.53	5.08	

In experiments performed in conjunction with this problem, two springs (one of nickel and one of piano wire) were employed. By the methods just outlined, the value of c adopted for the nickel coil was 2.75 and for the piano wire coil, 2.65. Thus, for the nickel coil,

$$f_j=\frac{3(2.75)^{\frac{1}{2}}\Lambda_j}{6.28}=\frac{\Lambda_j}{1.26},$$

and for the piano wire coil,

$$f_j=\frac{3(2.65)^{\frac{1}{2}}\Lambda_j}{6.28}=\frac{\Lambda_j}{1.29}.$$

Table I shows the results of this case.

IIA. Vertex Fixed, Base Free

In this case, the boundary conditions to be met are that $E(0,t)=0$, and $\partial E/\partial x$ be zero at $z=1$. As in the previous case, in order to fulfill the condition at the vertex, A, (Eq. (6)), must be made identically zero. Thus, for a particular solution, we choose:

$$E(z,t)=(\Lambda/2)^{\frac{1}{2}}z^2BJ_{2/3}(\Lambda z^3)\cos(\lambda t). \tag{8}$$

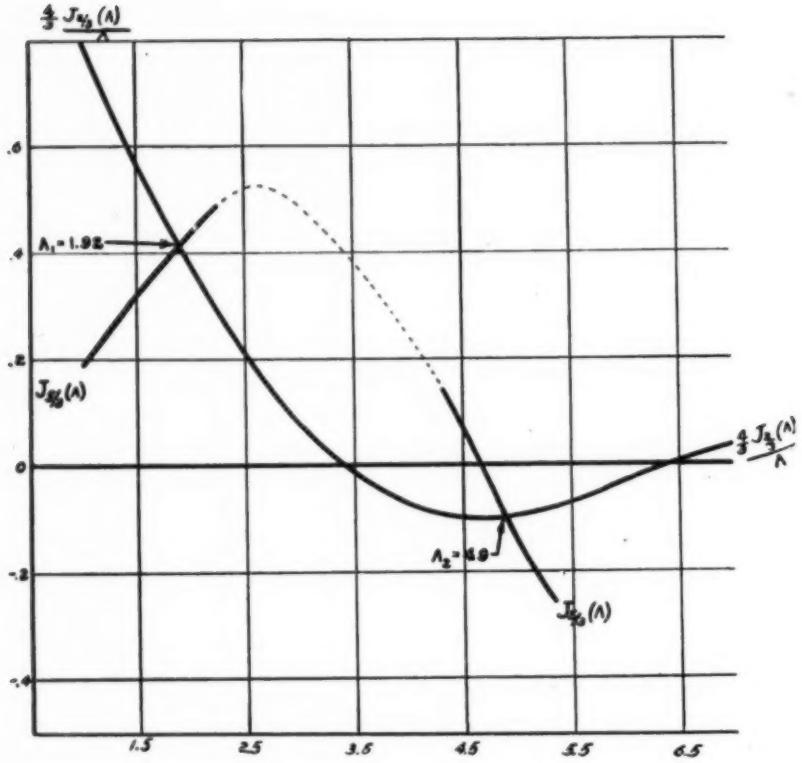

FIG. 2. Graphical solution for first two roots, Λ_1 and Λ_2 of Eq. (9).

$\partial E/\partial x$ must be zero for $z=1$, that is,

$$(\Lambda z^{\frac{3}{2}})J_{2/3}'(\Lambda z^{\frac{3}{2}}) = -\tfrac{2}{3}J_{2/3}(\Lambda z^{\frac{3}{2}}) \quad \text{for } z=1.$$

Hence, the equivalent expression to be satisfied is:

$$J_{5/3}(\Lambda) = \frac{4}{3}\frac{J_{2/3}(\Lambda)}{(\Lambda)}. \tag{9}$$

The roots of this equation will determine the values of Λ which will satisfy the boundary conditions at the base of the spring. Equation (9) may be solved graphically from tabulated values of $J_{5/3}(\Lambda)$ and of $4/3[J_{2/3}(\Lambda)/(\Lambda)]$. By inspection of Fig. 2, Eq. (9) is satisfied when $\Lambda = 1.92, 4.9, \cdots,$. Using the formulas developed in Section I, the natural frequencies may be computed. Table II shows the results of this case.

IIB. Base Fixed, Vertex Free

In this case, the boundary conditions to be met are that $E(1, t)=0$, and that $\partial E/\partial x$ be zero at $z=0$. It is advantageous at this point to write the general solution of Eq. (4) in the form:

$$W(y) = (y/2)^{\frac{1}{2}}\{AJ_{-2/3}(y)+BJ_{2/3}(y)\},$$

and noting that $y=0$ when $z=0$, $y=\Lambda$ when $z=1$. Now, from the definition of $J_{-2/3}(y)$, it is evident that

$$\lim_{y\to 0}[(y/2)^{\frac{1}{2}}J_{-2/3}(y)] = \frac{1}{\pi(-2/3)},$$

where $\pi(n)=\Gamma(n+1)$. Thus, when $y=0$, $E(z, t) = E(0, t) \neq 0$, as is required by boundary conditions, and the solution is not trivial. Inclusion of $J_{2/3}(y)$ in the solution is unnecessary to meet boundary conditions and B can be taken as zero, thus reducing our solution to:

$$E(y, t) = (y/2)^{\frac{1}{2}}AJ_{-2/3}(y)\cos(\lambda t), \tag{10}$$

TABLE II.

	Root	Λ_j	f_j(c/sec.)	f_j(experimentally)
Ni	1st	1.92	1.53	1.53
	2nd	4.9	3.9	
	3rd	8.1	6.4	
Piano wire	1st	1.92	1.49	1.51
	2nd	4.9	3.8	
	3rd	8.1	6.3	

or, in terms of z:

$$E(z, t) = [(\Lambda/2)^{\frac{1}{2}}A]z^{\frac{1}{2}}J_{-2/3}(\Lambda z^{\frac{3}{2}}) \cos(\lambda t). \quad (11)$$

We now aim to satisfy the condition that $\partial E/\partial x$ be zero at $z=0$, using Eq. (11) as the particular solution of Eq. (1). This requires the following relationship to be satisfied:

$$3z(\Lambda z^{\frac{3}{2}})J_{-2/3}'(\Lambda z^{\frac{3}{2}}) = -2zJ_{-2/3}(\Lambda z^{\frac{3}{2}}) \quad \text{for } z=0,$$

or the equivalent form:

$$3z[(-2/3)J_{-2/3}(\Lambda z^{\frac{3}{2}}) - \Lambda z^{\frac{3}{2}}J_{1/3}(\Lambda z^{\frac{3}{2}})] = -2zJ_{-2/3}(\Lambda z^{\frac{3}{2}}).$$

Terms in $J_{-2/3}(\Lambda z^{\frac{3}{2}})$ are mutually annihilated and the following relationship remains to be satisfied:

$$-3\Lambda z^{\frac{4}{2}}J_{1/3}(\Lambda z^{\frac{3}{2}}) = 0 \quad \text{for } z=0. \quad (12)$$

But this is true for $z=0$, hence, Eq. (11) satisfies the boundary condition at the vertex.

To satisfy the boundary condition at the base, $E(1, t)=0$, the choice of Λ must be restricted to roots of the equation $J_{-2/3}(\Lambda)=0$. Hence, the boundary conditions of this case are satisfied by the particular solution (11) where Λ_j are roots of $J_{-2/3}(\Lambda)=0$. The first three roots of this equation are $\Lambda_1=1.25$, $\Lambda_2=4.43$, and $\Lambda_3=7.58$, while other roots may be deduced by adding π successively to each former root.[2] After converting these roots to fundamental frequencies, the results of this case may be stated in tabular form (Table III).

IIIA. Weight Attached to Base, Vertex Fixed

The boundary conditions in this case are that $E(z, t)$ be zero at $z=0$ and that $K\partial E/\partial x = M\partial^2 E/\partial t^2$ at $z=1$, where $K=Gd^4/8z^3$, the spring "constant" in this problem, and M the mass of the attached weight.

In order to satisfy the boundary condition at the vertex, A in the general solution of Eq. (1) must be taken as zero. Hence,

$$(\Lambda/2)^{\frac{1}{2}}Bz^{\frac{1}{2}}J_{2/3}(\Lambda z^{\frac{3}{2}}) \cos(\lambda t) \quad (13)$$

satisfies the physical conditions imposed at the point of support. To fulfill the boundary condition at $z=1$ (point of attachment of weight), the following equality must hold:

$$\frac{aGd^4}{4}\{4J_{2/3}(\Lambda) - 3\Lambda J_{5/3}(\Lambda)\} = 9Mc\Lambda^2 J_{2/3}(\Lambda),$$

or, writing this equation in a form more easily accessible to computation,

$$\left\{1 - \left[\frac{9Mc}{aGd^4}\right]\Lambda^2\right\} \cdot \frac{4}{3}\frac{J_{2/3}(\Lambda)}{(\Lambda)} = J_{5/3}(\Lambda). \quad (14)$$

Thus, the particular solution of Eq. (1) which satisfies the conditions of this case is Eq. (13) wherein Λ_j are roots of Eq. (14). The defining equation for Λ_j, (14), and hence, for the fundamental frequencies of this system, may be solved by graphical means. The right member in Eq. (9) tabulated for Case IIA, is present here again. The function to the left of the equals sign in Eq. (14) is then built up as a tabulated function of Λ and is plotted on the same sheet as $J_{5/3}(\Lambda)$. The intersection of these curves gives the roots Λ_j. Three different weights (60, 80, and 110 grams) are used in each case. For the coils used here, it was found that $aGd^4=5.22$ for the nickel coil, and for the piano wire coil, a corresponding value of $aGd^4=3.72$. Figure 3 gives, by inspection, the roots of Eq. (14) necessary for the fulfillment of the boundary conditions of this case. These roots are then converted into natural frequencies, yielding the following summary (Table IV).

TABLE III.

	Root	Λ_j	f_j(c/sec.)	f_j(experimentally)
Ni	1st	1.25	1.00	1.04
	2nd	4.43	3.52	
	3rd	7.58	6.04	
Piano wire	1st	1.25	.96	.92
	2nd	4.43	3.44	
	3rd	7.58	5.88	

IIIB. Weight Attached to Vertex, Base Fixed

The boundary conditions in this case are that $E(z, t)$ be zero at $z=1$, and that $-K\partial E/\partial x = M\partial^2 E/\partial t^2$ at $z=0$, where $K=Gd^4/8z^3$, the spring "constant" in this problem, and M the mass of the attached weights.

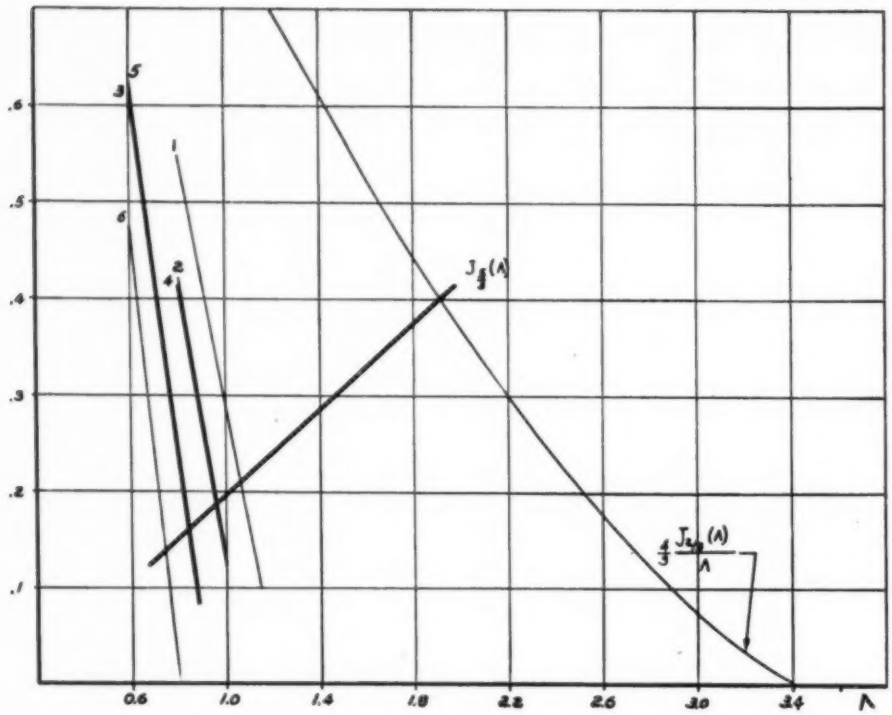

FIG. 3. Graphical solution of Eq. (14) for six values of $9Mc/aGd^4$.

To fulfill the boundary conditions of this problem, it is necessary to employ Bessel functions of orders $\frac{2}{3}$ *and* $-\frac{2}{3}$. The solution taken is the general one:

$$E(z,t)=(\Lambda/2)^{\frac{1}{2}}z^2 \times\{AJ_{-2/3}(\Lambda z^3)+BJ_{2/3}(\Lambda z^3)\}\cos(\lambda t). \quad (15)$$

The following two equalities must hold for the solution of this case:

$$\frac{aGd^4}{4z^2}(\Lambda/2)^{\frac{1}{2}}\{3A(\Lambda z^3)J_{-2/3}'(\Lambda z^3)+3B(\Lambda z^3)J_{2/3}'(\Lambda z^3) +2AJ_{-2/3}(\Lambda z^3)+2BJ_{2/3}(\Lambda z^3)\}$$
$$=9Mc\Lambda^2(\Lambda/2)^{\frac{1}{2}}z^2\{AJ_{-2/3}(\Lambda z^3)+BJ_{2/3}(\Lambda z^3)\}, \quad (16)$$

for $z=0$, *and*

$$(\Lambda/2)^{\frac{1}{2}}z^2\{AJ_{-2/3}(\Lambda z^3)+BJ_{2/3}(\Lambda z^3)\} \times\cos(\lambda t)=0 \quad (17)$$

for $z=1$. The condition of Eq. (17) reduces to:

$$AJ_{-2/3}(\Lambda)+BJ_{2/3}(\Lambda)=0. \quad (18)$$

In order to reduce Eq. (16) it is advisable to convert the derivatives of Bessel functions into related Bessel functions, and then to take limits of each term as $z\to 0$. Doing this, the condition to be met at the vertex becomes:

$$\left[\frac{aGd^4\Lambda^{\frac{1}{2}}}{(0.90275)4^{\frac{1}{2}}}\right]B_j=-\left[\frac{9Mc\Lambda^2 4^{\frac{1}{2}}}{(2.67893)\Lambda^{\frac{1}{2}}}\right]A_j. \quad (19)$$

Applying also condition (18), A_j and B_j can be eliminated, and the final ratio obtains:

$$\left\{-\left[\frac{aGd^4}{Mc}\right](59.4)\right\}\Lambda^{-\frac{1}{2}}=-\frac{J_{2/3}(\Lambda)}{J_{-2/3}(\Lambda)}, \quad (20)$$

where M has been converted into grams. The values of Λ_j which satisfy Eq. (20) are the ones which, when put into solution (15), will have both boundary conditions satisfied. Equation (20) may be solved graphically. $J_{2/3}(\Lambda)$ and

TABLE IV.

Wire	Mass attached in grams	1st frequency Λ_1	f_1	f_1(experimentally)
Nickel	60	1.06	.84	.84
	80	.96	.76	.74
	110	.84	.66	.64
Piano wire	60	.96	.74	.73
	80	.85	.66	.64
	110	.74	.57	.56

TABLE V.

Wire	Mass attached in grams	1st frequency Λ_1	f_1	f_1(experimentally)
Nickel	60	.89	.71	.71
	80	.82	.66	.65
	110	.74	.59	.58
Piano wire	60	.81	.62	.61
	80	.75	.58	.56
	110	.66	.51	.50

TABLE VI.

Ratio of diameters	1st root Λ_1	nickel coil f_1 theory	nickel coil f_1 exp.	piano wire coil f_1 theory	piano wire coil f_1 exp.
Case I (1: ∞)	3.38	(see results of Case I)			
1:10½, (1:2.154)	3.6	2.86	2.86	2.80	2.81
1:8½, (1:2.000)	3.7	2.94	2.94	2.88	2.89
1:6½, (1:1.817)	3.85	3.05	3.02	2.99	2.97

$J_{-2/3}(\Lambda)$ have been tabulated against Λ as independent variable. aGd^4/Mc will have a constant value, depending on the spring used and the mass suspended. Figure 4 shows the final determination of the roots of Eq. (20). It gives, by inspection, the roots of Eq. (20) necessary for the fulfillment of the boundary conditions of this case. These roots may be converted into natural frequencies in the usual way. The following is a tabulation of the results of the theory and their experimental verification (Table V).

IV. Two Intermediate Points Fixed

Next considered is the general case of the spring fastened at any two intermediate points. The

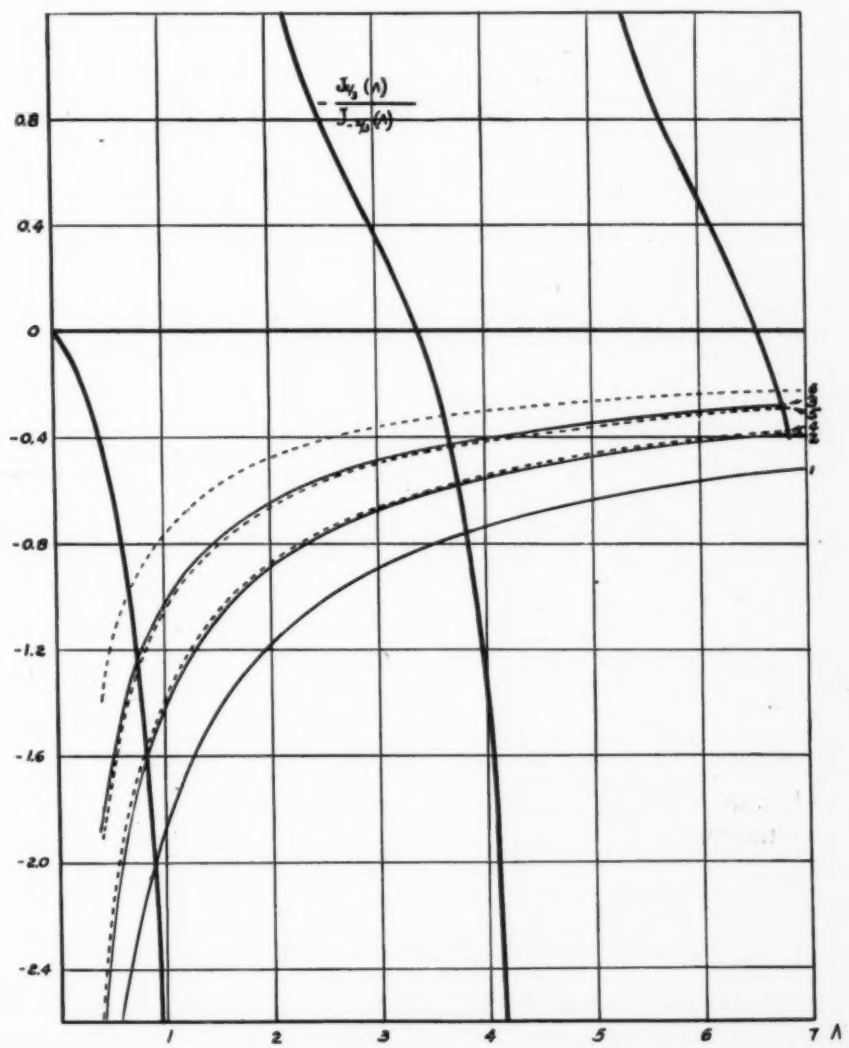

FIG. 4. Graphical solution of Eq. (20) for six values of aGd^4/Mc.

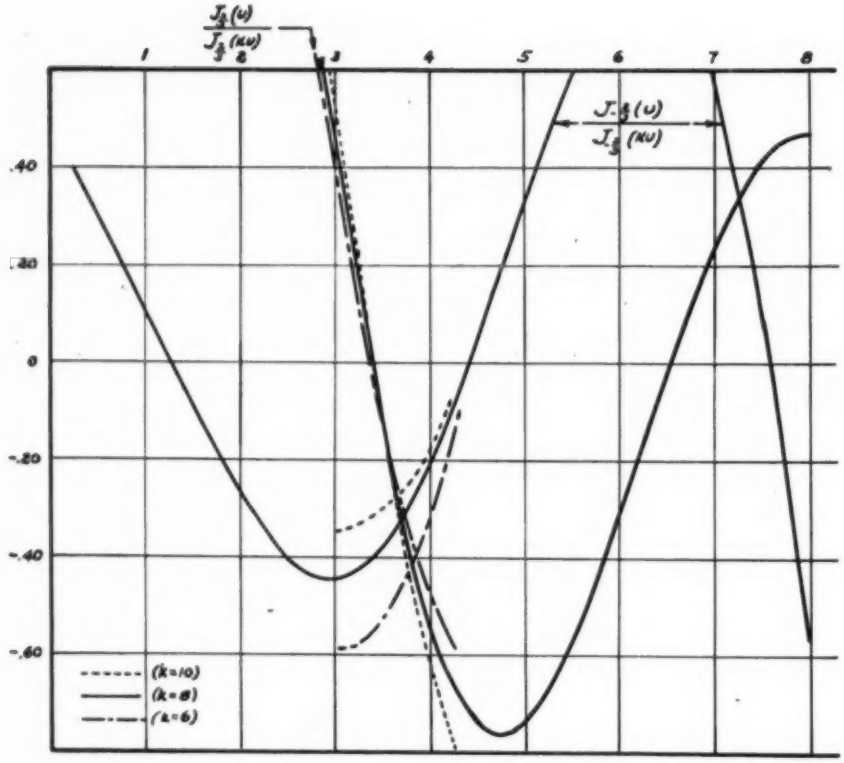

FIG. 5. Graphical solution of Eq. (24) when ratios of largest diameter of coil to smallest are as $1:10^{\frac{1}{3}}$, 1:2, and $1:6^{\frac{1}{3}}$.

boundary conditions, stated mathematically, are that $E(z', t)=0$ for $z'=a$ and for $z'=b$. There is no loss in generality if the widest upper boundary is taken to have the value 1. This can be done since in Eq. (1), c is defined as $a^2Gd^4/2\pi mD_0^6$, where D_0 is the diameter of the widest turn of wire. This is, in effect, thinking of the upper bound as the base of the spring. Thus, the boundary conditions to be used are: $E(1, t)=0=E(b, t)$, where $0<b<1$. We take as a solution of Eq. (4) the general solution:

$$E(z,t)=(\Lambda/2)^{\frac{1}{2}}z^{\frac{1}{2}}\{AJ_{-2/3}(\Lambda z^3)+BJ_{2/3}(\Lambda z^3)\}\times\cos(\lambda t). \quad (21)$$

To satisfy boundary conditions at $z=1$ and at $z=b$, the following equalities must be met simultaneously:

$$AJ_{-2/3}(\Lambda)+BJ_{2/3}(\Lambda)=0, \quad (22)$$

$$AJ_{-2/3}(\Lambda b^3)+BJ_{2/3}(\Lambda b^3)=0. \quad (23)$$

The solution of this pair of simultaneous equations depends upon the satisfaction of the following relationship:

$$\frac{J_{-2/3}(\Lambda)}{J_{-2/3}(\Lambda b^3)}=\frac{J_{2/3}(\Lambda)}{J_{2/3}(\Lambda b^3)}. \quad (24)$$

Equation (24) may be solved graphically for specific values of b^3. Values of $J_n(k\Lambda_j)$ for $n=\frac{2}{3}$ and $-\frac{2}{3}$, and for $k=6$, 8, and 10 are derived from tabulated values of $J_{-2/3}(x)$ and $J_{2/3}(x)$ by a shift of axis of the independent variable. It will be noted that this case degenerates into Case I when k becomes infinite (that is, when the lower diameter is taken as zero). Figure 5 shows the solution of Eq. (24) for values of $b^3=6$, 8, and 10. It gives, by inspection, the values of Λ_j which will satisfy Eq. (21) and both boundary conditions. Λ_j may be translated into f_j and in the usual way. Table VI below gives the results of this case.

ACKNOWLEDGMENT

Special appreciation is due Professor D. A. Wells for having suggested this problem and for having offered many stimulating suggestions during its composition.

An Introduction to the Mathematical Theory of Plasticity

W. PRAGER
Brown University, Providence, Rhode Island
(Received December 12, 1946)

The paper aims at introducing the reader to the principal theories of plasticity. Since a presentation of the general stress-strain relations used in these theories would require too much space, the discussion is restricted to the mechanical behavior of plastic materials under shear. Theories of plastic deformation (Hencky, Nadai) and theories of plastic flow (Saint Venant-Lévy-Mises, Prandtl-Reuss, Prager) are illustrated by the example of a prismatic bar under torsion.

1. INTRODUCTION

IN designing a structural member or a machine part the engineer, as a rule, uses formulas which are based on the theory of elasticity in a more or less rigorous manner. The highest stress predicted by these formulas is then compared with the maximum stress of the same type which the material can stand without failure. A so-called factor of safety is derived from this comparison. Now, in all but the very simplest cases the factor of safety obtained in this manner will differ considerably from the factor of safety defined as the ratio of the ultimate load to the design load. The reason for this is, of course, the fact that the stresses set up by the ultimate load will exceed the elastic limit of the material and that, consequently, the theory of elasticity is unable to predict these stresses. In order to obtain the second factor of safety, the only one with a physical meaning, the mechanical behavior of the material beyond the elastic limit must be taken into account. This behavior must also be taken into consideration in the study of manufacturing processes which aim at obtaining a favorable stress distribution under service conditions by setting up suitable initial stresses through previous plastic deformations. Another important field of application of the theory of plasticity is furnished by the phenomenon of creep. Under a constant load acting over a long period of time and at a high temperature a slow but steady increase of the deformation may take place. The problem of predicting the total deformation due to creep which may occur during the lifetime of a structure is of an obvious importance. In the cases mentioned so far, the plastic deformations must be rather small, as otherwise they would endanger the safety of the structure. This assumption of small deformations will no longer be justified in the study of technological processes like rolling or drawing. However, in an introduction to the theory of plasticity, it would certainly be unwise to try to cope at the same time with the difficulties arising from the consideration of finite deformations and from the unelastic behavior of the material. In the following it will, therefore, be assumed that the deformations, though greater than those possible within the elastic range, can still be treated as small. In order to show that such an assumption is reasonable, let us consider a bar of mild steel in simple tension. At the elastic limit the unit extension is of the order of one per mille. Now, we certainly are entitled to treat a unit extension of one percent still as small, but it is already far greater than any unit extension possible within the elastic range.

2. ELASTIC TORSION

The essential characteristic of the mechanical behavior of an elastic material is adequately expressed in Hooke's famous statement "*ut tensio sic vis.*" No similarly concise description of the mechanical behavior of plastic materials is possible, and a mathematical theory attempting to take into consideration all mechanical phenomena observed in the plastic range would not be practical. A workable mathematical theory must idealize the mechanical behavior of structural materials to a certain extent, and different idealizations are being used in the various fields of application. The fact that there exist almost as many theories of plasticity as writers on this subject is often a source of confusion to the student beginning to explore this field.

In the following, some of the more important theories of plasticity will be discussed briefly. Since a presentation of the general stress-strain relations used in the mathematical theory of plasticity would require too much space, the following discussion is restricted to the mechanical behavior of plastic materials under shear such as occurs at a generic point of a cylindrical or prismatic bar in torsion. Using a system of rectangular coordinates x, y, z, with the z axis parallel to the generators of the cylindrical or prismatic surface of the bar, we let τ_x and τ_y denote the components of the shearing stress acting at a generic point of a cross section. We shall assume that all other stress components vanish and that τ_x and τ_y are independent of z.

The equation of equilibrium,[1]

$$\partial\tau_x/\partial x+\partial\tau_y/\partial y=0 \tag{1}$$

is fulfilled if the stress components are derived from a stress function $\psi(x, y)$ in accordance with

$$\tau_x=\partial\psi/\partial y, \quad \tau_y=-\partial\psi/\partial x. \tag{2}$$

The condition that the cylindrical or prismatic surface of the bar is free from stresses requires that the stress function ψ has a constant value, for instance zero, along the boundary of the cross section of the bar.[1]

In order to obtain a differential equation for the stress function, we must consider the deformations of the bar and make use of the stress-strain relations. As in elastic torsion, the displacement components are assumed to be of the form

$$u=-yz\theta, \quad v=xz\theta, \quad w=\varphi(x, y, \theta), \tag{3}$$

where θ denotes the angle of twist per unit length, and the function φ represents the warping of an originally plane cross section of the bar.[2] The shear strains corresponding to the displacements (3) are[3]

$$\gamma_x=\partial\varphi/\partial x-y\theta, \quad \gamma_y=\partial\varphi/\partial y+x\theta. \tag{4}$$

Up to this point, our discussion of the torsion problem applies equally well to elastic and plastic materials. Further progress, however, depends on the introduction of a stress-strain relation, and different materials require different stress-strain relations. For the purpose of the present discussion, the stress-strain relation of an *isotropic* material is best expressed as a relation between the vector $\boldsymbol{\tau}$ with the components τ_x, τ_y and the vector $\boldsymbol{\gamma}$ with the components γ_x, γ_y, both vectors being considered as functions of time, as is the angle θ. In addition to the vectors $\boldsymbol{\tau}$ and $\boldsymbol{\gamma}$, a stress-strain relation may therefore contain their derivatives with respect to time, $\partial\boldsymbol{\tau}/\partial t$, $\partial\boldsymbol{\gamma}/\partial t$, $\partial^2\boldsymbol{\tau}/\partial t^2$, etc. In expressing the stress-strain relation in vector form, we make certain that it is independent of the choice of the coordinate axes x, y, as it must be for an isotropic material.

For an elastic material, the stress-strain relation (Hooke's law) has the following particularly simple form

$$\boldsymbol{\tau}=G_0\boldsymbol{\gamma}, \tag{5}$$

where G_0 is the shear modulus, a characteristic constant of the material. Introducing (2) and (4) into the scalar equations equivalent to (5), we obtain

$$\begin{aligned}\partial\psi/\partial y&=G_0(\partial\varphi/\partial x-y\theta),\\ -\partial\psi/\partial x&=G_0(\partial\varphi/\partial y+x\theta).\end{aligned} \tag{6}$$

Elimination of the warping function φ from Eqs. (6) furnishes the following differential equation for the stress function:

$$\partial^2\psi/\partial x^2+\partial^2\psi/\partial y^2=-2G_0\theta, \tag{7}$$

where G_0 and θ may be considered as given constants. Together with the condition that $\psi=0$ on the boundary of the cross section, Eq. (7) completely defines the stress function ψ.

As L. Prandtl[4] has pointed out, the function ψ satisfying (7) and vanishing along the boundary can be obtained by experiment. Let us consider a thin membrane, for instance a soap film, which is uniformly stretched over an opening in a rigid plane plate. The edge of the opening is given the shape of the contour of the cross section for which we desire to solve the boundary value problem formulated above. Furthermore, the membrane is fastened to the edge of the opening.

[1] See, for instance, S. Timoshenko, *Theory of Elasticity* (McGraw-Hill Book Company, Inc., New York, 1934) p. 230.

[2] J. Mandel, Ann. Ponts Chaussées **116**, 1–33 (1946) assumes $w=\theta\varphi(x, y)$. Such proportionality between warping and angle of twist can hardly be expected in the plastic range.

[3] See, for instance, S. Timoshenko, reference 1, p. 233.

[4] L. Prandtl, Jahresber. Deutsch. Math.-Ver. **13**, 31–36 (1904).

If we now have a small excess pressure p on one side of the plate, the membrane will be deformed and it can easily be shown that the deflections ω of the membrane out of its original plane will satisfy the differential equation

$$\partial^2\omega/\partial x^2+\partial^2\omega/\partial y^2=-p/T, \tag{8}$$

where T is the uniform surface tension in the membrane. Along the edge of the opening we have $\omega=0$. Choosing the value of p/T in a suitable manner, we can therefore obtain the surface $z=\psi(x, y)$ by experiment. Equations (2) show that the magnitude of the vector τ is represented by the slope of the deformed membrane, and that the vector τ is tangential to the contour lines of the deformed membrane.[5]

3. STRESS-STRAIN RELATIONS FOR PLASTIC MATERIALS UNDER SHEAR

In its initial phase, engineering research in plasticity was concerned with the limits of the elastic range rather than the phenomena occurring beyond this range. The condition that a given state of stress and strain is on the boundary of the elastic domain is expressed mathematically by the vanishing of a certain expression in the components of stress and strain (*yield condition*). For isotropic materials, this expression must be invariant with respect to rotation of the coordinate axes. Since Hooke's law holds up to the boundary of the elastic domain, all strain components which might appear in the yield condition can be expressed in terms of stress components. The yield conditions for an isotropic material then stipulates the vanishing of a certain stress invariant. In the torsion problem, where the state of stress at a point is defined by the vector τ, the only yield condition of this kind is

$$|\tau|-k=0, \tag{9}$$

where $|\tau|$ denotes the *intensity of stress*, i.e., the magnitude of the vector τ, and k the yield stress in pure shear.

The yield condition (9) establishes the limit up to which the stress distribution can be obtained from the theory of elasticity. To carry the stress analysis beyond this point, we must explore the stress-strain relations in the plastic range. It was already pointed out above that, for the torsion problem, a stress-strain relation reduces to a relation between the vectors τ and γ and their derivatives with respect to time. We shall restrict the following discussion to stress-strain relations which do not involve time derivatives of an order higher than the first. Moreover, we shall neglect all viscosity effects. This means that we shall only admit stress-strain relations which are homogeneous in the time rates of stress and strain. In spite of these restrictions which are suggested by the results of experiments on metals such as steel, copper, and aluminum, we still retain considerable freedom in fitting stress-strain relations to experimental evidence.

With each *homogenous* state of stress and strain in a plastic body there is associated a certain *permanent strain*, i.e., the residual strain after the stress is reduced to zero by unloading the body. That part of the strain which disappears upon unloading is called the *elastic strain*. In the case of the torsion problem, we shall denote the elastic and permanent strains by γ' and γ'', respectively. Experience shows that the elastic strain is related to the stress by Hooke's law:

$$\tau=G_0\gamma'. \tag{10}$$

In establishing stress-strain relations for plastic materials, we must distinguish between *loading* and *unloading*. An infinitesimal change of the state of stress and strain in a plastic material is said to constitute loading if it involves a change of the permanent strain. On the other hand, during an infinitesimal change of stress and strain which constitutes unloading the permanent strain remains constant. In the case of the torsion problem, we have $\partial\gamma/\partial t=\partial\gamma'/\partial t$ for unloading, and Eq. (10) suggests

$$\partial\tau/\partial t=G_0\partial\gamma/\partial t \tag{11}$$

as the stress-strain relation for unloading. Equation (11) is used in all theories of plasticity as the stress-strain relation for unloading; these theories therefore differ only in the stress-strain relations for loading. Moreover, even for loading the elastic strain is supposed to be related to the stress by Hooke's law, so that the task of establishing a stress-strain relation for a plastic

[5] For a comprehensive survey of the elastic torsion problem see T. J. Higgins, J. App. Phys. 10, 248–259 (1942).

material consists essentially in defining the manner in which the permanent strain, or its rate of change, depend on the stress. For the torsion problem, in particular, we must define the manner in which γ'' or $\partial\gamma''/\partial t$ depend on τ.

Let us first consider the case where γ'' is made to depend on τ (*theories of plastic deformation*). The isotropy of the material requires then that these two vectors have the same direction. This may be expressed by the equation

$$G_0\gamma''=(\lambda-1)\tau, \tag{12}$$

where λ is a scalar factor of proportionality which, as a rule, will be a function of the coordinates x, y, and the time. To obtain a proper relation between γ'' and τ we must supplement Eq. (12) by a relation between the intensities $|\gamma''|$ and $|\tau|$:

$$|\tau|=G_0f(|\gamma''|). \tag{13}$$

In the following, Eq. (13) will be called the *flow condition*. The flow condition enables us to eliminate the factor of proportionality, λ, from Eq. (12). In the following, we shall consider two kinds of flow conditions:

(a) *for perfectly plastic materials:* $G_0f=k$ $=$const.,

(b) *for materials with strain-hardening:* for the small permanent strains to which this discussion is restricted, f is a monotonically increasing function of its argument; it is then convenient to write the inverse of (13) in the form

$$G_0|\gamma''|=|\tau|[g(|\tau|/G_0)-1]. \tag{14}$$

The elastic strain is given by Eq. (10), the permanent strain by (12) and (13). Combining Eqs. (10) and (12), we obtain the following relation for the total strain $\gamma=\gamma'+\gamma''$:

$$G_0\gamma=\lambda\tau. \tag{15}$$

In the case of a perfectly plastic material Eq. (15) together with the flow condition $|\tau|=k$ constitute the stress-strain relations for loading. This stress-strain relation must, of course, be supplemented by Hooke's law, Eq. (5), which is supposed to be valid as long as $|\tau|<k$. Stress-strain relations of this type were first discussed by H. Hencky.[6] In the case of a material with strain-hardening the form (14) of the flow condition enables us to eliminate λ from Eq. (15). Since both γ' and γ'' have the direction of τ, we have

$$G_0|\gamma''|=G_0[|\gamma|-|\gamma'|]=G_0|\gamma|-|\tau|.$$

Equating the last member of this continued equation to the right-hand side of (14), we find

$$G_0|\gamma|=|\tau|g(|\tau|/G_0).$$

Comparing this to the equation obtained by taking absolute values on both sides of (15), we find

$$\lambda=g(|\tau|/G_0).$$

The stress-strain relation for the loading of a material with strain-hardening therefore takes the form

$$G_0\gamma=\tau g(|\tau|/G_0). \tag{16}$$

Setting $G_0/g=G$, we may write (16) in the form $\tau=G\gamma$, where G is a function of $|\tau|/G_0$. This stress-strain relation which, of course, applies to loading only, has the form of Hooke's law, but the shear modulus G, the so-called *secant modulus*, depends on the intensity of stress. The relation $\tau=G\gamma$ covers the elastic as well as the plastic range, if G is made to equal G_0 for $|\tau|<k$. The practical stress analysis is simplified, however, if a single analytic function $G(|\tau|/G_0)$ is used for both the elastic and the plastic range. To obtain good results one must, of course, choose a function which departs but little from the initial value G_0 as long as $|\tau|<k$. On account of its mathematical simplicity, this type of stress-strain relation which was introduced by A. Nadai[7] is widely used in the modern literature;[8] it gives a continuous transition from the elastic to the plastic state.

The stress-strain relations of Hencky and Nadai are sometimes criticized because they let the stress depend on the instantaneous strain only and not on the history of straining as might

[6] H. Hencky, Zeits. f. angew. Math. Mech. **4**, 323–334 (1924).

[7] A. Nadai, *Plasticity, a Mechanics of the Plastic State of Matter* (McGraw-Hill Book Company, Inc., New York, 1931), p. 75.

[8] See, for instance, B. Finzi, Atti Ac. Sci. Torino, Cl. Sci. Fiz. Mat. Nat. **76**, 222–238 (1941); F. P. Cozzone, J. Aero. Sci. **10**, 137–151 (1943); A. A. Ilyushin, Prikladnaia Mat. Mekh. **7**, 245–272 (1943); L. M. Kachanov, *ibid.* **6**, 187–196 (1942); E. Melan, Oesterreich. Ing.-Arch. **1**, 14–21 (1946). W. R. Osgood, J. Aero. Sci. **11**, 213–226 (1944); W. W. Sokolovsky, J. Appl. Mech. **13**, A1–A10 (1946).

be expected for plastic materials. We shall return to this criticism after discussing some rival theories of plasticity.

Let us now consider the case where $\partial\gamma''/\partial t$ is made to depend on τ (*theories of plastic flow*). The isotropy of the material requires that these two vectors have the same direction, and we may write

$$G_0\partial\gamma''/\partial t=\mu\tau, \tag{17}$$

where μ is a factor or proportionality similar to the factor λ appearing in (12). Combining Eqs. (10) and (17), we obtain the following relation for the total strain $\gamma=\gamma'+\gamma''$:

$$G_0\partial\gamma/\partial t=\partial\tau/\partial t+\mu\tau. \tag{18}$$

For a perfectly plastic material with the flow condition $|\tau|=k$ or $\tau\cdot\tau=k^2$, we have $\tau\cdot\partial\tau/\partial t=0$. Scalar multiplication of each side of Eq. (18) by τ yields therefore

$$\mu=G_0\tau\cdot\partial\gamma/k^2\partial t=G_0\dot{W}/k^2, \tag{19}$$

where $\dot{W}=\tau\cdot\partial\gamma/\partial t$ denotes the rate at which work is done. Substituting (19) into (18) we obtain

$$G_0\partial\gamma/\partial t=\partial\tau/\partial t+G_0\dot{W}\tau/k^2 \text{ with } |\tau|=k. \tag{20}$$

This stress-strain relation for loading must, of course, be supplemented by Hooke's law, Eq. (5), which is supposed to be valid as long as $|\tau|<k$. Stress-strain relations of this type were first discussed by L. Prandtl[9] and E. Reuss.[10]

As has already been indicated above, the sharp distinction between the elastic and plastic ranges with separate stress-strain relations complicates any stress analysis considerably. It therefore seems desirable to modify Eq. (20) so as to obtain a gradual transition from the elastic to the plastic state and take account of strain-hardening at the same time. As the present author[11] has shown, this can be accomplished without difficulty. In fact, let us drop the condition $|\tau|=k$ in (20). Scalar multiplication of each side of this equation by τ then furnishes

$$G_0\dot{W}=\tfrac{1}{2}\dot{S}+G_0\dot{W}S/k^2, \tag{21}$$

where $S=\tau\cdot\tau=|\tau|^2$ is a measure of the intensity of stress and the dot denotes differentiation with respect to time. Solving (21) for $\dot{W}$ and substituting into (20), we obtain

$$G_0\frac{\partial\gamma}{\partial t}=\frac{\partial\tau}{\partial t}+\frac{\dot{S}/k^2}{2(1-S/k^2)}\tau. \tag{22}$$

Let us apply this stress-strain relation to the case of pure shear, where $\tau_y=\gamma_y=0$. Equation (22) then takes the form

$$G_0\dot{\gamma}_x=\dot{\tau}_x+\frac{\tau_x\dot{\tau}_x/k^2}{1-\tau_x^2/k^2}\tau_x=\frac{\dot{\tau}_x}{1-\tau_x^2/k^2}. \tag{23}$$

With the initial condition $\tau_x=0$ for $\gamma_x=0$, integration of (23) furnishes

$$\tau_x=k\tanh(G_0\gamma_x/k).$$

The graph of τ_x *vs.* γ_x has the initial slope G_0 and the asymptote $\tau_x=k$. The stress-strain relation (23) thus provides a continuous transition from elastic behavior governed by Hooke's law to the flow of a perfectly plastic material.

Equation (23) is easily modified so as to include strain-hardening. To this end we write

$$G_0\frac{\partial\gamma}{\partial t}=\frac{\partial\tau}{\partial t}+\frac{1}{2}\left(\frac{G_0}{G^*}-1\right)\frac{\dot{S}}{S}\tau, \tag{24}$$

where G^* denotes the so-called *tangent modulus* which depends on the stress intensity S. Indeed, specializing as in (23), we obtain

$$G_0\dot{\gamma}_x=\dot{\tau}_x+\left(\frac{G_0}{G^*}-1\right)\frac{\tau_x\dot{\tau}_x}{\tau_x^2}\tau_x=\frac{G_0}{G^*}\dot{\tau}_x$$

or

$$d\tau_x/d\gamma_x=G^*.$$

From a graph of τ_x *vs.* γ_x the tangent modulus G^* can be found as a function of τ_x^2; the quantity G^* appearing in (24) is the same function of S. The stress-strain relation (24) was suggested in 1942 by H. J. Laning in an unpublished manuscript; more general stress-strain relations of this type are discussed by G. H. Handelman, C. C. Lin, and W. Prager.[12]

The first term on the right-hand side of Eq. (18) represents the rate of change of the elastic

[9] L. Prandtl, Proc. 1st Internat. Congr. Appl. Mech., Delft, 1924, pp. 43–54.

[10] E. Reuss, Zeits. f. angew. Math. Mech. **10**, 266–274 (1930).

[11] W. Prager, Proc. 5th Internat. Congr. Appl. Mech., Cambridge, Massachusetts, 1938, pp. 234–237.

[12] G. H. Handelman, C. C. Lin, and W. Prager, Quart. App. Math. **4**, 397–407 (1947).

strain. For perfectly plastic materials, it has sometimes been suggested to neglect the elastic strains at the side of the often much larger permanent strains. Equation (18) then takes the form

$$\partial\gamma/\partial t=\mu'\tau \text{ with } |\tau|=k. \tag{25}$$

Stress-strain relations of this type were the first to be used in the theory of plasticity, in the two-dimensional case by B. de Saint Venant,[13] and in the three-dimensional case by M. Lévy[14] and R. v. Mises.[15] As will be shown below, serious objections can be raised against the neglection of elastic strains.[16] In view of this fact, the amount of effort which has been spent on developing this particular theory of plasticity is surprising.[17]

4. PLASTIC TORSION

In applying the stress-strain relations of the preceding section to the torsion problem, let us first consider perfectly plastic materials. These possess a clearly defined yield point below which they obey Hooke's law (Hencky, Prandtl-Reuss) or are rigid (Saint Venant-Lévy-Mises); in the plastic range they flow under constant $|\tau|$. Once the applied torque is sufficiently large to produce yielding, the cross section can be divided into elastic (or rigid) and plastic regions. In the latter we have $|\tau|=k$ or, in terms of the stress function,

$$(\partial\psi/\partial x)^2+(\partial\psi/\partial y)^2=k^2. \tag{26}$$

As the applied torque increases the plastic regions expand until, finally, they cover the entire cross section.

Let us first consider this final stage of the torsion test. Here Eq. (26) is satisfied throughout the cross section. The left-hand side of this equation is the square of the slope of the tangent plane of the surface $z=\psi(x, y)$ with respect to the plane $z=0$. According to (26) the surface $z=\psi(x, y)$ therefore is a surface of constant slope. We can produce such a surface experimentally by heaping sand on a horizontal tray which has the shape of the cross section. Indeed, the slope of such a sand hill has a constant value corresponding to the angle of friction, and the boundary condition $\psi=0$ is enforced by the shape of the tray. For a bar of quadratic cross section, for instance, the surface $z=\psi(x, y)$ is a pyramid, for a rectangular cross section it has the form of a roof and for a circular cross section the form of a cone.

In the case of a perfectly plastic material, and for a torque which produces plastic flow throughout the entire test specimen, the stress distribution can thus be obtained without reference to any specific relation between stresses and strains. This fact is usually expressed by stating that, under these circumstances, the stress distribution in torsion is statically *determinate*.[18]

So far, we have assumed that the torque is sufficiently large to produce plastic flow throughout the entire test specimen. For smaller torques only part of the material will become plastic. According to the theories of Hencky and Prandtl-Reuss, the stress function ψ will satisfy Eq. (7) [with $(\partial\psi/\partial x)^2+(\partial\psi/\partial y)^2<k^2$] in the elastic region of the cross section and Eq. (26) in the plastic region. Continuity of the stress vector τ at the boundary between elastic and plastic regions requires continuity of the first derivatives of ψ. The complete problem for the stress function has therefore the following form: *to determine a function $\psi(x,y)$ with continuous first derivatives, which vanishes along the contour of the cross section and satisfies Eq. (7) with $(\partial\psi/\partial x)^2+(\partial\psi/\partial y)^2<k^2$ in part of the cross section and Eq. (26) in the rest.*[19] As Nadai[18] has pointed out, Prandtl's membrane analogy can easily be modified so as to enable us to solve this problem by experiment. Let us consider the square cross section as an example. A membrane is then stretched uniformly over a square opening in a rigid plate and fastened to the edge of this opening. Over the opening we erect a pyramidal surface of the slope which corresponds to the yield stress k. If now the membrane is deformed by slowly increasing pres-

[13] B. de Saint Venant, Comptes rendus **70**, 473–480 (1870).
[14] M. Lévy, Comptes rendus **70**, 1323–1325 (1870).
[15] R. v. Mises, Goettinger Nachrichten 582–592 (1913).
[16] See also W. Prager, J. App. Phys. **15**, 65–71 (1944).
[17] Excellent surveys of the Saint Venant-Mises theory of plasticity have been given by H. Geiringer, *Fondements mathématiques de la théorie des corps plastiques isotropes* (Gauthier-Villars, Paris, 1937), and S. G. Mikhlin in the chapter entitled "The mathematical theory of plasticity" of the book *Some New Methods in the Mechanics of Continuous Media* (Russian), (Izd. A. N. USSR, 1938), pp. 157–216.
[18] This was first pointed out by A. Nadai, Zeits. f. angew. Math. Mech. **3**, 442–454 (1923).
[19] For an ingenious manner of constructing particular solutions of this problem by an inverse method see V. V. Sokolovsky, Prikladnaia Mat. Mekh. **6**, 241–246 (1942).

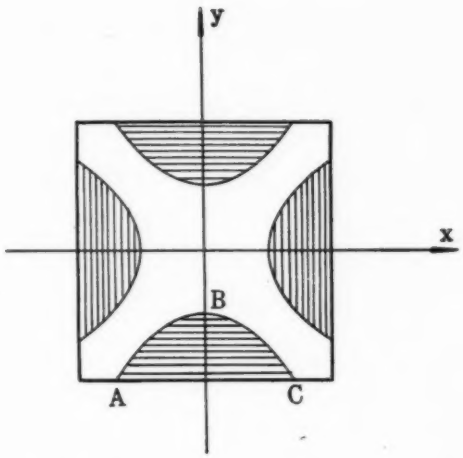

FIG. 1. Elastic and plastic regions in the cross section of a prismatic bar under torsion.

sure on one side of the plate, it will at first assume a shape which corresponds to the stress function in the elastic case. As the pressure increases, however, the membrane will partly be pressed against the pyramidal surface. Where this is the case, the membrane represents the plastic stress function satisfying Eq. (26). Where the membrane is not in contact with the pyramidal surface it represents the elastic stress function satisfying Eq. (7).

Having determined the stresses by means of this so-called soap film—sand hill analogy, we can determine the strains. Let us first apply the theory of Hencky, again considering a square cross section as an example. In Fig. 1, let the shaded areas be the plastic regions as obtained from the soap film—sand hill analogy and the unshaded cruciform area the elastic region. Since the stress function, and hence the stresses, are determined by the analogy, the strains in the elastic region can be found by applying Hooke's law. As Eqs. (4) show, this means that, in the elastic region, the warping function φ can be determined to within an immaterial constant. To show how the warping function in the plastic region is found, we consider the shaded area ABC in Fig. 1. Here $\tau_x=k$, $\tau_y=0$, and the y component of Hencky's stress-strain relation (15) gives

$$\gamma_y=\partial\varphi/\partial y+x\theta=0, \tag{27}$$

while the x component does not furnish any information on account of the presence of the unknown factor λ. Integration of (27) furnishes

$$\varphi=-xy\theta+f(x). \tag{28}$$

Along the arc ABC the warping function φ is known from the elastic solution, and this enables us to determine the function $f(x)$ in (28).

Next, let us apply the theory of Prandtl and Reuss to the same problem. The soap film—sand hill analogy shows that, for any given torque, this theory furnishes the same stress distribution as that of Hencky. Moreover, it can be shown that the warping function, too, is the same for both theories.[20] Indeed, let us consider a generic point P of the cross section. As the torque is increased, the boundary between the elastic and plastic regions sweeps across the section of the bar. Once P has been engulfed in the plastic region, the stress τ at this point remains constant. For instance, if P is engulfed in the shaded area ABC of Fig. 1, the stress at P will have the constant components $\tau_x=k$, $\tau_y=0$. Accordingly, $\partial\tau/\partial t$ is zero, and the y component of the stress-strain relation (18) of the Prandtl-Reuss theory furnishes $\dot{\gamma}_x=0$, while the x component does not give any information on account of the presence of the unknown factor μ. The strain component γ_x therefore retains whatever value it has at the instant when the boundary between the elastic and plastic regions sweeps across P. On account of the continuity of the stress vector, however, the stress components at P just before this point is engulfed into the plastic region must be $\tau_x=k$, $\tau_y=0$. At this instant we therefore have $\gamma_y=0$ at P, by Hooke's law. Since from this instant on $\dot{\gamma}_y=0$ at P, we have $\gamma_y=0$ at a generic point P inside the shaded area ABC of Fig. 1. From this and the identity of the stress distributions for the two theories follows the identity of the warping functions.

The theories of Hencky and Prandtl-Reuss are thus seen to furnish two identical predictions in the case of the torsion problem. This result must not be unduly generalized, however. As a rule, the predictions furnished by the two theories

[20] This was first pointed out by the present author in H. Geiringer and W. Prager, "Mechanik isotroper Koerper im plastischen Zustand," Ergebnisse d. exakt. Nat. wiss. **13**, 310–363 (1934), p. 331.

differ; conditions under which they agree were investigated by A. A. Ilyushin.[21]

As regards the theory of Saint Venant-Lévy-Mises, it does not give a solution of the torsion problem except in the case where the torque is sufficiently large to produce plastic flow throughout the entire test specimen. Indeed, the stress distribution in the plastic part being the same as was studied above, Eq. (25) gives

$$\dot{\gamma}_{\theta}=\partial\dot{\varphi}/\partial y+x\dot{\theta}=0$$

or

$$\dot{\varphi}=-xy\dot{\theta}+f(x) \tag{29}$$

for a point in the shaded region ABC in Fig. 1. Since the cruciform unshaded region now is supposed to be rigid, we have $\dot{\varphi}=0$ along the arc ABC. This condition enables us to determine $f(x)$, and hence $\dot{\varphi}$, inside the shaded area ABC provided that its boundary, the arc ABC, is known. *The theory of Saint Venant-Lévy-Mises does not furnish any condition, however, from which this boundary between the rigid and plastic regions could be determined. Moreover, the stress distribution in the rigid part is indeterminate.*

Let us review the results obtained so far. The Saint-Venant-Lévy-Mises theory is applicable only if the torque is large enough to produce plastic flow throughout the entire bar. For smaller torques the theories of Hencky and Prandtl-Reuss furnish identical results. In all but the very simplest cases, however, the theoretical determination of the boundary between the elastic and plastic regions encounters practically unsurmountable mathematical difficulties.[22] These difficulties are avoided by the theories of Nadai and Prager which stipulate a continuous transition from the elastic to the plastic state.

Let us first apply Nadai's theory to the torsion problem. In terms of the stress function the intensity of stress, on which the shear modulus depends, is given by

$$|\tau|=\left[\left(\frac{\partial\psi}{\partial x}\right)^2+\left(\frac{\partial\psi}{\partial y}\right)^2\right]^{\frac{1}{2}}=|\text{grad}\psi|.$$

The stress-strain relation $\tau=G\gamma$ therefore gives

$$\frac{1}{G}\frac{\partial\psi}{\partial y}=\frac{\partial\varphi}{\partial x}-y\theta, \qquad -\frac{1}{G}\frac{\partial\psi}{\partial x}=\frac{\partial\varphi}{\partial y}+x\theta.$$

Elimination of φ between these equations furnishes

$$\frac{\partial}{\partial x}\left(\frac{1}{G}\frac{\partial\psi}{\partial x}\right)+\frac{\partial}{\partial y}\left(\frac{1}{G}\frac{\partial\psi}{\partial y}\right)=-2\theta \tag{30}$$

which equation replaces Eq. (7). Here G is a function of $|\text{grad}\,\psi|$, and the stress function ψ vanishes on the contour of the cross section. Equation (30) is non-linear, and somewhat reminiscent of equations which are encountered in connection with steady two-dimensional flows of compressible fluids. Integration methods developed in fluid dynamics might therefore prove useful; so far, however, the boundary value problem formulated in connection with Eq. (30) has been solved only in a few special cases.[23]

Finally, let us apply the stress-strain relation (24) to the torsion problem. To this end, we set

$$\int_0^s\frac{1}{2}\left(\frac{G_0}{G^*(s)}-1\right)\frac{ds}{s}=-\log A(S).$$

This enables us to write Eq. (24) in the form

$$G_0\frac{\partial\gamma}{\partial t}=A\frac{\partial}{\partial t}(\tau/A). \tag{31}$$

Introducing the warping function and the stress function into the two scalar equations equivalent to (31) and eliminating the warping function between them we obtain[24]

$$\frac{\partial}{\partial x}\left[A\frac{\partial}{\partial t}\left(\frac{1}{A}\frac{\partial\psi}{\partial x}\right)\right]+\frac{\partial}{\partial y}\left[A\frac{\partial}{\partial t}\left(\frac{1}{A}\frac{\partial\psi}{\partial y}\right)\right]=-2G_0\frac{\partial\theta}{\partial t}. \tag{32}$$

This equation contains the time rates of change

[21] A. A. Ilyushin, Prikladnaia Mat. Mekh. 9, 207–218 (1945).

[22] For a numerical treatment of this problem by relaxation methods see D. G. Christopherson, Trans. A.S.M.E. 62, A1–A4, and F. S. Shaw, Austral. Counc. Aeronaut. Rep. ACA-11 (1944). See also R. V. Southwell, *Relaxation methods in theoretical physics* (Oxford Press, 1946).

[23] The as yet unpublished Ph.D. thesis of G. H. Handelman (Brown University, 1946) is concerned with the application of this theory to thin-walled sections. See also L. A. Galin, Prikladnaia Mat. Mekh. 8, 307–322 (1944).

[24] This equation was first established in W. Prager, "Theory of plasticity," (mimeographed lecture notes) Brown University, Providence, Rhode Island, 1942, p. 112.

of ψ and θ in a homogeneous manner. Accordingly, the time scale is irrelevant and the angle of twist θ may be taken as measure for the time. Thus,

$$\frac{\partial}{\partial x}\left[A\frac{\partial}{\partial\theta}\left(\frac{1}{A}\frac{\partial\psi}{\partial x}\right)\right]+\frac{\partial}{\partial y}\left[A\frac{\partial}{\partial\theta}\left(\frac{1}{A}\frac{\partial\psi}{\partial y}\right)\right]=-2G_0. \quad (33)$$

Considered as an equation for $\psi(x, y, \theta)$, Eq. (33) is non-linear. It is worth noting, however, that this equation is linear in $\partial\psi/\partial\theta$ with coefficients which depend on ψ. This remark suggests the possibility of integrating (33) approximately by solving a number of linear problems for $\partial\psi/\partial\theta$ with coefficients which depend on the function ψ built up from the previously obtained values of $\partial\psi/\partial\theta$. Physically speaking, this procedure amounts to producing the desired angle of twist in a series of small steps, and assuming that during each step the tangent modulus at any point of the cross section retains the value which corresponds to the stress intensity existing at the beginning of this step at the point under consideration.

For perfectly plastic materials, the theories of plastic deformation and of plastic flow furnished the same solution of the torsion problem; except for the circular cross section these theories will yield different results, however, when strain-hardening is taken into account. Torsion of a cylindrical bar of non-circular cross section may therefore afford an opportunity of deciding experimentally between these two theories.

On the Theory of Noise in Radio Receivers with Square Law Detectors*

MARK KAC
Department of Mathematics, Cornell University, Ithaca, New York

AND

A. J. F. SIEGERT**
Radiation Laboratory, Massachusetts Institute of Technology, Cambridge, Massachusetts

(Received September 13, 1946)

For the video output V of a receiver, consisting of an i-f stage, a quadratic detector, and a video amplifier, the probability density $P(V)$ has been obtained for noise alone and for noise and signal. The results are expressed in terms of eigenvalues and eigenfunctions of the integral equation

$$\int_0^\infty K(t)\rho(s-t)f(t)dt=\lambda f(s),$$

where $\rho(\tau)$ is the i-f correlation function (i.e., the Fourier transform of the i-f power spectrum) and $K(t)$ is the response function of the video amplifier (i.e., the Fourier transform of the video amplitude spectrum). Two special cases are discussed in which the integral equation can be solved explicitly. Approximations for general amplifiers are given in the limiting cases of wide and narrow videos. Some applications of the method to other problems are shown in Sections 7B and 9.

I. THE RECEIVER MODEL

THE response of a linear circuit to noise has been investigated by several authors. The probability densities and correlation coefficients of the noise outputs of some types of detectors are also known.[1] To find the probability density of the noise voltage output of the next stage

* The major part of this paper is based on work done for the Office of Scientific Research and Development under contract OEMsr-429 with Cornell University and contract OEMsr-262 with Massachusetts Institute of Technology.

** Now at the Physics Department, Syracuse University, Syracuse, New York.

[1] References to the work in this field can be found in the articles by S. O. Rice, Bell Sys. Tech. J. **23**, 282 (1944); **24**, 46 (1945), and M. C. Wang and G. E. Uhlenbeck, Rev. Mod. Phys. **17**, 323 (1946).

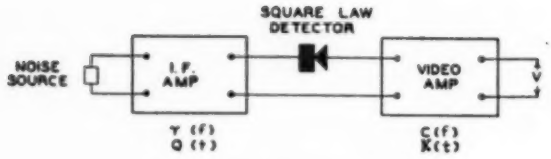

FIG. 1. The receiver model.

(video or audio amplifier) is a problem of a different type, since after the detector, the noise voltage is no longer Gaussianly distributed.

In this paper we have, therefore, calculated the probability density $P(V)$ of the noise voltage V at the end terminals of a receiver consisting of an intermediate-frequency amplifier, a quadratic detector and a video (or audio) amplifier (Fig. 1). The response of both amplifiers is assumed to be linear and characterized by the steady-state response function $\gamma(f)$ and $C(f)$, respectively, or the response functions $Q(t)$ and $K(t)$, such that the output voltages of the amplifiers are $\gamma(f)e^{2\pi ift}$ and $C(f)e^{2\pi ift}$, respectively, if the input voltage is $e^{2\pi ift}$. If, therefore, the video input voltage is $v(t)$, the video output voltage V is given by

$$\begin{aligned} V(t) &= \int_{-\infty}^{\infty} df C(f) e^{2\pi ift} \int_{-\infty}^{\infty} dt' e^{-2\pi ift'} v(t') \\ &= \int_{-\infty}^{\infty} dt' K(t-t') v(t') \end{aligned} \tag{1.11}$$

where

$$K(\tau) = \int_{-\infty}^{\infty} df C(f) e^{2\pi if\tau}. \tag{1.12}$$

Since $V(t)$ can depend only on the values which $v(t')$ assumes at times $t' \leqq t$, it follows that $K(\tau) = 0$ for $\tau < 0$, which means that all poles of $C(f)$ lie above the real axis. Since K must be real, we have $C(-f) = C^*(f)$. Both conditions are fulfilled for passive networks. We shall normalize K by

$$\int_0^{\infty} K(t)dt = 1.$$

In writing i-f voltages $V_{\text{I.F.}}^{(i)}$ and $V_{\text{I.F.}}^{(o)}$ for input and output it is generally convenient to consider them as modulated carriers, i.e., we write

$$\begin{aligned} V_{\text{I.F.}}^{(i)} &= Re\{u(t)e^{2\pi if_0 t}\} \\ &= x(t)\cos 2\pi f_0 t + y(t)\sin 2\pi f_0 t, \end{aligned}$$

where

$$u(t) = x(t) - iy(t),$$

and f_0 is the carrier frequency. The i-f output voltage is then

$$\begin{aligned} V_{\text{I.F.}}^{(o)} &= Re\left\{ \int_{-\infty}^{\infty} df e^{2\pi ift} \gamma(f) \right. \\ &\qquad \left. \times \int_{-\infty}^{\infty} dt' e^{-2\pi ift'} u(t') e^{2\pi if_0 t'} \right\} \\ &= Re\left\{ e^{2\pi if_0 t} \int_{-\infty}^{\infty} dt' u(t') \right. \\ &\qquad \left. \times \int_{-\infty}^{\infty} df e^{2\pi i(f-f_0)(t-t')} \gamma(f) \right\} \\ &= Re\{U(t)e^{2\pi if_0 t}\} \end{aligned}$$

where

$$U(t) = \int_{-\infty}^{\infty} dt' Q(t-t') u(t'),$$

and

$$Q(\tau) = \int_{-\infty}^{\infty} df e^{2\pi i(f-f_0)\tau} \gamma(f) = \int_{-\infty}^{\infty} df' e^{2\pi if'\tau} \gamma(f'+f_0).$$

We shall normalize γ and Q by demanding that

$$\int_{-\infty}^{\infty} Q^2(\tau)d\tau = 1;$$

then we have

$$\begin{aligned} \int_{-\infty}^{\infty} Q^2(\tau)d\tau &= \int\int\int_{-\infty}^{\infty} d\tau df' df'' e^{2\pi i(f'+f'')\tau} \gamma(f'+f_0) \\ &\qquad \times \gamma(f''+f_0) = 1, \end{aligned}$$

or

$$\int_{-\infty}^{\infty} df' \gamma(f_0+f')\gamma(f_0-f') = 1.$$

The calculations are appreciably simplified by assuming a symmetrical pass band* for the i-f amplifier, i.e.,

$$\gamma(f_0+f') = \gamma^*(f_0-f'). \tag{1.20}$$

We also put $|\gamma(f_0+f)| = B(f)$. Inserting this in the normalization equation we have

$$\int_{-\infty}^{\infty} |\gamma^2(f)| df = 1,$$

i.e., the power spectrum is normalized. The sym-

* See, however, footnote 3, Section IV.

metry of γ implies that Q is real and $V_{\text{I.F.}}^{(o)}$ can now be written as

$$V_{\text{I.F.}}^{(o)} = X(t)\cos 2\pi f_0 t + Y(t)\sin 2\pi f_0 t \quad (1.21)$$

with

$$X(t) = \int_{-\infty}^{\infty} dt' Q(t-t')x(t')$$
$$Y(t) = \int_{-\infty}^{\infty} dt' Q(t-t')y(t'). \quad (1.22)$$

$Q(\tau)$ must of course vanish for $\tau < 0$.

The detector is assumed to yield the output

$$X^2(t) + Y^2(t), \quad (1.31)$$

if the input voltage is

$$X(t)\cos 2\pi f_0 t + Y(t)\sin 2\pi f_0 t. \quad (1.32)$$

In order that this be a reasonable model of an actual detector it is necessary to assume

$$\left|\frac{x'(t)}{x(t)}\right| \ll f_0 \quad \text{and} \quad \left|\frac{y'(t)}{y(t)}\right| \ll f_0,$$

which implies that the width of the pass band of the i-f amplifier is small compared to the intermediate frequency f_0.

II. REPRESENTATION OF NOISE

The i-f output noise voltage (omitting the irrelevant d.c. component) is represented[2] as

$$V_{\text{I.F.}}^{(o)} = \frac{\sqrt{N}}{\sqrt{T}} \sum_{k=1}^{\infty} |\gamma(f_k')| \times (X_k' \cos 2\pi f_k' t + Y_k' \sin 2\pi f_k' t) \quad (2.11)$$

with

$$f_k' = k/T,$$

where X_1', Y_1', X_2', $Y_2' \cdots$ are independent normally distributed random variables each having the probability density

$$\pi^{-\frac{1}{2}} \exp(-u^2).$$

The representation holds only for the time interval $0 < t < T$, but this is adequate if T is chosen large compared to the time during which observations are made. We shall later let $T \to \infty$. The properties of $\gamma(f)$ were discussed above and N denotes the input noise power per unit frequency.

[2] S. O. Rice, "Mathematical analysis of random noise," Bell Sys. Tech. J. **23**, 282 (1944), see p. 328.

According to (1.31) and (1.32), the detector output voltage arising from this i-f input voltage is given by

$$X^2(t) + Y^2(t) = V_D^{(o)},$$

where

$$X(t) = \frac{\sqrt{N}}{\sqrt{T}} \sum_{k=1}^{\infty} |\gamma(f_k')| [X_k' \cos 2\pi (f_k' - f_0)t + Y_k' \sin 2\pi (f_k' - f_0)t]$$
$$Y(t) = \frac{\sqrt{N}}{\sqrt{T}} \sum_{k=1}^{\infty} |\gamma(f_k')| [-X_k' \sin 2\pi (f_k' - f_0) + Y_k' \cos 2\pi (f_k' - f_0)t]. \quad (2.12)$$

Making use of (1.20) and the fact that the band width of the i-f amplifier is small compared to the intermediate frequency f_0, we may write

$$X(t) = \frac{\sqrt{N}}{\sqrt{T}} \sum_{-\infty}^{\infty} B(f_k)(X_k \cos 2\pi f_k t + Y_k \sin 2\pi f_k t),$$
$$Y(t) = \frac{\sqrt{N}}{\sqrt{T}} \sum_{-\infty}^{\infty} B(f_k) \times (-X_k \sin 2\pi f_k t + Y_k \cos 2\pi f_k t), \quad (2.13)$$

where

$$f_k = k/T, \quad B(f_k) = |\gamma(f_k + f_0)|,$$
$$X_k = X'_{k+k_0} \quad \text{and} \quad Y_k = Y'_{k+k_0} \quad (2.14)$$

with $k_0 = Tf_0$, assumed to be an integer.

The video output voltage $V(t)$ is given by (1.11) as

$$V(t) = \int_{-\infty}^{\infty} K(t-t')[X^2(t') + Y^2(t')]dt' = \int_0^{\infty} K(u)[X^2(t-u) + Y^2(t-u)]du. \quad (2.15)$$

In the derivation of Chapter 3 we shall consider the probability distribution of the slightly modified quantity

$$V_T(t) = \int_0^T K(u)[X^2(t-u) + Y^2(t-u)]du, \quad (2.16)$$

and then pass to the limit as $T \to \infty$.

III. "WHITE NOISE"

The i-f output $X(t)\cos 2\pi f_0 t + Y(t)\sin 2\pi f_0 t$ with $X(t)$, $Y(t)$ given by (2.13) can be described

as caused by the "white noise"

$$x(t)\cos 2\pi f_0 t + y(t)\sin 2\pi f_0 t,$$

where $x(t)$ and $y(t)$ are given by

$$x(t) = \frac{\sqrt{N}}{\sqrt{T}} \sum_{k=-L}^{L} (X_k \cos 2\pi f_k t + Y_k \sin 2\pi f_k t)$$

$$y(t) = \frac{\sqrt{N}}{\sqrt{T}} \sum_{k=-L}^{L} (-X_k \sin 2\pi f_k t + Y_k \cos 2\pi f_k t),$$

where L is a number so large that the frequencies $f_0 \pm L/T$ lie outside of the pass band of the i-f amplifier. This "white noise" is the input thermal and shot noise which actually is known to have a constant power spectrum up to very high frequencies.

In the derivation of the next section it will be advantageous to represent $x(t)$ and $y(t)$ in a different orthogonal system, and we will now show that the expansion coefficients in any other complete orthogonal system are Gaussianly distributed and independent of each other, if L is sufficiently large, i.e., if the power spectrum is constant up to sufficiently high frequencies.

Let $\phi_j(t)$ be an orthonormal, complete set in the interval $(0, T)$. Expanding $x(t)$ in this system we have

$$x(t) = \sum_{1}^{\infty} u_j \phi_j(t), \tag{3.1}$$

where

$$u_j = \left(\frac{N}{T}\right)^{\frac{1}{2}} \sum_{k=-L}^{L} \left(X_k \int_0^T \phi_j(t) \cos 2\pi f_k t dt + Y_k \int_0^T \phi_j(t) \sin 2\pi f_k t dt \right). \tag{3.2}$$

The coefficients u_j are thus linear combinations of the Gaussian variables X_k, Y_k and are, therefore, Gaussianly distributed. To prove independence of linear combinations of independent Gaussian variables, it is necessary only to show that $\langle u_l u_j \rangle = 0$ for $l \neq j$. Using the statistical properties of X_k and Y_k, we have

$$\langle u_l u_j \rangle_{Av} = \frac{1}{2}\frac{N}{T} \int_0^T \int_0^T ds dt \phi_l(t) \phi_j(s) \times \sum_{-L}^{L} \cos 2\pi f_k (s-t). \tag{3.3}$$

For sufficiently large L

$$\frac{1}{T} \sum_{-L}^{L} \cos 2\pi f_k (s-t)$$

can be replaced by $\delta(s-t)$ and, therefore,

$$\langle u_l u_j \rangle_{Av} \rightarrow \frac{N}{2} \delta_{jl}. \tag{3.4}$$

In the same way we can show, for the coefficients v_j of $y(t)$, that

$$\langle v_l v_j \rangle_{Av} \rightarrow \frac{N}{2} \delta_{lj} \tag{3.5}$$

and

$$\langle u_k v_l \rangle_{Av} \rightarrow 0. \tag{3.6}$$

IV. DERIVATION OF PROBABILITY DENSITY FOR NOISE ALONE

To derive the probability density $P(V)$ we use the above representation for the incoming "white noise" writing the i-f input voltage[3] as

$$V_{\text{I.F.}}^{(i)} = x(t)\cos 2\pi f_0 t + y(t)\sin 2\pi f_0 t, \tag{4.11}$$

with

$$x(t) = \sum_j u_j \phi_j(t)$$

and

$$y(t) = \sum_j v_j \phi_j(t). \tag{4.12}$$

Choosing N as unit of power we have

$$\langle u_k u_l \rangle_{Av} = \langle v_k v_l \rangle_{Av} = \tfrac{1}{2}\delta_{lk}. \tag{4.13}$$

The i-f output voltate $V_{\text{I.F.}}^{(o)}$ is given by

$$V_{\text{I.F.}}^{(o)} = X(t)\cos 2\pi f_0 t + Y(t)\sin 2\pi f_0 t, \tag{4.14}$$

where

$$X(t) = \int_{-\infty}^{\infty} Q(t-\tau)x(\tau)d\tau,$$

$$Y(t) = \int_{-\infty}^{\infty} Q(t-\tau)y(\tau)d\tau. \tag{4.15}$$

---

[3] The authors are aware that the results of this section can be obtained in a more elegant way by using the representation (4.12) for $V_{\text{I.F.}}^{(i)}$ rather than for the components $x(t)$ and $y(t)$, and by defining the quadratic detector by

$$V_D^{(o)} = [V_{\text{I.F.}}^{(o)}]^2$$

rather than by Eq. (4.31), provided that the I.F. and video band widths are small compared with f_0 [cf. Phys. Rev. **70**, 449, C6 (1946)]. The simplifying assumption of symmetrical I.F. pass band can then be easily dispensed with. The method presented here was chosen to keep the continuity with the existing literature.

The correlation coefficient

$$\rho(\tau)=\langle X(t)X(t+\tau)\rangle_{Av}/\langle X^2(t)\rangle_{Av} \quad (4.21)$$

can be expressed in terms of the function Q as follows:

$$\begin{aligned}\langle X(t)X(t+\tau)\rangle_{Av}&=\int_{-\infty}^{\infty}\int Q(t-\tau_1)Q(t+\tau-\tau_2)\\&\quad\times\langle X(\tau_1)X(\tau_2)\rangle_{Av}d\tau_1 d\tau_2\\&=\frac{1}{2}\int_{-\infty}^{\infty}Q(t-\tau_1)Q(t+\tau-\tau_1)d\tau_1\\&=\frac{1}{2}\int_{-\infty}^{\infty}Q(\theta)Q(\theta+\tau)d\theta, \quad (4.22)\end{aligned}$$

$$\langle X^2(t)\rangle_{Av}=\frac{1}{2}\int_{-\infty}^{\infty}Q^2(\theta)d\theta=\tfrac{1}{2}, \quad (4.23)$$

and therefore

$$\rho(\tau)=\int_{-\infty}^{\infty}Q(\theta)Q(\theta+\tau)d\theta. \quad (4.24)$$

We note that

$$\begin{aligned}&\int_{-\infty}^{\infty}e^{2\pi if\tau}\rho(\tau)d\tau\\&=\int_{-\infty}^{\infty}\int_{-\infty}^{\infty}Q(\theta)Q(\theta+\tau)e^{2\pi if\tau}d\theta d\tau\\&=\int\int_{-\infty}^{\infty}\int\int df'df''\gamma(f'+f_0)\gamma(f''+f_0)\\&\qquad\times e^{2\pi i[f'\theta+f''(\theta+\tau)+f\tau]}d\theta d\tau\\&=\int_{-\infty}^{\infty}\int df'df''\gamma(f'+f_0)\gamma(f''+f_0)\\&\qquad\times\delta(f'+f'')\delta(f''+f)\\&=\gamma(f+f_0)\gamma(f_0-f)=|\gamma^2(f+f_0)| \quad (4.25)\end{aligned}$$

which is a special case of the Wiener-Khintchine relation.

The detector output voltage $V_D{}^{(o)}$ is, therefore,

$$\begin{aligned}V_D{}^{(o)}&=X^2(t)+Y^2(t)\\&=\int_{-\infty}^{\infty}\int Q(t-\tau_1)Q(t-\tau_2)\\&\quad\times[x(\tau_1)x(\tau_2)+y(\tau_1)y(\tau_2)]d\tau_1 d\tau_2, \quad (4.31)\end{aligned}$$

and the output of the video amplifier

$$\begin{aligned}V(t)&=\int_{-\infty}^{\infty}K(t-\theta)[X^2(\theta)+Y^2(\theta)]d\theta\\&=\int_{-\infty}^{\infty}K(t-\theta)d\theta\int_{-\infty}^{\infty}\int Q(\theta-\tau_1)Q(\theta-\tau_2)\\&\quad\times[x(\tau_1)x(\tau_2)+y(\tau_1)y(\tau_2)]d\tau_1 d\tau_2. \quad (4.32)\end{aligned}$$

Changing variables to

$$\theta'=t-\theta,\quad \tau_1'=t-\tau_1,\quad \tau_2'=t-\tau_2, \quad (4.33)$$

we have

$$\begin{aligned}V(t)&=\int_{-\infty}^{\infty}K(\theta')d\theta'\int_{-\infty}^{\infty}\int Q(\tau_1'-\theta')Q(\tau_2'-\theta')\\&\quad\times[x(t-\tau_1')x(t-\gamma_2')\\&\qquad+y(t-\tau_1')y(t-\tau_2')]d\tau_1' d\tau_2'. \quad (4.34)\end{aligned}$$

If the i-f input noise voltage is a homogeneous random function $x(t-\tau)$ and $y(t-\tau)$ are given by

$$\begin{aligned}x(t-\tau)&=\textstyle\sum_j u_j'\phi_j(\tau),\\y(t-\tau)&=\textstyle\sum_j v_j'\phi_j(\tau),\end{aligned} \quad (4.35)$$

where u_j' and v_j' are random variables with the same properties as u_j and v_j, and we have—omitting the primes—

$$\begin{aligned}V(t)&=\int_{-\infty}^{\infty}K(\theta)d\theta\int_{-\infty}^{\infty}\int Q(\tau_1-\theta)Q(\tau_2-\theta)\\&\quad\times\textstyle\sum_{ij}(u_iu_j+v_iv_j)\phi_i(\tau_1)\phi_j(\tau_2)d\tau_1 d\tau_2 \quad (4.36)\\&=\textstyle\sum_{ij}(u_iu_j+v_iv_j)\\&\quad\times\displaystyle\int_{-\infty}^{\infty}\int\Lambda(\tau_1,\tau_2)\phi_i(\tau_1)\phi_j(\tau_2)d\tau_1 d\tau_2 \quad (4.37)\end{aligned}$$

with

$$\Lambda(\tau_1,\tau_2)=\int_{-\infty}^{\infty}K(\theta)d\theta Q(\tau_1-\theta)Q(\tau_2-\theta). \quad (4.38)$$

We note that t does not appear anymore on the r.h.s., that means that $V(t)$ is a homogeneous random function. This is caused by the fact that the input noise is itself a homogeneous random function.

The essential step in our calculation is now to choose as the function $\phi_i(\tau)$ the normalized eigenfunctions of the integral equation

$$\int_{-\infty}^{\infty} A(\tau_1, \tau_2)\phi(\tau_2)d\tau_2 = \lambda\phi(\tau_1). \quad (4.41)$$

Then $V(t)$ is expressed as

$$V = \sum_i (u_i^2 + v_i^2)\lambda_i, \quad (4.42)$$

where the quantities λ_i are the eigenvalues of the integral equation. The quantities

$$u_i^2 + v_i^2 = Z_i \quad (4.43)$$

are independent and their probability densities $W(Z_i)$ are given by

$$W(Z_i) = \begin{cases} e^{-Z_i} & \text{if } Z_i > 0, \\ 0 & \text{if } Z_i < 0, \end{cases} \quad (4.44)$$

because u_i and v_i are independent Gaussian variables of spread $\frac{1}{2}$. The probability distribution of the sum representing V is therefore

$$\begin{aligned} P(V)dV &= dV \int_0^{\infty} \cdots \int_0^{\infty} \delta(V - \textstyle\sum_i \lambda_i Z_i) \prod_k W(Z_k) dZ_k \\ &= dV \frac{1}{2\pi} \int_{-\infty}^{\infty} d\xi e^{-iV\xi} \int_0^{\infty} \cdots \int_0^{\infty} \prod_k e^{-Z_k(1-i\lambda_k\xi)} dZ_k \\ &= dV \frac{1}{2\pi} \int_{-\infty}^{\infty} d\xi e^{-iV\xi} \frac{1}{\prod_k (1 - i\lambda_k\xi)}. \end{aligned} \quad (4.45)$$

For $V>0$ the path of integration is closed in the lower half plane and contracted around all poles $\xi_s = -i/\lambda_s$ with $\lambda_s > 0$ and *vice versa*. We thus obtain

$$P(V) = \frac{1}{2\pi} \sum_s{}^{+} \oint^{(1/i\lambda_s, -)} \frac{d\xi}{(-i\lambda_s)\left(\xi - \frac{1}{i\lambda_s}\right)} \frac{e^{-iV\xi}}{\prod_k{}'(1 - i\lambda_k\xi)} = \sum_s{}^{+} \frac{e^{(-V/\lambda_s)}}{\lambda_s \prod_k{}'\left(1 - \frac{\lambda_k}{\lambda_s}\right)} \quad \text{for } V>0 \quad (4.46)$$

where $\sum_s{}^{+}$ means summation over all values of s for which $\lambda_s > 0$. For $V<0$ we obtain

$$P(V) = \frac{1}{2\pi} \sum_n{}^{(-)} \oint \frac{d\xi}{(-i\lambda_n)\left(\xi - \frac{1}{i\lambda_n}\right)} \frac{e^{-iV\xi}}{\prod_k{}'(1 - i\lambda_k\xi)} = \sum_n{}^{(-)} \frac{e^{(-V/\lambda_n)}}{\lambda_n \prod_k{}'\left(1 - \frac{\lambda_k}{\lambda_n}\right)} \quad (4.47)$$

where $\sum_n{}^{(-)}$ indicates summation over all n for which $\lambda_n < 0$. The product is extended always over all k with exception of $k=n$.

It is sometimes more convenient to have the integral equation in a different form, involving the functions K and ρ rather than K and Q. This form is obtained by introducing the new unknown

$$f(\theta) = \int_{-\infty}^{\infty} Q(\tau_2 - \theta)\phi(\tau_2)d\tau_2, \quad (4.51)$$

so that

$$\int_{-\infty}^{\infty} d\theta K(\theta)Q(\tau_1 - \theta)f(\theta) = \lambda\phi(\tau_1). \quad (4.52)$$

Multiplying both sides with $Q(\tau_1 - \theta')$ and integrating over τ_1 we obtain

$$\int_{-\infty}^{\infty} K(\theta)d\theta \int_{-\infty}^{\infty} d\tau_1 Q(\tau_1 - \theta') \times Q(\tau_1 - \theta)f(\theta) = \lambda f(\theta'). \quad (4.53)$$

We can now write

$$\int_{-\infty}^{\infty} Q(\tau_1 - \theta')Q(\tau_1 - \theta)d\tau_1 = \int_{-\infty}^{\infty} d\tau Q(\tau)Q(\tau + \theta' - \theta) = \rho(\theta' - \theta), \quad (4.54)$$

and have the integral equation in the form

$$\int_{-\infty}^{\infty} K(\theta)\rho(\theta' - \theta)f(\theta)d\theta = \lambda f(\theta'),$$

or, since $K(\theta)=0$ for $\theta<0$,

$$\int_0^\infty K(\theta)\rho(\theta'-\theta)f(\theta)d\theta=\lambda f(\theta'). \quad (4.55)$$

Finally, by writing $(K(\theta))^{\frac{1}{2}}f(\theta)=\Phi(\theta)$ we can bring the equation into the form which will be derived directly in Section 6:

$$\int_0^\infty [K(\theta')]^{\frac{1}{2}}\rho(\theta'-\theta)[K(\theta)]^{\frac{1}{2}}\Phi(\theta)d\theta=\lambda\Phi(\theta'). \quad (4.56)$$

By means of the expression

$$V=\sum \lambda_j Z_j, \quad (4.61)$$

we can easily verify formulas for the moments. For the first two moments we have for instance

$$\langle V\rangle_{Av}=\sum \lambda_j\langle Z_j\rangle_{Av}=\sum \lambda_j=\int_0^\infty K(s)ds=1, \quad (4.62)$$

$$\langle V^2\rangle_{Av}=\sum \lambda_j^2\langle Z_j^2\rangle_{Av}+\sum_{j\neq k}\lambda_j\lambda_k\langle Z_jZ_k\rangle_{Av}$$

$$=\sum_1^\infty \lambda_j^2+(\sum \lambda_j)^2 \quad (4.63)$$

$$=1+\sum \lambda_j^2.$$

For the fluctuation

$$\sigma^2=\langle V^2\rangle_{Av}-\langle V\rangle_{Av}^2. \quad (4.64)$$

We thus obtain

$$\sigma^2=\sum \lambda_j^2=\int_0^\infty\int_0^\infty K(s)K(t)\rho^2(s-t)dsdt, \quad (4.65)$$

this being the trace of the first iterated kernel.

V. DERIVATION OF THE PROBABILITY DENSITY FOR SIGNAL AND NOISE

For the case of signal and noise only one derivation will be given here, since the direct derivation runs parallel to the analogous derivation for noise alone. The i-f input voltage $V_{\text{I.F.}}^{(i)}$ is in this case given by

$$V_{\text{I.F.}}^{(i)}=[x(t)+\alpha(t)]\cos 2\pi f_0 t+[y(t)+\beta(t)]\sin 2\pi f_0 t, \quad (5.11)$$

where $x(t)$, $y(t)$ are the input white noise amplitudes, and $\alpha(t)$, $\beta(t)$ are the input signal amplitudes. The i-f output voltage is then given by

$$V_{\text{I.F.}}^{(o)}=[X(t)+p(t)]\cos 2\pi f_0 t+[Y(t)+q(t)]\sin 2\pi f_0 t, \quad (5.12)$$

where X and Y are defined as above and

$$p(t)=\int_{-\infty}^\infty Q(t-\tau)\alpha(\tau)d\tau \quad \text{and} \quad q(t)=\int_{-\infty}^\infty Q(t-\tau)\beta(\tau)d\tau \quad (5.13)$$

are the signal amplitudes after the i-f amplifier. The detector output voltage is then

$$V_D^{(o)}=[X(t)+p(t)]^2+[Y(t)+q(t)]^2 \quad (5.14)$$

and the output of the video amplifier is

$$V(t)=\int_{-\infty}^\infty K(t-\theta)d\theta\{[X(\theta)+p(\theta)]^2+[Y(\theta+q(\theta)]^2\}$$

$$=\int_{-\infty}^\infty K(t-\theta)d\theta\int_{-\infty}^\infty\int Q(\theta-\tau_1)Q(\theta-\tau_2)\{[X(\tau_1)+\alpha(\tau_1)][x(\tau_2)+\alpha(\tau_2)]$$

$$+[y(\tau_1)+\beta(\tau_1)][y(\tau_2)+\beta(\tau_2)]\}d\tau_1 d\tau_2. \quad (5.15)$$

Changing variables to

$$\theta'=t-\theta,\ \tau_1'=t-\tau_1,\ \tau_2'=t-\tau_2, \quad (5.16)$$

we obtain

$$V(t)=\int_{-\infty}^{\infty}K(\theta')d\theta'\iint_{-\infty}^{\infty}Q(\tau_1'-\theta')Q(\tau_2'-\theta')\{[x(t-\tau_1')+\alpha(t-\tau_1')][x(t-\tau_2')+\alpha(t-\tau_2')]$$
$$+[y(t-\tau_1')+\beta(t-\tau_1')][y(t-\tau_2')+\beta(t-\tau_2')]\}d\tau_1'd\tau_2'$$
$$=\int_{-\infty}^{\infty}\Lambda(\tau_1,\tau_2)d\tau_1d\tau_2\{[x(t-\tau_1)+\alpha(t-\tau_1)][x(t-\tau_2)+\alpha(t-\tau_2)]$$
$$+[y(t-\tau_1)+\beta(t-\tau_1)][y(t-\tau_2)+\beta(t-\tau_2)]\}. \quad (5.17)$$

We now expand noise and signal amplitudes in terms of the eigen functions ϕ_j of Λ, writing

$$\begin{aligned} x(t-\tau)&=\textstyle\sum_j u_j\phi_j(\tau), \quad \alpha(t-\tau)=\sum_j\alpha_j(t)\phi_j(\tau),\\ y(t-\tau)&=\textstyle\sum_j v_j\phi_j(\tau), \quad \beta(t-\tau)=\sum_j\beta_j(t)\phi_j(\tau), \end{aligned} \quad (5.18)$$

and obtain

$$V(t)=\textstyle\sum_j\lambda_j\{[u_j+\alpha_j(t)]^2+[v_j+\beta_j(t)]^2\}. \quad (5.19)$$

The probability density of the variables u_j and v_j are $\pi^{-\frac{1}{2}}\exp(-u_j^2)$ and $\pi^{-\frac{1}{2}}\exp(-v_j^2)$, respectively, and the characteristic function for $V(t)$ is, therefore, given by

$$\langle e^{i\xi V}\rangle_{Av}=\int_{-\infty}^{\infty}\cdots\int\exp\{i\xi\textstyle\sum_j\lambda_j[(u_j+\alpha_j)^2+(v_j+\beta_j)^2]\}\prod_j\dfrac{\exp[-(u_j^2+v_j^2)]}{\pi}du_jdv_j$$

$$=\prod_j\frac{1}{\pi}\iint_{-\infty}^{\infty}du_jdv_j\exp\{-[(u_j^2+v_j^2)(1-i\xi\lambda_j)-2i\xi\lambda_j(u_j\alpha_j+v_j\beta_j)]+i\xi\lambda_j(\alpha_j^2+\beta_j^2)\}$$

$$=\prod_j\frac{1}{\pi}\iint_{-\infty}^{\infty}du_jdv_j\exp\left\{\left(-u_j(1-i\xi\lambda_j)^{\frac{1}{2}}-\frac{i\xi\lambda_j\alpha_j}{(1-i\xi\lambda_j)^{\frac{1}{2}}}\right)^2-\left(v_j(1-i\xi\lambda_j)^{\frac{1}{2}}-\frac{i\xi\lambda_j\beta_j}{(1-i\xi\lambda_j)^{\frac{1}{2}}}\right)^2\right\}$$
$$\times\exp\left[-\frac{\lambda_j^2\xi^2(\alpha_j^2+\beta_j^2)}{1-i\xi\lambda_j}+i\xi\lambda_j(\alpha_j^2+\beta_j^2)\right], \quad (5.21)$$

$$\langle e^{i\xi V}\rangle_{Av}=\prod_j\frac{\exp[i\xi\lambda_j(\alpha_j^2+\beta_j^2)/(1-i\xi\lambda_j)]}{1-i\xi\lambda_j}. \quad (5.22)$$

The Fourier inversion integral of this expression which represents the probability density cannot be evaluated in closed form.

We shall check this expression by deriving the known [4] probability density for the voltage after a quadratic detector. This distribution is obtained in the limit of infinitely wide video band width, which implies that

$$\int_0^{\infty}K(\theta)\psi(\theta)d\theta=\psi(0) \quad (5.31)$$

for any function $\psi(\theta)$. Then $\Lambda(\tau_1\tau_2)$ becomes simply the product $Q(\tau_1)Q(\tau_2)$ and the integral equation reduces to

$$Q(\tau_1)\int_{-\infty}^{\infty}Q(\tau_2)\phi(\tau_2)d\tau_2=\lambda\phi(\tau_1). \quad (5.32)$$

The only eigenfunction of this integral equation is of the form $CQ(\tau_1)$ where C is a constant, and from

[4] S. A. Goudsmit, RL 43-21; K. A. Norton and V. D. Landon, Proc. I.R.E. **30**, 425, Sept. 42; J. C. Slater, RL V-23; D. G. Fink, Report T8; D. O. North, RCA Tech. Rep. PTR6C.

$\int_{-\infty}^{\infty} Q^2(\tau)d\tau = 1$ we have $C=1$ and $\lambda=1$. The characteristic function, therefore, reduces to

$$\frac{\exp i\xi(\alpha^2+\beta^2)/(1-i\xi)}{1-i\xi},$$

where

$$\alpha = \int_{-\infty}^{\infty} \alpha(t-\tau)Q(\tau)d\tau = \int_{-\infty}^{\infty} \alpha(\tau')Q(\tau-\tau')d\tau' = p(t),$$
$$\beta = \int_{-\infty}^{\infty} \beta(t-\tau)Q(\tau)d\tau = \int_{-\infty}^{\infty} \beta(\tau')Q(t-\tau')d\tau' = q(t). \tag{5.33}$$

Calling the signal after the detector $s^2 = s^2(t)$ we have

$$s^2(t) = p^2(t)+q^2(t) = \alpha^2+\beta^2, \tag{5.34}$$

and

$$P(V) = \frac{1}{2\pi}\int_{-\infty}^{\infty} \frac{\exp(-i\xi V + i\xi s^2/(i-i\xi))}{(1-i\xi)}d\xi$$
$$= \frac{1}{2\pi}\oint^{-i,-} \frac{\exp(-i\xi V + i\xi s^2/(1-i\xi))}{1-i\xi}d\xi \tag{5.35}$$

for $V>0$ and zero otherwise. With $u = 1-i\xi$ this becomes

$$P(V) = \exp(-V-s^2)\frac{1}{2\pi i}\int^{0,+} \exp[Vu+s^2/u]du/u$$
$$= \exp(-V-s^2)J_0(2is\sqrt{V}) \text{ for } V>0 \text{ and} \tag{5.36}$$

zero otherwise, where J_0 is the Bessel function of order 0. This result is in agreement with the earlier results.

VI. DIRECT DERIVATION FOR NOISE ALONE

In order to give a direct derivation of the results obtained in Section 4, we investigate the probability density of the function

$$V(t) = \int_0^T K(u)[x^2(t-u)+y^2(t-u)]du \tag{6.11}*$$

and let, at an appropriate instant, T approach infinity. For the sake of simplicity, we shall restrict ourselves to the case $K(u)>0$. We divide the interval $(0, T)$ into a large number n of equal subintervals and consider the expression

$$\frac{T}{n}\sum_{j=1}^{n}[x^2(t-u_j)+y^2(t-u_j)]K(u_j); \tag{6.12}$$
$$\frac{j-1}{n}T < u_j < \frac{j}{n}T.$$

* For convenience, x and y are used in this section to denote the quantities formerly denoted by X and Y.

The characteristic function of the joint probability density of

$$x_1 = x(t-u_1), \quad x_2 = x(t-u_2), \quad \cdots, \quad x_n = x(t-u_n)$$

defined as the average

$$\left\langle \exp\left[i\sum_1^n \xi_j x(t-u_j)\right]\right\rangle_{Av}$$

is easily found to be

$$\exp\left[-\frac{1}{4}\sum_{j,k=1}^{n} \rho_T(u_j-u_k)\xi_j\xi_k\right] \tag{6.13}$$

where the correlation coefficients ρ_T for the finite interval T are defined as

$$\rho_T(t) = \frac{1}{T}\sum_{-\infty}^{\infty} A(f_k)\cos 2\pi f_k t, \tag{6.14}$$

and

$$A(f) = B^2(f) = |\gamma^2(f\pm f_0)|. \tag{6.15}$$

Thus the joint probability density of

$$x_1, x_2, x_3, \cdots, x_n$$

is given by the formula

$$\frac{1}{(2\pi)^n}\int_{-\infty}^{\infty}\cdots\int_{-\infty}^{\infty}\exp\left\{-i\sum_1^n \xi_j x_j\right\}$$
$$\times\exp\left\{-\frac{1}{4}\sum_1^n \rho_T(u_j-u_k)\xi_j\xi_k\right\}d\xi_1\cdots d\xi_n$$
$$=\frac{1}{(\sqrt{\pi})^n}\frac{1}{\sqrt{D}}\exp\left\{-\sum_1^n \alpha_{jk}x_j x_k\right\}, \quad (6.16)$$

where the matrix $[\alpha_{jk}]$ is the inverse of the correlation matrix $[\rho_T(u_j-u_k)]$ and D the determinant of the correlation matrix.

We next find the characteristic function of

$$\frac{T}{n}\sum_1^n K(u_j)x^2(t-u_j),$$

i.e., the average

$$\left\langle\exp\left\{\frac{i\xi T}{n}\sum_1^n K(u_j)x^2(t-u_j)\right\}\right\rangle_{Av}.$$

We have

$$\left\langle\exp\left\{\frac{i\xi T}{n}\sum_1^n K(u_j)x^2(t-u_j)\right\}\right\rangle_{Av}$$
$$=\frac{1}{(\sqrt{\pi})^n}\frac{1}{\sqrt{D}}\int_{-\infty}^{\infty}\cdots\int_{-\infty}^{\infty}\exp\left\{\frac{i\xi T}{n}\sum_1^n K(u_j)x_j^2\right\}$$
$$\times\exp\left\{-\sum_1^n \alpha_{jk}x_j x_k\right\}dx_1\cdots dx_n. \quad (6.21)$$

Since $K(u_j)>0$ we can introduce the new variables

$$x_j'=[K(u_j)]^{\frac{1}{2}}x_j. \quad (6.22)$$

Obtaining

$$\left\langle\exp\left\{\frac{i\xi T}{n}\sum_1^n K(u_j)x^2(t-u_j)\right\}\right\rangle_{Av}$$
$$=\frac{1}{(\sqrt{\pi})^n}\frac{1}{\sqrt{\ }}\frac{1}{\prod_1^n[K(u_j)]^{\frac{1}{2}}}$$
$$\times\int_{-\infty}^{\infty}\cdots\int_{-\infty}^{\infty}\exp\left\{\frac{i\xi T}{n}\sum_1^n x_j'^2\right\}$$
$$\times\exp\left\{-\sum_1^n \beta_{jk}x_j'x_k'\right\}dx_1'\cdots dx_n', \quad (6.23)$$

where

$$\beta_{jk}=\frac{\alpha_{jk}}{[K(u_j)]^{\frac{1}{2}}[K(u_k)]^{\frac{1}{2}}}. \quad (6.24)$$

Let $\mu_1^{(n)}, \mu_2^{(n)}, \cdots, \mu_n^{(n)}$ be the eigenvalues of the matrix $[\beta_{jk}]$; then changing the coordinates in the last integral to "principal axes" of the "ellipsoid"

$$\sum_1^n \beta_{jk}x_j'x_k'=1 \quad (6.25)$$

and noting that $\sum x_j'^2$ remains invariant under the transformation, we get easily

$$\left\langle\exp\left\{\frac{i\xi T}{n}\sum_1^n K(u_j)x^2(t-u_j)\right\}\right\rangle_{Av}$$
$$=\frac{1}{\sqrt{D}\prod_1^n[K(u_j)]^{\frac{1}{2}}}\frac{1}{\prod_1^n\left(\mu_j^{(n)}-\frac{i\xi T}{n}\right)^{\frac{1}{2}}}. \quad (6.26)$$

Since we have assumed that $A(f)$ is an even function we can show without much difficulty that

$$\sum_1^n K(u_j)x^2(t-u_j) \quad \text{and} \quad \sum_1^n K(u_j)y^2(t-u_j)$$

are independent in the statistical sense of the word. Thus the characteristic function of

$$\frac{T}{n}\sum_1^n K(u_j)\{x^2(t-u_j)+y^2(t-u_j)\} \quad (6.27)$$

is

$$\frac{1}{D\prod_1^n K(u_j)\prod_1^n\left(\mu_j^{(n)}-\frac{i\xi T}{n}\right)}$$

we now observe that the matrix $[\beta_{jk}]$ is the inverse of the matrix

$$[(K(u_j))^{\frac{1}{2}}\rho_T(u_j-u_k)(K(u_k))^{\frac{1}{2}}] \quad (6.28)$$

and that the determinant of (6.28) is

$$D\prod_1^n K(u_j).$$

Denoting by $\lambda_1^{(n)}, \lambda_2^{(n)}, \cdots, \lambda_n^{(n)}$, the eigenvalues of matrix (6.28) we see that the μ's are the inverses of the λ's and that

$$D\prod_1^n K(u_j)=\lambda_1^{(n)}\cdot\lambda_2^{(n)}\cdots\lambda_n^{(n)}.$$

These facts imply that the characteristic function of (6.27) is

$$1\Big/\prod_1^n\left(1-\frac{iT}{n}\lambda_j^{(n)}\xi\right). \tag{6.29}$$

It follows from Hilbert's treatment of integral equations that the eigenvalues of matrix (6.28) when multiplied by T/n approach, as n approaches infinity, the eigenvalues of the integral equation

$$\int_0^T [K(s)]^{\frac{1}{2}}\rho_T(s-t)[K(t)]^{\frac{1}{2}}f(t)dt=\lambda f(s), \tag{6.31}$$

provided these eigenvalues are simple. Since the distribution of (6.27) approaches that of $V(t)$ we deduce that the characteristic function of $V(t)$ is given by the formula

$$1\Big/\prod_1^\infty(1-i\lambda_j^{(T)}\xi), \tag{6.32}$$

where $\lambda_1^{(T)}$, $\lambda_2^{(T)}$, $\cdots$, are the eigenvalues of the integral equation (6.31). For large T we can replace the integral equation (6.31) by

$$\int_0^\infty [K(s)]^{\frac{1}{2}}\rho(s-t)[K(t)]^{\frac{1}{2}}f(t)dt=\lambda f(s), \tag{6.33}$$

and the characteristic function of $V(t)$ by

$$1/\prod_j(1-i\lambda_j\xi), \tag{6.34}$$

where λ_1, λ_2, λ_3, $\cdots$ are now the eigenvalues of the integral equation (6.34) which we again assume to be simple. The probability density $P(V)$ of V can now be expressed by means of the inversion formula

$$P(V)=\frac{1}{2\pi}\int_{-\infty}^{\infty}\frac{e^{-iV\xi}}{\prod_j(1-i\lambda_j\xi)}d\xi. \tag{6.35}$$

At the end of Section 4, the integration has been carried out by the method of residues. The justification of the formal integration is not quite simple since one must investigate the behavior of the entire function

$$\phi(Z)=\prod_1^\infty(1-i\lambda_jZ)$$

for large $|Z|$.[5] However, it can be considerably simplified if one assumes that for some $\nu(0<\nu<1)$ the series

$$\sum_1^\infty \lambda_j^\nu$$

converges. On the other hand it is easy to see that the exact probability density $P(V)$ is the limit, as n approaches infinity, of $P_n(V)$ where

$$P_n(V)=\sum_{s=1}^n\frac{\exp(-V/\lambda_s)}{\lambda_s\prod_1^{n\prime}(1-\lambda_j/\lambda_s)};\quad V>0. \tag{6.36}$$

$P_n(V)=0$; $V<0$ since with the assumption $K(u)>0$ negative eigenvalues cannot occur. In fact, the characteristic function corresponding to $P_n(V)$ which is seen to be

$$\prod_1^n\frac{1}{1-i\xi\lambda_j}$$

approaches the characteristic function associated with $P(V)$ thus $P_n(V)$ approaches $P(V)$.

VII. EXPLICIT SOLUTIONS IN SOME SPECIAL CASES

1. Single-Tuned I.F. with Simple Low Pass Video

For the special case of a single tuned i-f amplifier with the video amplifier acting as a simple low pass filter the integral equation can be solved explicitly and the eigenvalues can be expressed in terms of roots of Bessel functions. For one special ratio of video band width to i-f band width it is even possible to obtain $P(V)$ in closed form. For other ratios it is not too difficult to sum the series for $P(V)$ numerically.

The correlation function $\rho(t)$ is in this case

$$\rho(t)=e^{-\alpha|t|} \tag{7.11}$$

which is equivalent to writing

$$A(f)=\frac{\text{Const.}}{1+(2\pi f/\alpha)^2}. \tag{7.12}$$

[5] We note that $\phi(Z)=D(iZ)$ where $D(\mu)$ is the Fredholm Determinant of the above integral equation. It is noteworthy that this relationship between the characteristic function of $P(V)$ and the Fredholm Determinant persists, even in the general case in which $K(t)$ is not assumed positive (in which case the simple product representation need not hold, since $\Sigma\lambda$ need not converge). In the general case one must take the Fredholm Determinant of the kernel $K(t)\rho(s-t)$.

For the video we assume

$$K(u)=\begin{cases}0 & ,\ u>0\\ \beta\exp(-\beta u),\ u<0\end{cases} \tag{7.13}$$

i.e.,

$$C(f)=\frac{1}{1+2\pi if/\beta}. \tag{7.14}$$

The integral equation (6.33) now assumes the form

$$\beta\int_0^\infty e^{-\alpha|s-t|}e^{-(\beta/2)(s+t)}f(t)dt=\lambda f(s). \tag{7.15}$$

Putting

$$\psi(t)=\exp\left(\frac{\beta}{2}t\right)f(t) \tag{7.16}$$

we have

$$\int_0^\infty \exp(-\alpha|s-t|)\exp(-\beta t)\psi(t)dt=\frac{\lambda}{\beta}\psi(s). \tag{7.17}$$

This integral equation is solved by[6]

$$\psi(s)=J_{2\alpha/\beta}\left[2\left(\frac{2\alpha}{\beta\lambda}\right)^{\frac{1}{2}}e^{-\beta s/2}\right] \tag{7.18}$$

and the eigenvalues are determined by

$$J_{(2\alpha/\beta)-1}[2(2\alpha/\beta\lambda)^{\frac{1}{2}}]=0. \tag{7.19}$$

Thus the eigenvalues of our integral equation are expressible in terms of roots of Bessel functions and are seen to be simple. It is interesting to note that if $2\alpha/\beta=\frac{3}{2}$ we can express $P(V)$ in terms of one of the theta functions. In fact, if $2\alpha/\beta=\frac{3}{2}$, Eq. (7.19) assumes the form

$$J_{\frac{1}{2}}[(6/\lambda)^{\frac{1}{2}}]=0 \tag{7.21}$$

and since

$$J_{\frac{1}{2}}(x)=\left(\frac{2}{\pi}\right)^{\frac{1}{2}}\frac{\sin x}{\sqrt{x}} \tag{7.22}$$

we see that

$$\lambda_n=\frac{6}{\pi^2}\frac{1}{n^2}\quad(n=1,2,\cdots) \tag{7.23}$$

and formula (6.36) for $V>0$ becomes

$$P(V)=\frac{\pi^2}{6}\sum_{s=1}^{\infty}\frac{s^2\exp(-\pi^2s^2V/6)}{\prod_j{}'(1-(s^2/j^2))}. \tag{7.24}$$

[6] For the solution and discussion of the integral equation see M. L. Juncosa "An integral equation related to Bessel functions," Duke Math. J. 12, 465–471 (1945).

It can be shown quite easily that

$$\prod_j{}'\left(1-\frac{s^2}{j^2}\right)=-\frac{\cos\pi s}{2} \tag{7.25}$$

and therefore,

$$P(V)=\frac{\pi^2}{3}\sum_{s=1}^{\infty}(-1)^{s+1}s^2\exp(-\pi^2s^2V/6). \tag{7.26}$$

Introducing the theta-function notation

$$\theta(q;0)=1-2q+2q^4-2q^9+\cdots \tag{7.27}$$

we have

$$q\theta'(q;0)=-2\sum_{s=1}^{\infty}(-1)^{s+1}s^2q^{s^2} \tag{7.28}$$

and finally

$$P(V)=-\frac{\pi^2}{6}\exp\left(\frac{\pi^2V}{6}\right)\theta'(e^{-\pi^2V/6};0). \tag{7.29}$$

For other values of the ratio α/β we can calculate values of $P(V)$ and plot the corresponding graphs.

2. The Noise Power, Averaged over a Finite Time Interval

In some problems it is of interest to know the distribution of the average

$$M=\frac{1}{\tau}\int_0^\tau I^2(t)dt. \tag{7.31}$$

The derivation of Section 4 is clearly applicable to this case if we put

$$K(u)=\begin{cases}1/\tau,\ 0<u<\tau\\ 0\text{ elsewhere.}\end{cases} \tag{7.32}$$

The probability density is given by (4.46) replacing V by M except that the λ's are now eigenvalues of the integral equation

$$\frac{1}{\tau}\int_0^\tau \rho(s-t)f(t)dt=\lambda f(s). \tag{7.33}$$

In the simple case

$$\rho(t)=e^{-\alpha|t|} \tag{7.34}$$

the eigenvalues can be shown to be given by the formula

$$\lambda_m=\frac{2}{g}\frac{1}{1+y_m^2} \tag{7.35}$$

where y_m is the mth (positive) root of the equation

$$\tan gy = -2y/(1-y^2) \tag{7.36}$$

and $g = \alpha\tau$.

VIII. APPROXIMATIONS FOR $P(V)$

At the end of Section 5, it was shown that, for infinitely wide video, $P(V)$ becomes identical with the well-known probability density of the output voltage of a quadratic detector. We will derive now an approximation for the case that the video band width is very large compared with the i-f band width.

It can be shown that in this case one of the eigenvalues say λ_1, tends to unity while all others approach zero. In order to obtain the dependence of the eigenvalues on the band width ratio we shall write

$$A(f') = \frac{1}{B} a\left(\frac{f'}{B}\right) \tag{8.11}$$

and

$$C(f) = c\left(\frac{f-f_0}{b}\right), \tag{8.12}$$

where

$$\int_{-\infty}^{\infty} a(\nu)d\nu = 1 \tag{8.13}$$

and

$$c(f_0/b) = 1 \tag{8.14}$$

in conformity with our original normalization for $A(f)$ and $K(t)$. The limiting process is carried through for $B/b = \epsilon \to 0$, while the functions $a(\nu)$ and $c(\nu)$ remain unchanged. In terms of A and C our integral equation becomes

$$\int_{-\infty}^{\infty} A(f_1)C(f_2-f_1)g(f_2)df_2 = \lambda g(f_1) \tag{8.21}$$

and traces S_k are, therefore,

$S_1 = 1$,

$$S_2 = \int_{-\infty}^{\infty}\int d\nu_1 d\nu_2 a(\nu_1)a(\nu_2) \times c(\epsilon[\nu_2-\nu_1]-f_0/b)c(\epsilon[\nu_1-\nu_2]-f_0/b), \tag{8.22}$$

$$S_3 = \int_{-\infty}^{\infty}\int\int d\nu_1 d\nu_2 d\nu_3 a(\nu_1)a(\nu_2)a(\nu_3) \times c(\epsilon[\nu_2-\nu_1]-f_0/b)c(\epsilon[\nu_1-\nu_3]-f_0/b) \times c(\epsilon[\nu_3-\nu_2]-f_0/b),$$

etc. Expanding $c(\epsilon\nu - f_0/b)$ in a power series around f_0/b we shall write

$$c(\epsilon\nu - f_0/b) = 1 + C_1\epsilon\nu + C_2\epsilon^2\nu^2 + \cdots. \tag{8.23}$$

Assuming that

$$\int_{-\infty}^{\infty} a(\nu)\nu^4 d\nu$$

is finite we obtain the following approximations:

$$\begin{aligned} S_2 &\cong 1 + \alpha\epsilon^2 + 0(\epsilon^4), \\ S_3 &\cong 1 + 3\alpha\epsilon^2/2 + 0(\epsilon^4), \\ S_4 &\cong 1 + 2\alpha\epsilon^2 + 0(\epsilon^4), \end{aligned} \tag{8.24}$$

where

$$\alpha = 2(2C_2 - C_1^2)\int_{-\infty}^{\infty} a(\nu)\nu^2 d\nu \tag{8.25}$$

and essential use has been made of the fact that $a(\nu) = a(-\nu)$. Noticing that

$$\lambda_1^2 S_2 > S_4 \tag{8.26}$$

(since $S_n = \sum_1^\infty \lambda_k^n$, and λ_1 is by defintion the largest eigenvalue) we obtain

$$\lambda_1^2 > S_4/S_2 = 1 + \alpha\epsilon^2 + 0(\epsilon^4). \tag{8.27}$$

Therefore, $\sum_2^\infty \lambda_k^2$ is of order ϵ^4 or higher, and $\sum_2^\infty \lambda_k^4$ is of order ϵ^8 or higher. Now we notice that

$$(S_4)^{\frac{1}{4}} = \lambda_1 + 0(\epsilon^8) \tag{8.28}$$

so that

$$\lambda_1 = 1 + \alpha\epsilon^2/2 + 0(\epsilon^4). \tag{8.29}$$

Making use of the expression

$$V = \sum_1^\infty \lambda_k Z_k \tag{8.31}$$

[cf. Eqs. (4.42), (4.43)], we write

$$V = V_1 + v \tag{8.32}$$

with

$$V_1 = 1 - \lambda_1 + \lambda_1 Z_1 \tag{8.33}$$

and

$$v = \sum_2^\infty \lambda_k (Z_k - 1). \tag{8.34}$$

If $P_1(V_1)$ is the probability density of V_1, given by

$$P_1(V_1) = 0 \quad \text{for} \quad V_1 < 1 - \lambda_1 \tag{8.35}$$

and

$$P_1(V_1) = \lambda_1^{-1} \exp\frac{V_1 - (1-\lambda_1)}{\lambda_1} \quad \text{for} \quad V_1 > (1-\lambda_1),$$

and $w(v)$ is the probability density of v, we have

for $P(V)$ the exact expression

$$P(V)=\int_{-\infty}^{\infty} dvP_1(V-v)w(v)$$
$$=\int_{-\infty}^{V-1+\lambda_1} dvP_1(V-v)w(v). \quad (8.36)$$

Since the width of $w(v)$ is of order ϵ^2 we can use $P_1(V)$ as the first approximation of $P(V)$. To discuss the reliability of this appproximation we expand $P(V)$ in the form

$$P(V)=P_1(V)-P_1'(V)\int_{-\infty}^{V-1+\lambda_1} vdvw(v)$$
$$+\tfrac{1}{2}P_1''(V)\int_{-\infty}^{V-1+\lambda_1} v^2dvw(v)$$
$$+\frac{1}{3!}\int_{-\infty}^{V-1+\lambda_1} v^3dvw(v)P_1'''(V-\xi) \quad (8.37)$$

where, in the last term,

$$0<\xi<|v|.$$

For any fixed value of $V>0$, the integrals in the first and second term can be replaced by $\bar{v}=0$ and $\langle v^2\rangle=\sum_2^\infty \lambda_k^2$ with an error of order ϵ^4 or smaller, because

$$\int_{V-(1-\lambda_1)}^{\infty} vdvw(v)$$
$$<\int_0^\infty \frac{v^4}{[V-(1-\lambda_1)]^3}w(v)dv=0(\epsilon^8), \quad (8.38)$$
$$\int_{V-(1-\lambda_1)}^{\infty} v^2dvw(v)$$
$$<\int_0^\infty \frac{v^4}{[V-(1-\lambda_1)]^2}w(v)dv=0(\epsilon^8).$$

The last term in (8.37) can be shown to be of order ϵ^6 or higher. Thus we have

$$P(V)=P_1(V)+\tfrac{1}{2}P_1''(V)\langle v^2\rangle_{Av}+0(\epsilon^6) \quad (8.39)$$

for any fixed $V>0$. Substituting

$$\lambda_1=1+\alpha\epsilon^2/2+0(\epsilon^4)$$

and

$$\langle v^2\rangle_{Av}=\sum_{k=2}^{\infty}\lambda_k^2=0(\epsilon^4),$$

we see that for fixed $V>0$, $P_1(V)$ is a good approximation except for terms of order ϵ^4 and higher.

If, in addition, the existence of

$$\int_{-\infty}^{\infty} a(v)v^6dv \quad (8.41)$$

is assumed the approximation can be improved by including the term

$$\tfrac{1}{2}P_1''(V)\langle v^2\rangle_{Av}$$

where

$$\langle v^2\rangle_{Av}=S_2-(S_6)^{\frac{1}{3}}+0(\epsilon^{12}) \quad (8.42)$$

and λ_1 [which occurs in $P_1(V)$] is calculated from

$$\lambda_1=(S_4)^{\frac{1}{2}}+0(\epsilon^8). \quad (8.43)$$

Substituting these values we obtain an approximation for $P(V)$ valid up to terms of order ϵ^4 inclusive. In the neighborhood of $V=0$, no approximation which utilizes only the traces of a limited number of iterated kernels, can be expected to hold, since there—as can be seen from the general solution—the eigenvalues individually determine the shape.

The considerations of this section cannot be expected to be applicable to the case treated exactly in Section 7 since there not even

$$\int_{-\infty}^{\infty} a(v)v^2dv$$

exists. In that case one sees directly that the eigenvalues are such that

$$\lambda_1=1-0(\epsilon), \quad \sum_2^\infty \lambda_k^2=0(\epsilon^2).$$

In order to be able to obtain a general approximation for wide videos one must demand that the i-f spectrum falls off sufficiently rapidly at infinity.

In the opposite limit, $b/B\to 0$, similar considerations show that $P(V)$ becomes Gaussian with mean $\langle V\rangle_{Av}=1$ and spread proportional to $(b/B)^{\frac{1}{2}}$.

IX. APPLICATION TO A DISCRETE CASE

For some applications of noise theory it is desirable to have the characteristic function

$$\exp\left\langle i\sum_{k=1}^{n}\xi_kI_k\right\rangle_{Av}=\phi(\xi_1\cdots\xi_n) \quad (9.11)$$

of the joint probability of n successive values $I_1, I_2 \cdots, I_n$; $I_k = x^2(t_k) + y^2(t_k)$ of the detector output, from which the averages of products $\langle \prod_k I_k^{m_k} \rangle_{Av}$ (m_k integer) can be derived. $\phi(\xi_1 \cdots \xi_n)$ can be obtained by carrying through the idea of transformation to principal axes for the discrete case, that is, by a slight modification of Section 6. However, we shall derive $\phi(\xi_1 \cdots \xi_n)$ from the results of Section 4 since this seems the quicker way.

We simply chose for $K(t)$ the function

$$K(t) = \frac{1}{\xi} \sum_1^n \xi_k \delta(t - t_k) \tag{9.12}$$

where $\xi = \sum_1^n \xi_k$ for the sake of normalization, and the time variable t is chosen in such a way that all $t_k < 0$. For this choice of $K(t)$ we have

$$V = \int_0^\infty K(t)[x^2(t) + y^2(t)]dt = \frac{1}{\xi} \sum_1^n \xi_k I_k \tag{9.13}$$

and, provided that the I_k are normalized so that $\langle I_k \rangle_{Av} = 1$, we have

$$\phi(\xi_1 \cdots \xi_n) \equiv e^{i\Sigma \xi_k I_k} = \langle e^{i\xi V} \rangle_{Av} = \frac{1}{\prod_j (1 - i\lambda_j \xi)}. \tag{9.14}$$

The integral equation, whose eigenvalues are λ_j degenerates in this case into a system of linear equations for n discrete variables $f(t_k) = f_k$:

$$\frac{1}{\xi} \sum_{k=1}^n \xi_k \rho_{km} f_k = \lambda f_m, \tag{9.15}$$

where

$$\rho_{km} = \rho(t_k - t_m)$$

with

$$\Lambda = \xi \lambda.$$

We write these equations as

$$\sum_{k=1}^n \xi_k \rho_{km} f_k = \Lambda f_m. \tag{9.16}$$

To obtain ϕ, it is not necessary actually to determine the eigenvalues since the product $\prod_j (1 - i\Lambda_j)$ can be expressed in terms of the determinant $\det |\xi_k \rho_{km} + i\delta_{km}|$ as follows:
We note that

$\prod_1^n (iu - i\Lambda_j)$ is a polynomial in u which has zeros at $u = \Lambda_j$ and starts with $i^n u^n$. The determinant $\det |\xi_k \rho_{km} - u\delta_{km}|$ is a polynomial in u, which has the same roots and starts with $(-)^n u^n$. We therefore have

$$\prod_1^n (iu - i\lambda_j) = i^{-n} \det |\xi_k \rho_{km} - u\delta_{km}| \tag{9.17}$$

and, specially, for $u = -i$

$$\prod_1^n (1 - i\Lambda_j) = i^{-n} \det |\xi_k \rho_{km} + i\delta_{km}|.^7$$

The characteristic function is thus obtained as

$$\langle e^{i\Sigma \xi_k I_k} \rangle_{Av} = \frac{i^n}{\det |\xi_k \rho_{km} + i\delta_{km}|}. \tag{9.18}$$

While it has not been possible to evaluate the joint probability

$$W_n(I_1 \cdots I_n) = \frac{1}{(2\pi)^n} \int \cdots \int d\xi_1 \cdots d\xi_n \times \phi(\xi_1 \cdots \xi_n) e^{-i\Sigma \xi_k I_k}, \tag{9.19}$$

explicitly (except for $n = 1$ and $n = 2$, in which cases they are well known) one can obtain averages of the form

$$\langle \prod_k I_k^{m_k} \rangle_{Av} \text{ for integer values of } m_k,$$

by expanding both sides of (9.18) in power series in the variables ξ_k and by comparing coefficients.

[7] For the general kernel a corresponding relation can be derived between the above product and the Fredholm determinant of the kernel.

Heating and Cooling of Bolometer Elements

J. N. SHIVE
Bell Telephone Laboratories, Inc., Murray Hill, New Jersey
(Received January 20, 1947)

The analogy between thermal and electrical networks is used to obtain solutions to problems relating to the heating and cooling of air-backed and solid-backed bolometer elements exposed to radiation of periodically fluctuating intensity. From the equations derived, thermal response-frequency characteristics are computed for "typical" bolometer elements. Features of these characteristics are discussed, and the physical influences of the various thermal properties of the bolometer material and of the backing material are pointed out.

INTRODUCTION

IN some of the present-day applications of radiation bolometry the heat-sensitive receiver element is placed in series with another resistance, and a d.c. biasing voltage is applied across this series. The radiation incident upon the element is mechanically interrupted, as by a rotating sector disk, so that the element alternately heats and cools. Under these conditions an a.c. voltage is generated across the element, which, when amplified and measured, serves as an indication of the intensity of the incoming radiation.

The amplitude of the a.c. signal thus generated is approximately proportional to the biasing voltage across the receiver element. This, in turn, is limited by the rate at which the element can dissipate the Joule heat produced by the bias. If the element is placed in thermal contact with a solid backing through which this heat can be more rapidly dissipated, the bias voltage can be increased. The amplitude of the temperature fluctuation of the element due to the absorption of a given chopped radiation signal is reduced by the presence of such a backing, but this reduction, for certain ranges of chopping frequency, can be more than compensated for by the use of the higher biasing voltage made possible by the backing. In addition, the use of a backing brings about a faster approach to temperature equilibrium at each interruption of the radiation beam, so that the time constant of the element is correspondingly reduced, a consideration of importance, for example, in the rapid scanning of an infra-red spectrum.

There are a number of questions in connection with the backing of bolometer elements for which both experimental and theoretical answers have been sought. It is of importance to know, for example, what thermal properties and what geometry the backing should have in order to secure maximum dissipation of the bias heating with minimum reduction of the amplitude of the temperature fluctuations of the element. It is equally important to know the effect of such a backing on the frequency dependence of the element.

It is the purpose of this paper to demonstrate a method for obtaining answers to such questions by applying the mathematics of electrical network theory. The electrical analogy has long been useful in the solution of problems in mechanics and acoustics, and some applications have already been made in the field of heat flow.[1–4] Analytical expressions governing the behavior of bolometers

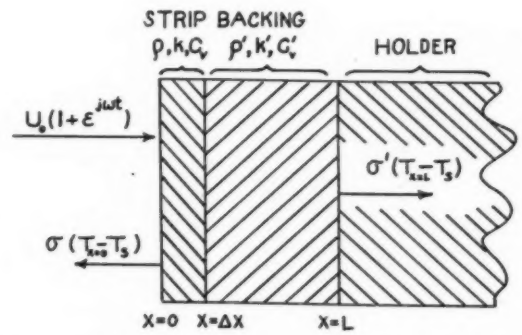

FIG. 1. Physical arrangement of bolometer strip, backing, and holder.

[1] V. Paschkis and M. P. Heisler, J. App. Phys. **17**, 246 (1946).
[2] C. D. McCann and H. E. Criner, Machine Design **17**, 137 (1945).
[3] V. Paschkis and H. D. Baker, Trans. A.S.M.E. **64**, 105 (1942).
[4] M. Avrami and V. Paschkis, Trans. A.I.C.E. **38**, 631 (1942).

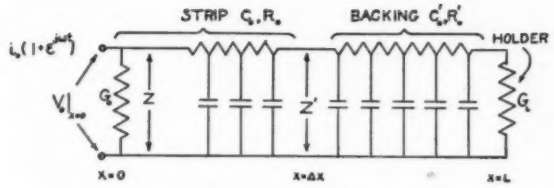

FIG. 2. Electrical analog of the bolometer assembly of Fig. 1.

will be developed from this analogy, and these will be employed in presenting graphical illustrations of the temperature fluctuation of the element in its dependence on the thermal properties of the bolometer and the backing, and on the chopping frequency.

General Equations for Backed Bolometers

Consider a thin strip of temperature-sensitive bolometer material of 1 sq. cm area and Δx thickness. Consider this strip to be fastened to a solid slab of backing material, also of 1 sq. cm area, and extending in thickness from $x=\Delta x$ to $x=L$. At $x=L$ let the backing slab be fastened in turn to some kind of holder or housing. This physical arrangement is sketched in Fig. 1.

Let the exposed front surface of the bolometer strip absorb an incident radiation signal of

$$U_0(1+\epsilon^{j\omega t})^* \qquad (1)$$

watts, where U_0 is half the radiant power per unit area in the unchopped beam, ω is 2π times the chopping frequency, and t is the time. Let heat be dissipated by reradiation and convection from the front face of the strip, according to Newton's law of cooling, at a rate of $\sigma(T_{x=0}-T_s)$ watts, where σ is the dissipation constant of the front face in watts per sq. cm per degree, $T_{x=0}$ is the instantaneous temperature of the front face, and T_s is the ambient temperature. Similarly let heat be lost from the rear surface of the backing slab to the holder at a rate $\sigma'(T_{x=L}-T_s)$ watts, where σ' is the backing-to-holder dissipation constant (here considered to be thermally nonreactive) and $T_{x=L}$ is the instantaneous temperature of the rear face of the backing. These various heat flows are indicated in Fig. 1. Consider the lateral surfaces of the bolometer and backing to be thermally insulated so that heat can flow only in the x coordinate.

Let k and k' be the thermal conductivities of the bolometer material and backing material, respectively, in watts per sq. cm per degree per cm, ρ and ρ' the respective densities in g per cc, and C_v and C_v' the respective specific heats in Joules per g degree. Then the respective thermal diffusivities K and K' are constants given by

$$K=k/\rho C_v \quad \text{and} \quad K'=k'/\rho' C_v'.$$

The electrical analog of the backed bolometer strip is a short transmission line (Fig. 2) having distributed series resistance R_0 and shunt capacity C_0 per unit length, looking into a longer transmission line representing the backing and having distributed series resistance R_0' and shunt capacity C_0' per unit length. The front-surface dissipation of the bolometer strip corresponds to a conductance G_0 hung across the input end of the short line, while the backing-to-holder dissipation corresponds to a conductance G_L terminating the long line. The following table of equivalents may be found useful in visualizing the correspondence of analogous thermal and electrical entities (Table I).

The problem is now that of finding the input voltage amplitude $V_0|_{x=0}$ as a function of frequency when a current

$$i_0(1+\epsilon^{j\omega t})$$

is fed into the network. The a.c. solution of this network may be obtained by considering the problem as that of a short line of input impedance Z (taken just inside the input dissipation conductance) and terminated at $x=\Delta x$ by the input

TABLE I.

Entity	Thermal	Electrical
Input flow, a.c. part	$U_{0\epsilon}{}^{j\omega t}$	$i_{0\epsilon}{}^{j\omega t}$
Input amplitude	$T_0\|_{x=0}$	$V_0\|_{x=0}$
Series resistance per unit length		
bolometer	$\frac{1}{k}$	R_0
backing	$\frac{1}{k'}$	R_0'
Shunt capacity per unit length		
bolometer	ρC_v	C_0
backing	$\rho' C_v'$	C_0'
Front-surface dissipation	$\sigma(T_{x=0}-T_s)$	$G_0V\|_{x=0}$
Backing-to-holder dissipation	$\sigma'(T_{x=L}-T_s)$	$G_LV\|_{x=L}$

* In (1) there is considered, for simplicity's sake, only the fundamental component of the multiply-harmonic radiant power input obtained by the usual mechanical chopping of the incident beam.

impedance Z' of the long line, which in turn is terminated at $x=L$ by the dissipation G_L. Thus, the solution is

$$\left.\begin{aligned} V_0|_{x=0} &= i_0/(G_0+1/Z) \\ \text{where } Z \text{ is given}^5 \text{ by} \\ Z &= Z_0\frac{Z_0\sinh\gamma\Delta x+Z'\cosh\gamma\Delta x}{Z_0\cosh\gamma\Delta x+Z'\sinh\gamma\Delta x}, \\ \text{and where, in turn, } Z' \text{ is given by} \\ Z' &= Z_0'\frac{Z_0'\sinh\gamma'(L-\Delta x)+\dfrac{1}{G_L}\cosh\gamma'(L-\Delta x)}{Z_0'\cosh\gamma'(L-\Delta x)+\dfrac{1}{G_L}\sinh\gamma'(L-\Delta x)}. \end{aligned}\right\} \tag{2}$$

In these equations Z_0 and γ are the characteristic impedance and propagation constant, respectively, of the short line representing the bolometer strip, and Z_0' and γ' are the corresponding constants for the long line representing the backing. For series-resistance shunt-capacity lines these quantities have the values:

$$\left.\begin{aligned} Z_0 &= (R_0/jC_0\omega)^{\frac{1}{2}} \\ \gamma &= (jR_0C_0\omega)^{\frac{1}{2}} \\ Z_0' &= (R_0'/jC_0'\omega)^{\frac{1}{2}} \\ \gamma' &= (jR_0'C_0'\omega)^{\frac{1}{2}} \end{aligned}\right\}. \tag{3}$$

With the quantities (3) replaced into (2), and with the corresponding thermal equivalents substituted into the resulting expressions, the amplitude of the temperature fluctuation at the front surface of the bolometer strip becomes

$$\left.\begin{aligned} T_0|_{x=0} &= U_0/(\sigma+1/Z_{\text{th}}), \\ \text{where} \\ Z_{\text{th}} &= \frac{1}{k}\left(\frac{K}{j\omega}\right)^{\frac{1}{2}}\frac{\dfrac{1}{k}\left(\dfrac{K}{j\omega}\right)^{\frac{1}{2}}\sinh\left(\dfrac{j\omega}{K}\right)^{\frac{1}{2}}\Delta x+Z'_{\text{th}}\cosh\left(\dfrac{j\omega}{K}\right)^{\frac{1}{2}}\Delta x}{\dfrac{1}{k}\left(\dfrac{K}{j\omega}\right)^{\frac{1}{2}}\cosh\left(\dfrac{j\omega}{K}\right)^{\frac{1}{2}}\Delta x+Z'_{\text{th}}\sinh\left(\dfrac{j\omega}{K}\right)^{\frac{1}{2}}\Delta x}, \\ \text{and where} \\ Z'_{\text{th}} &= \frac{1}{k'}\left(\frac{K'}{j\omega}\right)^{\frac{1}{2}}\frac{\dfrac{1}{k'}\left(\dfrac{K'}{j\omega}\right)^{\frac{1}{2}}\sinh\left(\dfrac{j\omega}{K'}\right)^{\frac{1}{2}}(L-\Delta x)+\dfrac{1}{\sigma'}\cosh\left(\dfrac{j\omega}{K'}\right)^{\frac{1}{2}}(L-\Delta x)}{\dfrac{1}{k'}\left(\dfrac{K'}{j\omega}\right)^{\frac{1}{2}}\cosh\left(\dfrac{j\omega}{K'}\right)^{\frac{1}{2}}(L-\Delta x)+\dfrac{1}{\sigma'}\sinh\left(\dfrac{j\omega}{K'}\right)^{\frac{1}{2}}(L-\Delta x)}. \end{aligned}\right\} \tag{4}$$

[5] A derivation of this expression for the input impedance of a distributed-constant line terminated by another impedance can be found, for instance, in Slater's *Microwave Transmission*, Chap. I.

The subscript th indicates that the impedances designated are thermal impedances.

Application to Air-Backed Bolometers

The above equations can equally well be applied to air-backed bolometers. For an air-backed element the only heat loss is by air dissipation at the front and rear surfaces. The thermal impedance of the backing in this case is replaced by the appropriate air-dissipation factor, so that Z'_{th} in (4) becomes simply $Z'_{th}=1/\sigma$. With this substitution the first two equations of (4) combine to give

$$T_0|_{x=0}=\frac{U_0}{\sigma+k\left(\frac{j\omega}{K}\right)^{\frac{1}{2}}\frac{\frac{1}{k}\left(\frac{K}{j\omega}\right)^{\frac{1}{2}}\cosh\left(\frac{j\omega}{K}\right)^{\frac{1}{2}}\Delta x+\frac{1}{\sigma}\sinh\left(\frac{j\omega}{K}\right)^{\frac{1}{2}}\Delta x}{\frac{1}{k}\left(\frac{K}{j\omega}\right)^{\frac{1}{2}}\sinh\left(\frac{j\omega}{K}\right)^{\frac{1}{2}}\Delta x+\frac{1}{\sigma}\cosh\left(\frac{j\omega}{K}\right)^{\frac{1}{2}}\Delta x}}. \tag{5}$$

Two approximations to (5) can be made, each being valid over a particular range of parameters, which simplify the task of interpreting physically the results obtained from (5). For small arguments the sinh is nearly equal to the argument and the cosh is nearly equal to unity. Thus, for

$$|(j\omega/K)^{\frac{1}{2}}\Delta x|\lesssim 0.3$$

Eq. (5) becomes

$$T_0|_{x=0}\simeq\frac{U_0(\sigma\Delta x+k)}{\sigma(\sigma\Delta x+2k)+\frac{jk^2\omega\Delta x}{K}}. \tag{5a}$$

For large arguments the sinh and cosh are nearly equal. Hence, if

$$|(j\omega/K)^{\frac{1}{2}}\Delta x|\gtrsim 1.8$$

Eq. (5) becomes

$$T_0|_{x=0}\simeq\frac{U_0}{\sigma+k(j\omega/K)^{\frac{1}{2}}}. \tag{5b}$$

Equations (5), (5a), and (5b) can be used to calculate theoretical response-frequency curves for various bolometers. By thermal response is meant the ratio $T_0|_{x=0}/U_0$ of the amplitude of the front-face temperature fluctuation to the amplitude of the incoming chopped radiation signal. Such a response-frequency curve is given by the solid curve of Fig. 3 for a typical bolometer strip made of thermistor material* and having:

$\Delta x=0.0018$ cm
$k=0.01$ watt/cm deg.
$\rho=5$ g/cc
$C_v=0.75$ joule/g deg.
$\sigma=0.005$ watt/sq. cm deg.

This curve is composed of the following three distinct regions, each being characteristic of a particular frequency range.

I. A frequency-independent region for very low frequencies in which, physically, the temperature of the entire flake is always in equilibrium with the incident radiation. From Eq.

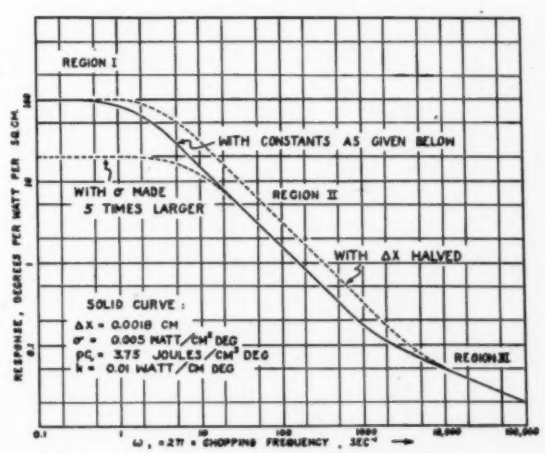
REGION I
WITH CONSTANTS AS GIVEN BELOW
WITH σ MADE 5 TIMES LARGER
REGION II
WITH ΔX HALVED
SOLID CURVE :
Δx = 0.0018 CM
σ = 0.005 WATT/CM² DEG
ρC_v = 3.75 JOULES/CM³ DEG
k = 0.01 WATT/CM DEG
REGION III
RESPONSE, DEGREES PER WATT PER SQ.CM.
ω, = 2π × CHOPPING FREQUENCY, SEC⁻¹

FIG. 3. Response-frequency characteristic for air-backed bolometer.

* Thermistor material is a mixture of certain semiconductor oxides. It has a large negative temperature coefficient of resistance.

(5a), appropriate to this region, it is apparent that the temperature fluctuations of the strip are in phase with the fluctuations of the incoming radiation.

II. An intermediate region in which the response is inversely proportional to the frequency. Here the strip temperature is no longer in equilibrium with the incoming radiation, and the phase of the former lags that of the latter by a quarter cycle. As will be shown below, the instantaneous temperature of the whole strip is effectively equal to that of the front surface over the entire frequency region for which this relationship holds. The thermal time constant of the strip is the reciprocal of the frequency at which the transition from region I to region II occurs.

III. A high frequency region in which the response obeys a $1/\sqrt{\omega}$ relationship, as given by (5b). Here the phase of the front-face temperature lags that of the incoming radiation by an eighth cycle.

The physical meaning of the transition from region II to region III can be understood from a consideration of the speed v and wave-length λ with which waves of temperature traverse the thickness of the strip in consequence of the periodic heating and cooling of the front face.

The propagation constant γ of the electrical line representing the bolometer, as given by Eq. (3) is: $\gamma=(jR_0C_0\omega)^{\frac{1}{2}}$. The imaginary part of this quantity, called the phase constant β, is: $\beta=(R_0C_0\omega/2)^{\frac{1}{2}}$. And the velocity v of electrical waves along this network is given by $v=\omega/\beta=(2\omega/R_0C_0)^{\frac{1}{2}}$. The thermal analog of this velocity expression is $v_{\text{therm}}=(2K\omega)^{\frac{1}{2}}$, while the wave-length λ of the temperature waves is

$$\lambda=\frac{2\pi v}{\omega}=2\pi(2K/\omega)^{\frac{1}{2}}.* \qquad (6)$$

Comparing (6) with the condition in (5b) for which the transition from region II to region III becomes practically complete, it is evident that $\lambda_{\text{III}}\lesssim 4\Delta x$. Thus, the transition corresponds, with increasing frequency, to the physical situation in which the temperature waves have become so short that their wave-length is comparable to the thickness of the strip, and the strip is no longer at the same instantaneous temperature throughout its entire thickness. Hence for chopping frequencies lying in region III various layers within the bolometer strip have temperatures different from $T|_{x=0}$, and the electrical output response of the bolometer bridge is no longer determined by $T_0|_{x=0}$, but rather by the average throughout the thickness of the strip of the local temperature fluctuation amplitude, with due regard for phase. It can be shown* that this electrical response continues to decrease like $1/\omega$ with increasing frequency, even though the front-face temperature fluctuation amplitude falls off like $1/\sqrt{\omega}$. It appears from these considerations that for chopping frequencies in regions I and II this solution could equally well have been obtained from a lumped-constant analogy as from a transmission line analogy.

In Fig. 3 are plotted two dashed curves showing how the response-frequency characteristic is altered if a change is made in the thickness of the strip or in the value of the dissipation constant. The dashed curve characteristic of the 5-times-greater dissipation constant becomes identical with the solid curve for $\omega\gtrsim 30$. It can be seen from this illustration that if, by backing or otherwise, the dissipation from the element can be increased, an advantage will be gained in the operation of the bolometer. For, with this 5-fold greater dissipation a $\sqrt{5}$-fold greater d.c. bias can be placed across the bolometer bridge, and for $\omega\gtrsim 30$ a $\sqrt{5}$-fold increase in the electrical signal to the amplifier will be obtained for a given radiation signal. Furthermore, the time constant has been decreased to $1/\sqrt{5}$ of its former value.

Unfortunately, there is no solid backing material whose dissipation is entirely conductive, and some thermal reactance due to the volume heat capacity of the material is inescapable. The effect of this reactance, as will be shown in the next section, is to modify the advantage gained by the use of a solid backing.

Application to Solid-Backed Bolometers

As an example of the kind of response-frequency curve to be expected for a solid-backed

* These expressions for wave-length and velocity of propagation of temperature waves in a semi-infinite medium were derived (otherwise) and used by Kelvin in his studies of the penetration of diurnal and annual waves of temperature into the earth.

* The author is particularly indebted to W. H. Brattain for helpful discussion of this subject.

bolometer there is shown in the solid curve of Fig. 4 the characteristic of the same strip bolometer as was used in the calculations for Fig. 3, but now fastened intimately to a rocksalt backing having the following dimensions and properties.

$$L = 0.1 \text{ cm}: \text{area} = 1 \text{ sq. cm}$$
$$k' = 0.07 \text{ watt/cm degree}$$
$$\rho' C_v' = 2 \text{ joules/cm}^3 \text{ degree}$$
$$\sigma' = 0.1 \text{ watt/cm}^2 \text{ degree}.$$

In the same figure appear a number of dashed curves showing the effects produced by varying, one or two at a time, some of the parameters of the backing. The caption adjacent to each dashed curve explains which parameter has been changed, and by how much. All of these curves have been computed from (4), using, wherever appropriate, the type of simplifications indicated in (5a) and (5b).

These curves exhibit features which are capable of simple physical explanation. The peculiar shape of the solid-line characteristic A is caused by the effect of the thermal reactance associated with the volume heat capacity of the backing. If this reactance could be eliminated, as for curve B which, to illustrate an extreme case, has been computed for $\rho' C_v' = 0$, the characteristic would resemble that of an air-backed unit with unachievably high surface dissipation. This circumstance is of importance in the practical selection of a backing material. It can be concluded generally that for backings having low $\rho' C_v'$ the response can be expected to remain frequency-independent out to higher chopping frequencies than for backings having comparable k' but higher $\rho' C_v'$.

Curve C, which has been computed for the extreme case $k' = 0$, appears to coincide exactly with the solid curve of Fig. 3 except in the frequency-independent region, where the limiting response is twice that of the air-backed unit. With $k' = 0$, the rear surface of the bolometer strip is thermally insulated, so that it now has only half the total dissipation of the air-backed unit. Of course, such a low-conductivity backing would be of no practical value in dissipating the bias heat of the element.

In curve D, to illustrate still another extreme case, the backing has been given an infinite

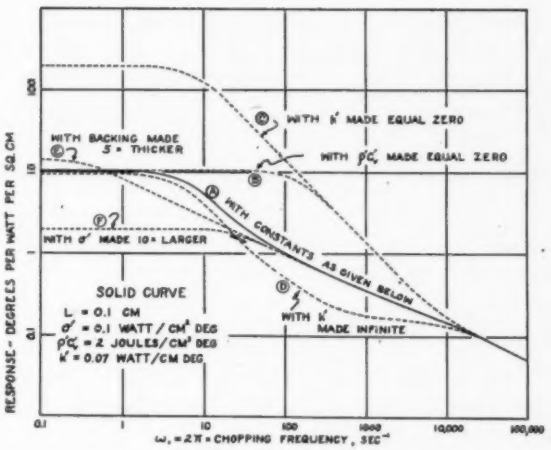

FIG. 4. Response-frequency characteristic for rocksalt-backed bolometer.

thermal conductivity. This is equivalent to placing the entire thermal capacity of the backing directly in contact with the rear surface of the bolometer strip. This unbuffered reactance brings about the rapid decrease in response in the range from $\omega = 10$ to $\omega = 100$ and results in the nearly frequency-independent response in the range from $\omega = 500$ to $\omega = 10{,}000$. In the latter range the frequency is so high that the heat capacity of the backing presents practically a "short-circuiting" reactance to the rear surface of the bolometer strip. Thus, while the temperature at the front surface of the strip is being driven by the fluctuation of the incoming radiation, the temperature of the rear surface is being held nearly constant by this reactance. And, while the whole strip is at the same phase throughout, it is not at the same temperature throughout. This state of affairs does not change much with increasing frequency until so high a frequency is reached that the wave-length of the thermal waves in the strip becomes shorter than the thickness of the strip. Then, of course, the front-surface temperature of the strip becomes independent of the nature and properties of the backing.

It is to be noted that in the solid curve A there appears some tendency toward a levelling-off in the neighborhood of $\omega \sim 100$. The reason is as explained in the last paragraph, except that here the full short-circuiting effect of the backing reactance is buffered by the distributed thermal

resistance of the backing, and the levelling-off is not as pronounced.

Curve E shows the modification in the response-frequency curve brought about by making the backing five times thicker than for the solid curve A. Increasing the thickness of the backing increases the heat capacity, and the parallel reactance of this extra capacity makes itself felt at a lower chopping frequency than for curve A. Curve E tends toward a higher low frequency limiting response than curve A because of the decrease in dissipation, brought about by the increased thermal resistance of the thicker backing.

Finally, curve F shows the effect of making the backing-to-holder dissipation ten times larger than for curve A. This increased dissipation lowers the low frequency limiting response and makes it necessary to go to higher chopping frequencies before coming to the fall-off due to the heat capacity of the backing.

It is often stated that an ideal backing material is one having a large value of the diffusivity K'. In making such a statement a distinction must be made whether the diffusivity is desired to be large by virtue of a large thermal conductivity k' or by virtue of a small volume heat capacity $\rho' C_v'$. A comparison of curves B and D shows why this distinction is necessary. In a bolometer assembly of such geometry and thermal properties as are considered here the highest permissible d.c. bias across the bolometer strip is determined chiefly by the backing-to-holder dissipation rather than by the thermal conductivity of the backing. As long as the latter is large enough (as it is for rocksalt) so that the backing offers a comparatively small thermal resistance between the element and the holder, there is little virtue in having k' still higher, as, for example, for quartz. However, any decrease in the value of $\rho' C_v'$ improves the response in the frequency region from $\omega \sim 1$ to $\omega \sim 1000$ and also decreases the time constant, both without affecting the permissible d.c. bias.

DISCUSSION

In the interest of simplifying the development of this presentation a number of short cuts and omissions have been employed which would have to be taken into account in the application of the method here outlined to any physical problem where accuracy of theoretical prediction is desired. There will be pointed out, in the next few paragraphs, the nature of some of these simplifications, their consequences, and, so far as possible, their specific remedies.

All the equations appearing in this paper were derived on the assumption of a single sinusoidal amplitude fluctuation of input radiant power. If the fluctuation is obtained with a sector disk producing a nearly square-wave input of radiant power, a more satisfactory solution would be obtained by solving the appropriate equation for the fundamental chopping frequency and two or three of its harmonics as well, assigning to each harmonic solution a weight corresponding to the Fourier coefficient of the particular harmonic in the square-wave expansion, and summing over the expansion.

While backed bolometers can be made for which the thermal contact between the element and its backing is intimate, it is usually necessary in practice to fasten the two together with a thin layer of cement whose thermal properties may contribute to the behavior of the whole. The backed bolometers discussed in connection with the curves of Fig. 4 have been idealized to the extent of neglecting this layer and its effects. A paper is now in preparation by W. van Roosbroeck in which some of these details are treated. Van Roosbroeck's treatment will also include a consideration of cases in which the incoming radiation, instead of being absorbed, as here assumed, at the front surface of the bolometer strip, is absorbed throughout the thickness of the strip.

In usual practice a backed bolometer is made of a narrow strip of sensitive material cemented to a backing slab much larger in area than the strip. Hence the physical problem is not one dimensional except in a small volume of the backing immediately adjacent to the strip. At larger distances away from the strip in the backing the heat flows along nearly radial lines and the isothermals are nearly semi-cylinders coaxial with the center line of the strip. The analogous electrical problem is one in which the series conductance and parallel capacitance of the transmission line representing the backing

increase nearly linearly with distance along the line. Except for special cases exact solutions for varying-parameter lines are not easily obtainable. However, approximate electrical analogs can be set up which are capable of solution. Such approximations, over certain frequency ranges are assisted by the fact that temperature waves in a semi-infinite solid are attenuated in amplitude by a factor $e^{-2\pi}$ per wave-length. Hence, for higher frequencies the temperature waves, which become shorter in wave-length with increasing frequency, do not penetrate far enough into the backing to get into the region where the fanning-out of the heat flow lines occurs, and the constant-parameter solutions already derived can be used as good approximations.

In deriving the equation for the solid-backed element the assumption was made that the holder presented a non-reactive dissipation to the rear surface of the backing slab. This assumption could lead to error only in frequency region *I* where the chopping rate is so low that the temperature waves penetrate clear through the backing. For higher frequencies the exact nature of the holder's impedance would not be of any consequence.

ACKNOWLEDGMENTS

The author is indebted for assistance in the development of this method and in the interpretation of some of its results to W. H. Brattain and J. A. Becker. The helpful advice of R. O. Grisdale in the arrangement of this manuscript is likewise acknowledged.

The Speed of Propagation of Brittle Cracks in Steel

G. Hudson* and M. Greenfield**
David Taylor Model Basin, USN, Washington, D. C.

(Received September 30, 1946)

Brittle failure was produced in notched steel tensile specimens. The speed of propagation of the brittle crack was measured and found to be approximately 40,400 in./sec.

THERE have been recent reports of the brittle failure of steel plate used in a variety of engineering structures. This rupture occurred when the steel was subjected to certain severe conditions. In the main these brittle failures may be characterized by the following:

(1) A crack is propagated with extreme rapidity through the steel plate,

(2) The surface of rupture created by this crack is orthogonal to the plane of the plate,

(3) This rupture surface shows a characteristic "herring-bone" pattern,

(4) There exist small permanent strains, often of less than 2 percent, in the neighborhood of the fractured surface. It was thought that a study of the speed of propagation of brittle cracks in steel might contribute to an understanding of the mechanisms of these phenomena.

A preliminary note on the beginning of this study has been given in an earlier paper.[1] This work was subsequently extended with a more refined technique, to include more variation in the path length over which the average velocity of the crack was measured, and a variation in the distance of this path from the point of initiation of the crack. In the present paper, in addition to reporting the later results which agree with the previous ones within the limit of experimental error, more details are given of the technique used.

It has been found possible to produce brittle failure in a steel tensile specimen at room temperatures in a controlled experiment of the following type. The specimens consisted of rectangular plates of a plain carbon structural steel (also known as medium steel) with a carbon content not exceeding 0.31. This steel had a minimum average ultimate strength of 60,000 lb./in.^{2}, and a minimum average yield strength of 34,000 lb./in.^{2}. This steel had not been heat treated. The specimens were approximately 2 feet long, $5\frac{3}{4}$ inches wide, and 1 inch thick. To fix

* Now at New York University, New York City, New York.

** Now at North American Aviation, Los Angeles, California.

[1] M. Greenfield and G. Hudson, Proc. Nat. Acad. **31**, 150 (1945).

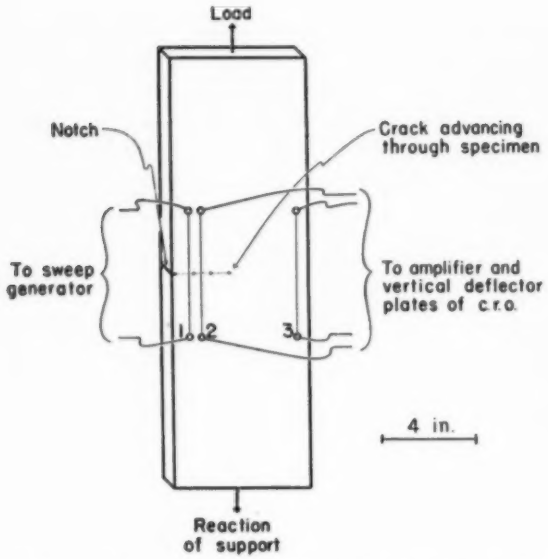

FIG. 1. Schematic diagram showing the positions of one-mil Nichrome break wires 1, 2, and 3 on the tensile specimen.

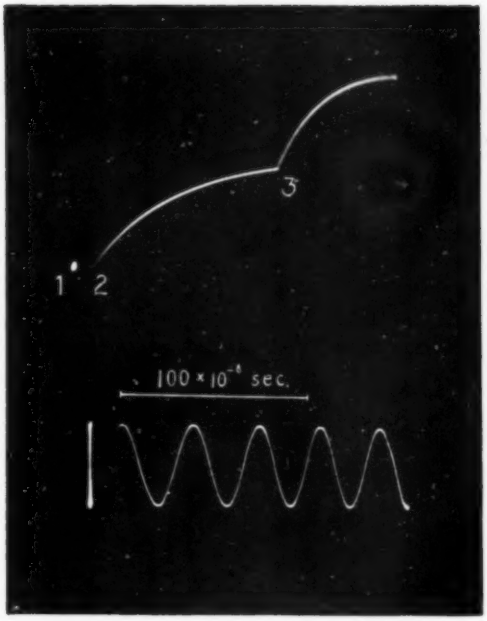

FIG. 2. A typical record obtained from the breaking of a tensile specimen like that shown in Fig. 1. The numbers 1, 2, and 3 designate the positions of the electron beam at the instants of breaking of wires 1, 2, and 3, respectively.

the point of initiation of the failure, a notch consisting of a milling saw cut of the order of $\frac{1}{32}$ inch in width and $\frac{1}{4}$ inch deep was machined into one edge of the specimen midway between its ends. See Fig. 1.

The specimen was placed in the grips of a tensile machine† and pulled to failure. A brittle crack initiated at the milling cut, as indicated by Fig. 1, was propagated across the specimen, at right angles to the edge.

An attempt was made to photograph the crack as it spread through the plate. The camera used was a Fastax Western Electric, operating at about 3000 frames per second. Even this speed was insufficient to catch the phenomenon, as the crack invariably spread across the specimen between two successive frames. It was possible, however, to infer by this method a lower limit of the order of 5000 in./sec. for the velocity.

The following method using electronic recording was finally adopted for determining the speed of propagation of the crack in these specimens. The specimens were first prepared by heating them to a temperature sufficient to melt but not boil a layer of medium de Khotinsky cement. This cement was spread smoothly on the surface of the metal in the region through which the crack was to be propagated. While the de Khotinsky was still fluid, several lengths of one-mil Nichrome wire were embedded in the cement, as shown schematically in Fig. 1. These wires were arranged to be approximately parallel, about one inch apart, and perpendicular to the expected path of the crack. The de Khotinsky thus served not only to cement the wire firmly to the tensile specimen,

† These specimens were actually tested in two different types of machines; one is a Baldwin Southwark hydraulic type with a 600,000 lb. capacity located at the David Taylor Model Basin, USN, Washington, D. C., and the other, an Olsen screw type with a 600,000 lb. capacity, located at the National Bureau of Standards, Washington, D. C.

TABLE I. Speed of propagation of brittle crack.

Testing machine	Specimen number	Wire numbers	Distance inches	Average velocity inches/second
TMB	E-1	2–3	2.23	42,700
TMB	E-3	2–3	4.41	37,900
NBS	F-3	2–3	1.01	36,500
	F-3	3–4	0.98	43,000
	F-3	4–5	0.96	39,500
	F-3	5–6	0.96	41,200
NBS	G-2	3–4	0.96	42,400
	G-2	4–6	1.99	41,600
NBS	G-3	2–4	1.97	44,200
	G-3	4–5	0.96	37,400
	G-3	5–6	0.98	43,700
NBS	G-5	3–4	1.00	41,200
	C-5	4–5	0.99	33,000
	C-5	5–6	0.98	41,000

Average of above velocities = 40,400 ± 2500 in./sec.

but also insulated the wire from the specimen. The ends of the wires which protruded from the cement were insulated from the specimen by strips of paper stuck to the specimen partly by the de Khotinsky cement and partly by Scotch Tape. After cooling the specimen, the ends of the wires were then soldered to binding posts on Bakelite strips. These were held by rubber bands to the specimen about two inches on either side of the path of the crack.

When a crack is propagated from the base of the saw cut, it breaks the fine wires in succession. The breaking of the first wire is used to start a single horizontal sweep of the electron beam on the screen of a cathode-ray oscillograph. Each of the succeeding wires, on breaking, introduces a voltage step on the vertical deflection plates by means of a simple voltage divider arrangement. The resulting staircase-like record may be photographed, e.g., see Fig. 2. The rounding off of the successive steps is caused by the impedance of the circuit used. A calibration wave for timing is provided by a standard oscillator. See Fig. 2.

The average velocity of the crack between any two successive wires is calculated by dividing the measured distance between them by the corresponding time interval measured from the oscillograph record.

Table I gives the final results. Column 1 states where the specimen was tested, i.e., either at the Taylor Model Basin or at the National Bureau of Standards. Column 2 is the specimen number. Columns 3 and 4 give, respectively, the numbers of the 1-mil Nichrome wires between which the speed was measured, and the distance between those wires. For example, Specimen F-3 had six (6) 1-mil Nichrome wires cemented to it. The breaking of the first wire started the single sweep across the c.r.o. screen. Then there were signal wires 2 through 6 spaced as indicated in column 4. Column 5 gives the average velocity for the corresponding distance listed in column 4.

The average of all the velocities listed in column 5 is 40,400 in./sec. with a mean absolute deviation of 2500 in./sec.

It is intended to continue this work to learn whether there is a significant variation of the velocity of the brittle crack with the thickness of the steel plate, its temperature, and its composition.

Use of the Broadcast Band in Geologic Mapping*

LARKIN KERWIN**
Massachusetts Institute of Technology, Cambridge, Massachusetts
(Received December 4, 1946)

A review of the literature indicates that a method of geologic mapping by means of observing the effect of geologic anomalies on electromagnetic field intensity should be practical. Field equipment is designed and assembled for that purpose and proves accurate and simple to use. Preliminary investigations with it successfully locate several anomalies.

INTRODUCTION

THE practicability of using high frequency electromagnetic waves in sub-surface geologic investigation is generally viewed as dubious. Joyce's theoretical conclusions from Maxwell's work[1] promise great attenuation under the assumed conditions. Eve,[2] Terman,[3] and Ollendorf support these considerations. However King predicted less attenuation, while Fritsch[4] declares that theoretical assumptions are never justified in practice and suggests that practical procedures are quite possible.

Relatively few experimental investigations

* This paper is based on a portion of a thesis entitled "The Development of Field Equipment Suitable for Measuring the Significant Properties of the Earth and Their Effect on Electromagnetic Wave Propagation," submitted for credits towards the degree of Master of Science at M.I.T. Financial support for the work was provided through a grant from The Geological Society of America, which is hereby gratefully acknowledged.

** Now with the Department of Physics, Laval University, Quebec.

[1] J. W. Joyce, Bureau of Mines Tech. Pap. No. 497 (1931).
[2] A. S. Eve and D. A. Keys, *Applied Geophysics* (Cambridge University Press, New York, 1929).
[3] F. E. Terman, *Radio Engineers' Handbook* (McGraw-Hill Book Company, Inc., New York, 1943), p. 698.
[4] V. Fritsch, Beit. Ang. Geophysik [4] **5**, pp. 375–395.

have been undertaken and these are inconclusive. Potter and Friis[5] determined that ordinary topographic variations did not have great effects on high frequency field intensities. On the other hand, Cloos,[6] Howell,[7] and Fritsch[8] found that field intensities did vary with the sub-surface geology. Joyce, Eve,[9] Allen, and Silverman and Sheffet[10] worked qualitatively in mines or tunnels and found in general that broadcast frequencies often penetrate the ground for considerable distances, but that higher frequencies were quickly absorbed. Joyce also did some quantitative work at 500 cycles, but it is highly doubtful if this frequency justified the use of electromagnetic wave theory in considering the results. The effect was undoubtedly a simple inductive one in view of the tremendous wave-length. Fritsch[11,12] lists many interesting results of successful underground propagation.

These results and others indicated that the effect of geology on the field intensity of electromagnetic waves might provide a useful method of geologic mapping. The Geologic Society of America provided a grant for the purpose of developing equipment, and preliminary results obtained with it last summer indicate that the band from 200 kc to 1000 kc will prove useful in future work.

It was decided that the investigation of the field patterns of various frequencies over the same area would provide useful information. Geologic anomalies would cause irregularities in the pattern which would vary with frequency according to the penetrating power of the various wave-lengths. Equipment was purchased and adapted or constructed to produce, monitor, and measure suitable electromagnetic fields.

EQUIPMENT

The field intensity recorder was assembled inside a wooden-bodied station wagon supplied by the Geotechnical Corporation. Its basic component was a modified Model DAE radio direction finder. The antenna consisted of a 14-inch shielded loop, mounted in a stationary cylinder provided with azimuth scale and commutator rings connected to a shielded lead. This loop was mounted on a spring tripod which was bolted to the floor of the station wagon. This mount was firm, but protected the loop from the shocks produced by the car's motion.

The associated receiver was mounted on a small oak table, directly in front of the operator's seat. This unit was of the superheterodyne type, covering the frequency range 240 kc to 2000 kc in three bands. It was provided with volume control, antenna tuning, and beat frequency oscillator, which made the receiving of unmodulated signals considerably easier. The case was provided with shock mounts screwed to the reinforced table top. In this unit the field produced a proportionate I.F. voltage, and that of the 2nd I.F. stage was selected as the most satisfactory for recording purposes. It was tapped to a jack on the panel, the signal from which was then proportional to the field strength, but could be controlled by the volume control circuit.

This voltage was measured by a vacuum-tube voltmeter of the "Vomax" type, installed immediately above the receiver on shock mounts attached to the latter's case. Sponge rubber pads were glued to the roof of the wagon and the voltmeter as added protection. For continuous recording, an Esterline-Angus recording milliammeter was used, having speeds up to six inches per minute. It was connected into the voltmeter circuit *via* a jack mounted on the meter face. By using this system throughout, any component could be removed for alteration or replacement without necessitating a rewiring job each time. For transportation and moderate speeds of recording the meter was mounted in sponge rubber padded clamps on a shelf under the table. Here it was easily available for inking, marking the chart, etc. The needle was weighed somewhat more than usual, and it was found that it would not jump from the paper if the car was driven at low speeds. For continuous operation at high speeds, a low frequency spring suspension should be used.

[5] R. K. Potter and H. T. Friis, Proc. I.R.E. [4] **20** (April, 1932).
[6] E. Cloos, Am. J. Sci. [166] **28** (October, 1934).
[7] Howell, Geophys. [2] **8** (April, 1943).
[8] V. Fritsch, Beit. Ang. Geophysik [3] **5**, pp. 315–364.
[9] Eve, A.I.M.E. Tech. Pub. No. 316.
[10] D. Silverman and D. Sheffet, Geophys. [4] **7** (October, 1942).
[11] V. Fritsch, Beit. Ang. Geophysik [1] **6**, pp. 100–119; [3] **6**, pp. 277–306; [4] **6**, pp. 407–412; [4] **7**, pp. 449–461.
[12] V. Fritsch, Neues Jahrb. f. Geol. B., Vol. 84, Series 1, pp. 90–116.

All of these units were operated with 110-volt, 60-cycle power. In the mobile unit this was provided by a Janette rotary converter operated by storage batteries. This produced a steady voltage at about 200 watts and operated silently. When well charged, the batteries provided 24 volts to operate the equipment for about 8 hours, more than a normal day's field work. A battery charger was mounted underneath the operator's seat and connected so that after the day's operations a long power cable could be connected to any convenient 110-volt outlet and the batteries charged overnight. This system proved completely satisfactory. A constant-voltage transformer proved useful for last-minute work at the day's end, in case the batteries began weakening. A general view of the equipment in the station wagon is given in Fig. 1.

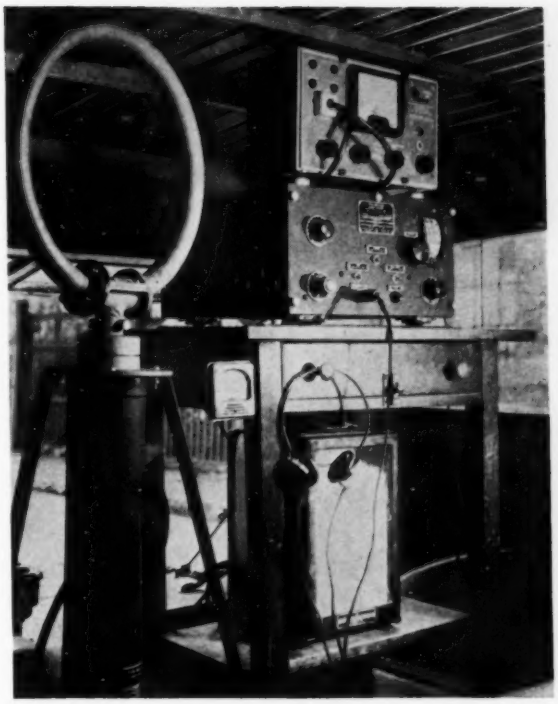

FIG. 1. Field intensity recording equipment mounted in station wagon.

It was intended that frequency ranges from 200 kc and up should be investigated. For preliminary work the broadcast band seemed suitable, and first field runs were made by recording the fields of various commercial transmitters as described later. For easily controllable work and for greater frequency range, a compact 75-watt transmitter was obtained. Known as the BC-375-E in the U. S. Army Signal Corps for whom it was designed, this transmitter provided continuously variable frequencies from 200 kc to 500 kc and from 1500 kc to 12,500 kc by means of six plug-in tuning units. This transmitter was designed to operate from 24-volt d.c. supply; plate voltages, etc., being supplied by a dynamotor. This supply provided approximately 750 watts. For portable operation battery operation was indicated, but was impractical because of the heavy drain of about 30 amperes. Accordingly, after some search a small gasoline driven generator was obtained which provided the required power, and delivered it through a number of "floating" storage batteries. This provided a smooth d.c. supply of about 28 volts for which the transmitter was easily modified.

During the process of taking field intensity measurements over various ground conditions, it was possible that the electromagnetic field would undergo certain variations independent of the geology. Fluctuations at the transmitter, atmospheric changes, the time of day at which readings were taken, etc. all contributed to fluctuation. It was therefore necessary to provide a stationary monitoring field intensity meter which would keep a record of these changes. The fact that relative field strengths and not absolute measurements were required simplified matters somewhat. A Hallicrafters Model SX-28 all-band receiver was obtained and provided with a simple fixed antenna. A vacuum-tube voltmeter was connected into the a.v.c. circuit of the receiver. Thus by the adjustment of the r-f amplifier amplitude and the use of a suitable voltmeter scale, a convenient deflection was obtained. This followed accurately the variations in field intensity. In order to obtain a continuous record of these changes, an Esterline Angus recording milliammeter was placed in the voltmeter circuit. This meter was adjusted to record at the rate of 1 foot per hour, which provided a satisfactory record of field strength changes without noting any minor fluctuations.

All of this equipment operated from 110-volt, 60-cycle current which was usually available near the scene of operations, or could be provided by a small motor generator.

In the course of the field work which was

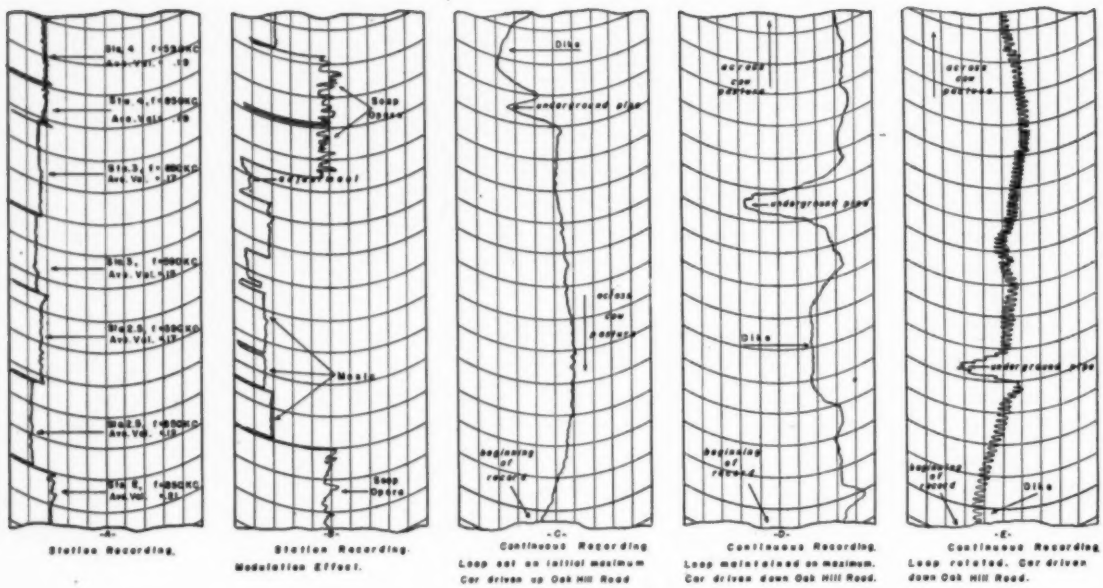

FIG. 2. Field intensity recordings (taken from recording meter chart).

extended over several weeks, the station wagon was driven over all kinds of roads, and a complete gamut of speeds. The equipment and mountings were thus subjected to a most thorough testing, and after a few adjustments following the first couple of days' experience, the apparatus proved entirely field-worthy. The only precaution taken was to remove the recording

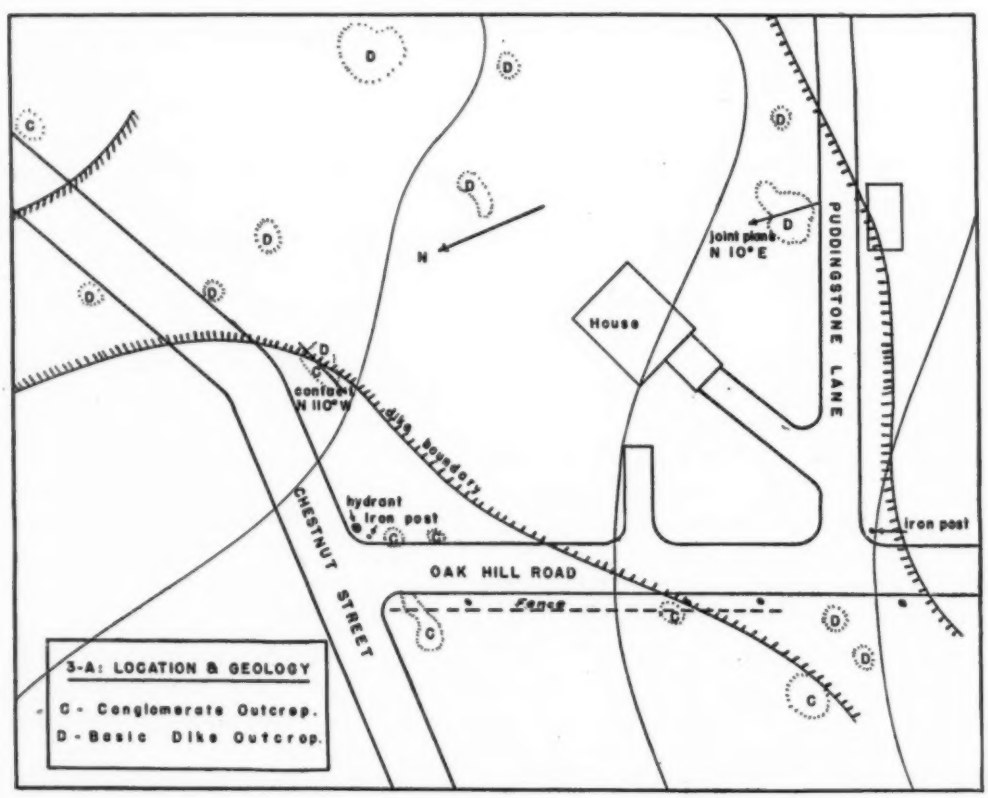

FIG. 3a. Area location and geology.

milliammeter needle if it was intended to proceed over rough ground at high speed. At low speeds it recorded satisfactorily. On this score, it is believed that future equipment patterned after this will provide a simple and rugged tool for the investigator.

FIELD PROCEDURE

For preliminary work, a dike situated in Newton, Massachusetts was selected as a suitable testing ground. This dike had been roughly located during a survey by Mr. Blumberg of Harvard, who kindly lent some of his field maps to this project. An extension of basic melophyre was found protruding through the roxbury conglomerate which was characteristic of the area. The contrast in the physical properties of these rocks is considerable, making them quite suitable for the purpose in hand.

The district was suburban, with considerable vegetation and the houses widely separated. Some time was spent in examining the geology in order to locate the dike factually if possible. In Fig. 3a the dike location based on surface geology is indicated.

Field intensity measurements were then made under a variety of conditions. First, detailed runs were made by taking field intensity records of about five minutes duration at points about twenty-five feet apart along the road. In each case the location of the loop and its orientation were established by taping and bearings taken with a Brunton-type pocket transit. The latter readings were taken from two directions and at some distance from the station wagon, eliminating the latter's effect on the compass. The bearings so taken were all consistent with those established from surveyed maps.

The duration of the five-minute reading was important in order to achieve an averaging effect. An example of the readings obtained over several stations as taken from the field chart is given in Fig. 2a. One of the disadvantages of using the broadcast band with the present equipment here became apparent. The modulating voltage had some effect on the instantaneous readings, although not the average. Therefore readings extending over some period of time were necessary to obtain accurate values. The type of program being broadcast also has an effect, as the modulation of musical programs is much

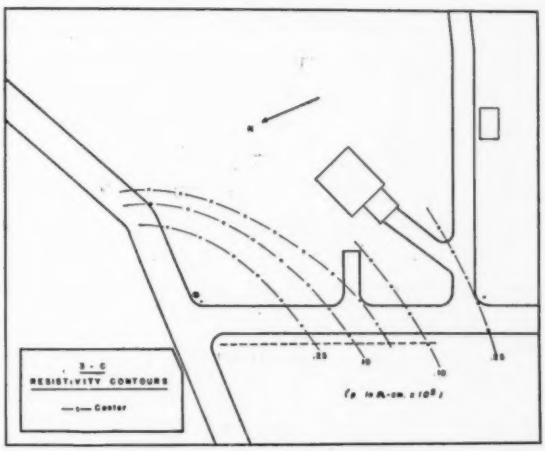

FIG. 3c. Resistivity contours.

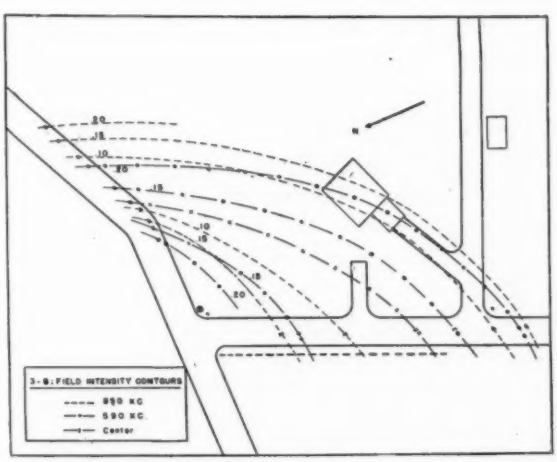

FIG. 3b. Field intensity contours.

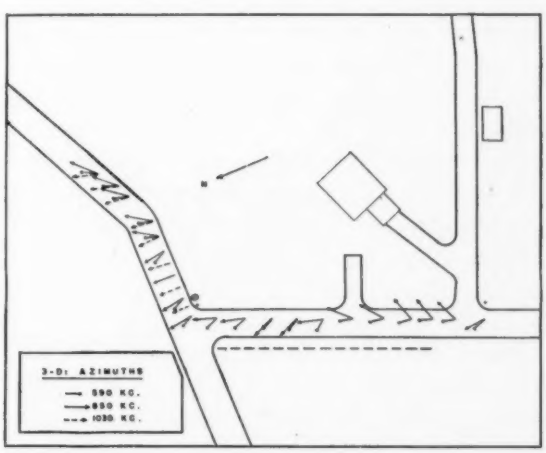

FIG. 3d. Field intensity azimuths.

smoother than those of the "soap-opera" type, and gave records which were much easier to interpret. An example is shown in Fig. 2b. These difficulties are avoided when using the unmodulated wave of the local transmitter.

The procedure was repeated several times, for several frequencies. Records were also made in the sunshine, rain, under dull clouds, and at night.

In addition to this, several types of continuous recording were investigated. By keeping the loop in a constant position of initial maximum strength and driving the station wagon slowly over the area, a figure such as that shown in Fig. 2c was recorded. This shows the prominent features which are marked. Other runs were made by keeping the loop manually oriented as much as possible in the direction of maximum intensity. The result is shown in Fig. 2d, where it is seen to bear close resemblance to the former record. Note that runs were made in varying directions and must be properly interpreted as to orientation. Continuously rotating the loop so as to produce an average effect gave a record such as shown in Fig. 2e, which follows the same general pattern as before.

A series of resistivity measurements was also made in the area in order to determine whether any relation existed between resistivity and field intensity. These measurements were made by inserting four metal stakes into the ground about twenty-five feet apart along the line of measurement. 150 volts, 60 cycle, as supplied by the small motor generator in the station wagon were applied between the two outer stakes. By measurements taken of the resistance between them the current put into the ground could be calculated. The voltage drop between the two inner stakes was then measured with a vacuum-tube voltmeter, and from these readings the resistivity was calculated.[13] By advancing the rear stake and changing terminals, successive readings were quickly taken. In this manner the resistivity was measured along the same direction as that in which the field intensity was recorded.

From the accumulated data, field intensity contours were drawn on the field map, and are shown in Fig. 3b. We see that the contours follow closely the direction of the dike as determined by the surface geology. Resistivity contours were also determined and are shown in Fig. 3c, where they assume the same general pattern as the other figures. The resistivity of the dike is substantially lower than the conglomerate, and as would be expected, the field intensity above the dike was also lower.

Azimuths of maximum field intensity are given in Fig. 3d, but they do not appear to convey any conclusive information. Over the dike, on Oak Hill Road, they seem to orient more towards the North than at other places.

Certain characteristics of the graphs drawn from the accumulated data are of some interest. It was observed that data taken at night showed considerably less variation than that taken by day. Measurements of low frequencies showed greater disturbance over the dike than did those of higher frequencies. Data taken during rainy weather showed the fields to be in general stronger and less affected by geology. Low intensities over the dike pointed to its higher conductivity, as was verified by resistivity measurements. The low frequency irregularities were more widespread than the others, indicating that the ground anomaly was more than a surface effect. To some extent here, and more so in urban areas later investigated, the effects of manholes, steel rails, etc. were quite obvious and easily detected.

Besides the detailed investigations in this area, other districts were investigated, using both stationary and rotating loop techniques. In the more urban area of Hammond Street, Brookline, a similar dibase dike protruding through the conglomerate was located by this method, and its presence verified by an examination of the surface geology. The boundaries of the dike were fairly sharply recorded as the field weakened over it. In Medford there is a noted extrusion of Medford dibase through Lynn volcanic complex. In this instance the resistivity of the dike is higher than the surrounding rocks, and the field intensity increased over it.

It was also observed that topography appeared to have relatively little effect. In driving over stretches of country in Arlington where the geology was uniform, the field remained essen-

[13] C. A. Heiland, *Geophysical Exploration* (Prentice-Hall, Inc., New York, 1940), p. 709.

tially constant except for manhole effects, etc., whether the receiver was passing over rolling hills, proceeding through cuttings, or on level ground. A notable exception was observed on the top of Pine Hill, a prominence beside the Medford Dike and very close to the transmitting antenna of the broadcast station being recorded. At the top of the hill the signal was extremely strong, but it weakened considerably as the bulk of the mountain was interposed sharply between the receiver and transmitter.

For most of these field measurements the field itself remained very constant, as shown by the monitoring station. Variations were observed between daytime and nighttime records, and with weather; but over considerable periods (3–4 hours) if the weather and daylight conditions were constant the field remained quite steady.

In general it is considered that the results obtained thus far show sufficient promise to warrant a continuation of the research. The equipment has proven sufficiently rugged, sensitive and simple to operate over long periods of field measurements. The cost of operation involves only the depreciation of equipment, and station wagon expenses. The method of field intensity recording has been used to locate a geologic anomaly as determined by other independent means, and has generally located other geologic features. Accordingly, further work on the subject is being done.

MODIFICATIONS

In light of past experience, several modifications are recommended for the equipment, and will be incorporated into it shortly. The portable transmitter will provide a much more satisfactory field from the point of view of modulation as well as that of situation and pattern. For continuous recording, the milliammeter is being equipped with speedometer drive. This will permit operation by one person rather than the operator and driver previously necessary. The loop antenna is being supplemented by a vertical antenna, the two being interchangeable by means of a switch. This will eliminate the necessity of rotating the loop when azimuths are not being taken. A switching system in the charging circuit will make that operation somewhat more convenient to perform. The monitoring unit is being made self-sufficient by powering it with another rotary converter operating from 12 volts d.c. The SX-28 Hallicrafters receiver is being replaced by a smaller, more portable one.

Considerable attention is being devoted to frequencies below the broadcast band, as field experience here supports the general theory that low frequencies are more suitable. Experiments will also be performed on bands above the broadcast, up to about 12,000 kc.

ACKNOWLEDGMENT

The writer expresses his sincere personal appreciation to Dr. R. F. Beers of the Geological Society of America and the Geotechnical Corporation; and to Dr. W. B. Nottingham of the Institute Department of Physics for their unstinted and practical assistance as well as moral encouragement.

A Note on a Paper by Faust and Beck

WILLIAM M. STONE
Iowa State College, Ames, Iowa
(Received October 31, 1946)

An infinite sum transformation is defined and applied to a system of linear difference equations discussed by Faust and Beck in their paper on single tuned amplifiers. Some transforms of the more common functions are given and points of superiority of the transform method over the classical methods of solution of difference equations are emphasized.

IN their paper, "Oscillation Conditions in Single Tuned Amplifiers,"[1] Faust and Beck solved a simultaneous set of two first-order difference equations by classical methods. The purpose of this paper is to introduce the Generalized Laplace Transformation of Samuelson[2] and to illustrate its application to the same problem in circuit analysis. The advantages are that (1) a difference system is reduced to an algebraic system, (2) there are no extraneous constants introduced, and (3) no assumptions need be made as to the nature of the solution.

The generalized Laplace transformation is defined as

$$L\{F(k)\}_E = f(s) = \sum_0^\infty F(n)s^{-n-1}, \qquad (1)$$

where $F(k)$ must be of exponential order, $F(k)<M\alpha^k$, $k>K$, and defined for all positive integral values of k. The series is then uniformly convergent for all values of $s>\alpha$. The subscript refers to the shifting operator, $E^mF(k)=F(k+m)$, and serves to distinguish the generalized Laplace transformation from the ordinary case. Some transforms may be found by elementary summation but a more powerful method is readily available. By definition of the E operator

$$\begin{aligned} L\{E\cdot F(k)\}_E &= \sum_0^\infty F(n+1)s^{-n-1}, \\ &= s[F(0)s^{-1}+F(1)s^{-2}+\cdots]-F(0), \\ &= sf(s)-F(0), \end{aligned} \qquad (2)$$

which may be generalized at once by mathematical induction to the form

$$L\{E^m\cdot F(k)\}_E = s^m f(s) - \sum_{j=0}^{m-1} s^{m-1-j}F(j). \qquad (3)$$

Following is a list of some of the more useful transform pairs:

$F(k)$	$f(s)$
1	$1/(s-1)$
$a^k\cos wk$	$\dfrac{s-a\cos w}{s^2-2as\cos w+a^2}$
$a^k\sin wk$	$\dfrac{a\sin w}{s^2-2as\cos w+a^2}$
$a^k\cosh wk$	$\dfrac{s-as\cosh w}{s^2-2as\cosh w+a^2}$
$a^k\sinh wk$	$\dfrac{a\sinh w}{s^2-2as\cosh w+a^2}$
$a^kk^{(n)}$	$a^nn!/(s-a)^{n+1}$.

Here $k^{(n)}$ means the Newton factorial polynomial, $k(k-1)(k-2)\cdots(k-n+1)$.

Using capital letters for the object function, small letters for the transforms, Faust and Beck's equations for voltage and current may be written as

$$E(k+1)-E(k)-Z_1I(k)=0, \qquad (4)$$

$$E(k+1)+g_mZ_2E(k)-Z_2I(k+1)+Z_2I(k)=0. \qquad (5)$$

By means of (2) these may be transformed at once to an algebraic system:

$$(s-1)e(s)-Z_1i(s)=E(0), \qquad (6)$$

$$(s+g_mZ_2)e(s)-Z_2(s-1)i(s)=E(0)-I(0)Z_2. \qquad (7)$$

[1] Faust and Beck, J. App. Phys. **17**, 749 (1946).
[2] Samuelson, Bull. Am. Math. Soc., Abstract 52-3-86 (1946).

The solution of this system is found to be

$$e(s)=\frac{E(0)\left[s-\left(1+\frac{Z_1}{2Z_2}\right)\right]+I(0)Z_1-E(0)\frac{Z_1}{2Z_2}}{s^2-2s\left(1+\frac{Z_1}{2Z_2}\right)+1-g_mZ_1}, \tag{8}$$

$$i(s)=\frac{I(0)\left[s-\left(1-\frac{E(0)}{I(0)Z_2}\right)\right]+E(0)g_m}{s^2-2s\left(1+\frac{Z_1}{2Z_2}\right)+1-g_mZ_1}. \tag{9}$$

Substitute

$$a=(1-g_mZ_1)^{\frac{1}{2}}, \quad \cosh w=\frac{1+\frac{Z_1}{2Z_2}}{a}, \quad \sinh w=\frac{\left[\frac{Z_1}{Z_2}+\left(\frac{Z_1}{2Z_2}\right)^2+g_mZ_1\right]^{\frac{1}{2}}}{a},$$

$$=A/a, \qquad =B/a,$$

so that

$$e(s)=\frac{E(0)(s-A)+I(0)Z_1-E(0)\frac{Z_1}{2Z_2}}{s^2-2As+a^2}, \tag{10}$$

$$i(s)=\frac{I(0)\left[s-\left(1-\frac{E(0)}{I(0)Z_2}\right)\right]+E(0)g_m}{s^2-2As+a^2}. \tag{11}$$

Making the denominators conform with the list of transforms the object functions may be written as

$$E(k)=a^{k/2}\left[E(0)\cosh wk+\frac{I(0)Z_1-E(0)\frac{Z_1}{2Z_2}}{B}\sinh wk\right], \tag{12}$$

$$I(k)=a^{k/2}\left[I(0)\cosh wk+\frac{I(0)\frac{Z_1}{2Z_2}+\frac{E(0)}{Z_2}(1+g_mZ_2)}{B}\sinh wk\right]. \tag{13}$$

The boundary conditions are

$$I(n)=0, \tag{14}$$

$$E(0)=E_{in}+Z_gI(0), \tag{15}$$

where $I(n)$ is the current in the last mesh, $E(0)$ is the voltage in the input stage, E_{in} is the voltage of the input generator whose internal impedance is Z_g. Substitution of both conditions in (13)

and algebraic reduction leads to

$$E(0)=E_{in}\frac{B\cosh wn+\dfrac{Z_1}{2Z_2}\sinh wn}{B\cosh wn+\left[\dfrac{Z_1}{2Z_2}+Z_g\left(\dfrac{1}{Z_2}+g_m\right)\right]\sinh wn}, \tag{16}$$

$$I(0)=-E_{in}\frac{\left(\dfrac{1}{Z_2}+g_m\right)\sinh wn}{B\cosh wn+\left[\dfrac{Z_1}{2Z_2}+Z_g\left(\dfrac{1}{Z_2}+g_m\right)\right]\sinh wn}. \tag{17}$$

In practice the gain off all n stages is of most importance. If Z_g is set equal to Z_2 as is customary the gain of the n stages may be reduced to

$$\frac{E(n)}{E_{in}}=\frac{B(1-g_mZ_1)^{n/2}}{B\cosh wn+(A+g_mZ_2)\sinh wn}. \tag{18}$$

The well-known expansion formulas

$$\cosh wn=\sum_k\binom{n}{2k}(\cosh w)^{n-2k}(\sinh w)^{2k}, \tag{19}$$

$$\sinh wn=\sum_k\binom{n}{2k+1}(\cosh w)^{n-2k-1}(\sinh w)^{2k+1}, \tag{20}$$

where $\binom{n}{2k}$ represents the binomial coefficients as k takes on the values 0, 1, 2, . . ., lead to the form of (18)

$$\frac{E(n)}{E_{in}}=\frac{(1-g_mZ_1)^n}{\sum_k\binom{n+1}{2k+1}A^{n-2k}B^{2k}+g_mZ_2\sum_k\binom{n}{2k+1}A^{n-2k-1}B^{2k}}, \tag{21}$$

which is equivalent to the general formula for the gain given by Faust and Beck.

Internal Friction of Zinc Single Crystals*

IRVIN H. SWIFT†** AND JOHN E. RICHARDSON***
Department of Physics, The State University of Iowa, Iowa City, Iowa
(Received December 24, 1946)

Measurements were made of the internal friction of single crystal rods when vibrating longitudinally at 45 kilocycles per second. The decrement, or ratio of energy dissipated per cycle to twice the total vibrational energy, was used as a measure of the internal friction. At strain amplitudes below about 10^{-5} or 10^{-6} the decrement was independent of strain amplitude. The value of the constant decrement at low amplitudes, and the changes which occurred as the amplitude was increased, were both greatly dependent on the history of the specimen. The constant decrement for different crystals ranged from 7×10^{-5} to values higher than could be measured (about 200×10^{-5}). For some of the initially high-decrement crystals, values decreased with time (room temperature anneal). In general, for annealed crystals the decrement, measured as a function of increasing strain amplitude, remained almost constant up to and beyond the static elastic limit and then rose rapidly. It returned to the initial value when the strain amplitude was again reduced. On a second run, however, the rise in decrement occurred at much lower amplitude than on the initial one. It is concluded that the decrement is the result of two separate processes. The changing decrement at higher strain amplitudes is qualitatively explained with the use of dislocation theory.

INTRODUCTION

THE internal friction of single crystals of exceedingly pure zinc has been measured by Read,[1] and of less pure zinc by Read and Tyndall.[2] The decrement, which is the ratio of the energy dissipated per cycle to twice the total vibrational energy, was taken as a measure of the internal friction. Read found the decrement to be dependent on the past history of the specimen, strain or stress amplitude at which it was measured, time, etc. For the purer zinc decrements of the order of 10^{-5} were found at the lowest strain amplitudes but these, for most of the crystals, increased many fold with increasing amplitude. The present work consists of further observations of the behavior of the decrement of longitudinally oscillating zinc crystals under various circumstances and with partially controlled history.

EXPERIMENTAL METHOD

The zinc[3] used in this investigation was slightly less pure than that used by Read.[1] The crystals were grown by the Bridgman method in which a small casting is lowered through a furnace. The majority of the crystals were grown with the casting imbedded in dental investment compound and the rest were grown in the glass tube in which the original casting was made. The dental investment compound was easily softened by water after the crystals were grown and could then be removed with little danger of straining the crystals. The crystals had a cross-sectional area of 9 sq. mm and had fairly smooth surfaces.

The decrements were measured by essentially the same method as that used by Read[4] in which a composite oscillator is constructed by cementing to a quartz crystal a zinc crystal of the same cross-sectional area and cut with a fine jeweler's saw to a length such that the composite oscillator resonates at a frequency within less than 4 percent of the resonant frequency of the quartz crystal. The resonant frequency of the quartz crystal used in the present work was 45 kilocycles when vibrating longitudinally in the fundamental mode. The composite oscillator was suspended by silk fibers placed at displacement nodes of vibration between, but not touching, parallel plane electrodes. The assembly was then placed in a jar and the jar evacuated to a pressure of less than

* The main contents of two dissertations submitted in partial fulfillment of the requirements for degrees of Doctor of Philosophy in the Department of Physics in the Graduate College of the State University of Iowa.
** April, 1943.
*** June, 1946.
† Now at the Naval Ordnance Test Station, Inyokern, California.
[1] T. A. Read, Phys. Rev. 58, 371 (1940).
[2] T. A. Read and E. P. T. Tyndall, J. App. Phys. 17, 713 (1946).
[3] The zinc used was "Bunker Hill," a commercial zinc with not more than 0.01 percent impurity. Read and Tyndall (reference 2) report data from three crystals grown from this same zinc and two with additional impurity.
[4] The writers are indebted to Dr. Read for information about his bridge circuit, etc., in addition to that in reference 1.

0.1 mm of mercury. The quartz crystal was etched with hydroflouric acid before using and had a decrement of 2.7×10^{-5}.

The electrical apparatus consisted of an alternating-current bridge containing the composite oscillator as one arm and driven by a stable 35–100 kc oscillator. The detector used with the bridge consisted of an r-f amplifier, pentagrid converter, and associated oscillator which changed the high frequency signal from the bridge to an audible signal, and several stages of audio amplification. Its sensitivity with headphones was greater than that needed in any of the measurements. Either a vacuum thermocouple or a vacuum tube voltmeter were used to measure the voltage ϵ applied to the composite oscillator. The maximum strain amplitude, U_0, in the zinc specimen was then computed from the following formula:[5]

$$U_0=\frac{2\epsilon}{RV_0}(10K)^{\frac{1}{2}}\times10^3, \qquad (1)$$

where R is the electrical resistance of the composite oscillator at resonance, V_0 is the velocity of sound in the zinc specimen, and K is the constant relating the inductance L of the composite oscillator and the masses M_1 and M_2 of the cylinders in the equation:

$$L=K(M_1+M_2). \qquad (2)$$

The subscripts 1 and 2 in Eqs. (1) and (2) refer to the quartz and specimen, respectively.

The decrements of the zinc crystals were obtained from a knowledge of the inductance in the equivalent circuit, the resistance measured by the bridge, the resonant frequency of the composite oscillator, and the masses of the quartz and specimen. The constant K was evaluated with Eq. (11) in a paper by Cooke[6] and Eq. (2), from the observed variation of the reactance of the quartz crystal alone with frequency in the immediate neighborhood of the resonance frequency. It was determined to an accuracy of 1.5 percent. The accurate measurement of changes in frequency required in the plotting of the resonance curve was obtained as follows. The crystal controlled multivibrators of a piezoelectric frequency standard were adjusted in frequency until a harmonic of one of them was within about 50 cycles of the resonance frequency of the quartz crystal. The difference frequency obtained from this reference frequency and the frequency of the oscillator driving the bridge was amplified and used to drive a Cenco counter. The number of counts per second was then equal to the deviation of the unknown frequency from the crystal controlled reference frequency.

[5] This formula is an obvious modification of formula (1), reference 2, for stress amplitude. It may be obtained by equating the expression for total energy in electrical terms to that in mechanical terms, and solving for U_0.

[6] W. T. Cooke, Phys. Rev. **50**, 1158 (1936). Cooke's K is eight times the K used in Eq. (2).

EXPERIMENTAL RESULTS

Before describing the quantitative results, some qualitative observations may be of interest. It was noted that some of the crystals could be made to give a high pitched "ringing" sound when set into flexural oscillations by suspending them from the mid-point and tapping lightly. Later work showed that crystals for which this ringing was audible for 2 or 3 seconds had decrements of the order of 10^{-4} or less, whereas higher decrement crystals instead of ringing yielded a metallic or even wooden sound. A rough idea of the behavior of the decrement of a crystal could be obtained by subjecting it to this simple test. For example, eight crystals were tested just after they had been sawed to the desired length and then again after an anneal at 250°C for three hours. No noticeable difference was obtained at this time, but after storage at room temperature for several days a noticeable drop in the decrement, as judged by the increased time of ringing, was observed for some of the crystals while the rest showed little change. The crystals of the former class seemed to be persistent in their behavior. For example, crystal No. 1 (orientation 15°) would always return to a low decrement after two or three days' rest at room temperature without handling, regardless of its previous history. At one time when it was known to have a low decrement, it was accidently dropped onto the floor and bent considerably. It was then straightened by hand and left idle for several days after which it appeared to ring as well as ever. The data in Fig. 1 (curve A) and Fig. 8 (curve A) were taken on this crystal after it had rested nine days before it was mounted in the

apparatus and 7½ hours afterward. Other crystals behaved similarily although none of these were subjected to such drastic treatment. Crystals which did not develop a ring in a few days after growth did not do so after months of lying idle. Several crystals of this type were also annealed at 250°C and still did not develop a ring. These qualitative tests moreover showed very clearly how little handling was needed to increase the decrement. If a crystal which had a good ring was placed on a table and one end was elevated about a fourth of an inch and then dropped, the crystal thereafter would give only a metallic "clink" when tapped. In fact, while the crystals were being subjected to the ringing test, the gentle taps needed to set up the oscillations a few times would noticeably reduce the time of ringing. One or two days of rest at room temperature after the above treatment was however sufficient to restore the ringing properties of the crystals.

Nothing was found in the method of growth, amount of handling, etc., which gave any clue as to why some crystals had a low decrement while others had decrements which were too high to measure with the apparatus and which would not decrease with either a high or room temperature anneal. There was no apparent correlation of high and low decrement crystals with the degree of smoothness of their surfaces.

The writers observed, as did Read,[1] that the decrement measured at low amplitudes immediately after mounting in the apparatus was always much higher than after the crystal had been allowed to rest in the apparatus for some time undisturbed except for infrequent low amplitude measurements.[7] Two examples of this behavior are given in Fig. 1. Curves *A* and *B* are for two different crystals. The decrease in decrement with time after mounting was caused by, at least primarily, the self-annealing of the crystals at room temperature. Part of the decrease, particularly the initial rapid decrease, may have been caused by the drying of the cement between the specimen and the quartz. Calculations based on estimates of the thickness of the cement layer,

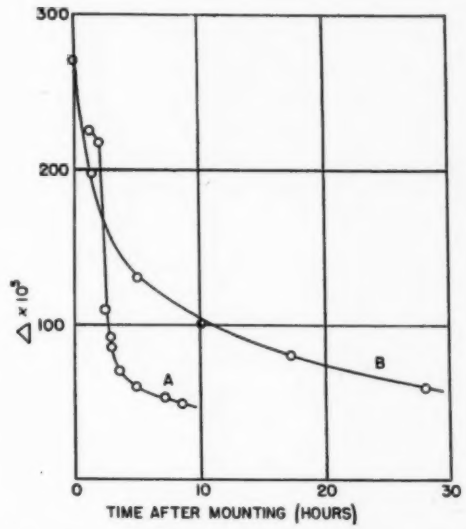

FIG. 1. Decrease of decrement with time after mounting, showing room temperature annealing. Curve *A* was taken on crystal No. 1.

etc., indicate, however, that the decrement of the cement would have to be as large as 100 to 1000 to cause the high decrements obtained. This seems improbable in view of the fact that the cement had dried for twenty or thirty minutes before the crystals were mounted. Also, Fig. 2 in Read's paper[1] shows a similar decrease of the decrement with time after mounting and his crystals were fastened to the quartz with beeswax and rosin which would show no drying effect.

Observations were made of the decrement as a function of maximum strain amplitude and time for thirteen crystals. It is not possible to present all of these data in full detail, but certain rather typical data are summarized and presented graphically. In Fig. 2 are shown curves of the decrement against strain amplitude for three crystals which had been allowed to rest in the apparatus for the following lengths of time: No. 2, two days; No. 3, three days; No. 4, thirty hours. In all cases the decrement had decreased to a nearly constant value before the data were taken. Crystal No. 4 (curve *C*) is particularly interesting as its decrement was practically constant to a value of maximum strain amplitude over five times that at the static elastic limit[2] (about 80×10^{-7}) for this crystal. Subsequent to the data in Fig. 2, crystal No. 4 was stored at room temperature for over six months. It was then remounted in the apparatus and the data

[7] The crystals of reference 2 made of the same zinc as the writers' did not show this decrease of decrement with time. These crystals however were of larger cross section than the writers' and the natural conclusion seems to be that they could be mounted without producing any detrimental strains.

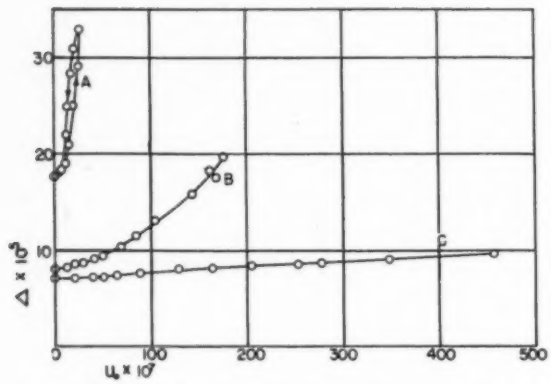

FIG. 2. Typical decrement *versus* maximum strain amplitude curves. Curve *A* was for crystal No. 2 ($\theta=71°$); curve *B* was for crystal No. 3 ($\theta=71°$); and curve *C* was for crystal No. 4 ($\theta=70°$).

shown in Fig. 3 were taken. The decrement had been allowed to reach a fairly constant value after mounting before the data were taken. The time given with each curve is the elapsed time after the taking of the first curve. The decrement was measured for increasing and then decreasing strain amplitude, as shown by the arrows. The decrement at the lowest strain amplitude decreased from 95×10^{-5} to 70×10^{-5} in the course of 143 hours, but did not come down to the previously measured value of 7.0×10^{-5} (Fig. 2). It may be seen from the lower branch of each of the curves shown in Fig. 3 that the strain amplitude required to increase the decrement by some amount, say 50 percent, increases considerably with elapsed time. In curve *J* the maximum strain amplitude was at the static elastic limit (80×10^{-7}) before the decrement started to increase very rapidly. Where two curves were taken with little intervening time, such as *B* and *C*, *G* and *H*, and *I* and *J*, the ascending branch of the second curve of a pair was nearly identical to the descending branch of the previous curve. After these data were taken, the crystal was removed from the apparatus and allowed to rest for 20 days. It was then remounted in the apparatus and left idle for seven days after which the data shown in curve *B*, Fig. 4, were obtained. The decrement in this curve shows only a gradual rise to a strain amplitude nearly three times that at the elastic limit. The decrement at low strain amplitude is still however about nine times as large as the first previously measured value (curve *C*, Fig. 2).

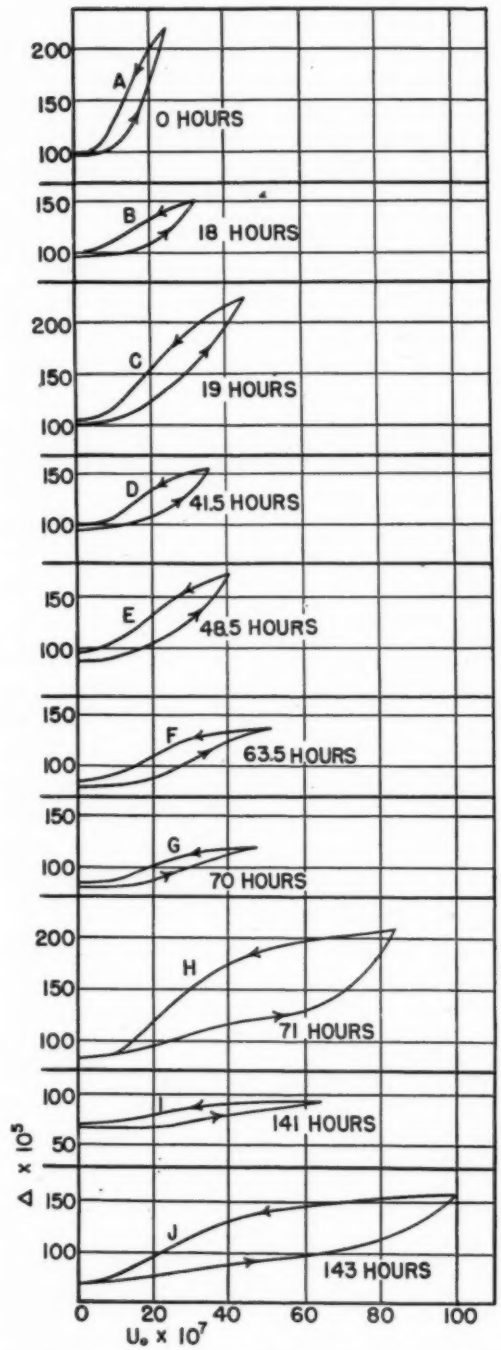

FIG. 3. Decrement *versus* maximum strain amplitude U_0 for crystal No. 4 ($\theta=70°$). The time given by each curve is the elapsed time after the first curve was taken. These curves show the effect of self-annealing at room temperature.

The curves shown in Fig. 5 demonstrate very well the phenomenon mentioned in connection with Fig. 3. These curves were taken on crystal

No. 6 ($\theta = 56°$) which was known to be strained prior to mounting. Data were first taken to a strain amplitude of 50×10^{-7} (curve 1) and the strain amplitude was then reduced to its lowest value. Curve 2 was then run to a strain amplitude of 80×10^{-7}, with curves 3 and 4 following in a similar fashion. From these curves it appears that previous runs affect subsequent runs only at strain amplitudes below the highest maximum strain amplitude obtained on the previous run. Thus, had the crystal been taken continuously from the minimum to the maximum strain amplitude (94×10^{-7}), it would probably have followed the lowest curve, which is a smooth continuation of curve 1. Also, while descending curves are not shown, they coincide quite well with the next ascending curve, as previously pointed out in connection with Fig. 3.

The curves shown in Fig. 6 taken on crystal No. 5 (orientation 80°) illustrate some effects of room temperature annealing. The decrement of this crystal remained constant until a critical value of strain amplitude was obtained and then started to rise. As successive runs were taken, this critical value of strain amplitude increased. The data for curve *A* were taken soon after the crystal was mounted. Data for curve *B* were taken 53 hours after *A* was taken; and curve *C*, 98 hours after *B*. Other sets of data were taken on the crystal during these two periods and therefore they should not be considered strictly as rest periods. Finally the crystal refused to anneal any further at room temperature and data could be very nearly repeated on successive runs taken several days apart. These later curves were substantially identical to curve *C*, Fig. 6. At this point the crystal was annealed for several days at 260°C, mounted in the apparatus, and left idle for a week. The decrement then remained nearly constant for a range of stress amplitude $2\frac{1}{2}$ times the value at the static elastic limit, as shown by curve *D*, Fig. 4. It will be noticed that after the high temperature anneal and remounting, the decrement at low strain amplitudes was higher than before the anneal (Fig. 6).

The two curves given in Fig. 7 indicate the diverse results that can be obtained when the conditions are very nearly the same. Curve *A* is

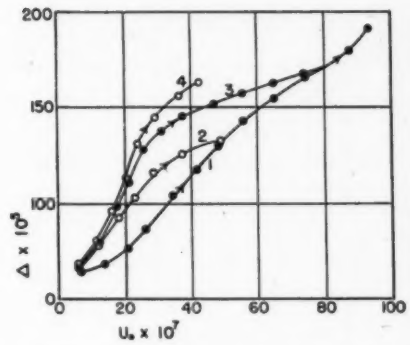

FIG. 5. Decrement *versus* maximum strain amplitude U_0 for crystal No. 6 ($\theta = 56°$), which was known to be strained before mounting in the apparatus. The curves are shown for increasing strain amplitude only and were taken in the order designated. They show that the decrement was influenced by previous runs only at strain amplitudes lower than the highest strain amplitude obtained on previous runs.

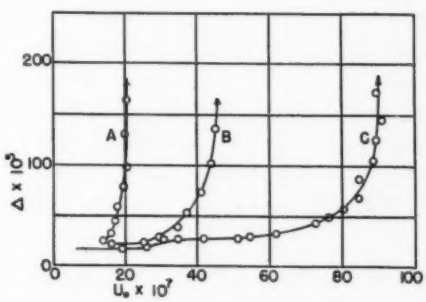

FIG. 6. Decrement *versus* maximum strain amplitude U_0 for crystal No. 5 ($\theta = 80°$). Curve *A* was taken soon after mounting, curve *B* 53 hours after *A*, and curve *C* 98 hours after *B*. Succeeding curves were very little different from curve *C*. As the crystal annealed at room temperature, the point of rise of the decrement occurred at higher strain amplitudes.

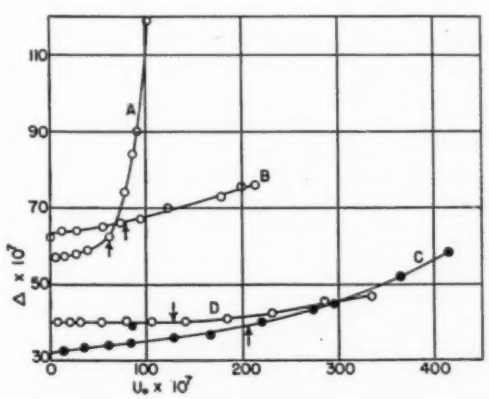

FIG. 4. Decrement *versus* maximum strain amplitude U_0 for crystals No. 9, 4, 10, and 5 corresponding to curves *A*, *B*, *C*, and *D*, respectively. All of these crystals had rested for a long period of time in the apparatus after mounting and before measurements were taken. The arrows on each curve designate the strain corresponding to the minimum static stress which will produce glide in the basal plane.

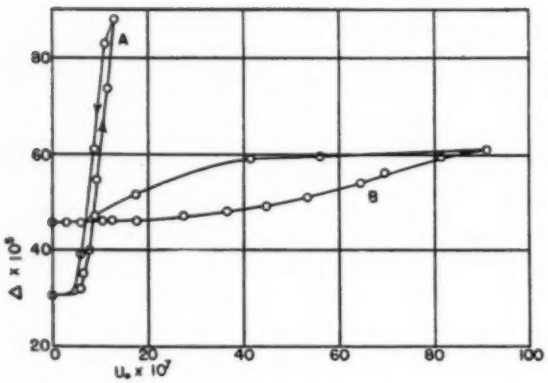

FIG. 7. Decrement *versus* maximum strain amplitude U_0. Curve *A* was for crystal No. 7a and curve *B* was for crystal No. 7b. Each of these two crystals were sections cut from one long 60° crystal.

for crystal No. 7a and curve *B* is for No. 7b. These two crystals were sections cut from the same original 60° crystal and annealed for two hours at 250°C. Crystal No. 7a was mounted four days after the anneal and curve *A* was taken after it had rested in the apparatus for one day. Crystal No. 7b was mounted eleven days after the anneal and curve *B* was taken after it had rested in the apparatus for two days. Curve *A* rises sharply at a low value of strain amplitude, while curve *B* shows a constant decrement as the strain amplitude is increased to a value of six or seven times that at which curve *A* starts to rise. The only known difference in the histories of the two crystals was in the time they were allowed to rest before and after mounting in the apparatus. Crystal No. 7b apparently had sufficient time to anneal at room temperature while No. 7a was still in a strained state. One other curve was taken on crystal No. 7b one day previous to curve *B* (one day after mounting), and it was nearly identical to curve *B* indicating that this crystal was in an annealed state (see discussion of Fig. 6).

Curve *A* of Fig. 8 was taken on the crystal (crystal No. 1, orientation 15°) which was dropped, bent, and subsequently straightened, as mentioned earlier. After the above treatment it was left idle for five days and mounted in the apparatus. At this time its resonant frequency was found to be too low and it was necessary to cut it to a shorter length. Three days after the sawing operation it was remounted in the apparatus and left idle for about eight hours except for occasional measurements of the decrement at very low strain amplitudes (curve *A*, Fig. 1). The data for curve *A*, Fig. 8 were then taken. Curve *B* represents data on crystal No. 8 (orientation 73°). It had rested for several days before mounting, and 34 hours after, before the data were taken. These two crystals had about the same resolved shear stress in the basal plane for a given tensile stress. The two curves are similar in form, indicating that crystal No. 1 had recovered fairly well from the severe strain given it.

The curves *A*, *B*, *C*, and *D* in Fig. 4 are for crystals which had been allowed to rest for long periods of time in the apparatus after they were mounted. The histories of crystals No. 4 and No. 5 have been given earlier in this paper. Crystal No. 9 (orientation 50°) and crystal No. 10 (orientation 20°) were left idle in the apparatus for about the same periods of time as crystals No. 4 and No. 5. The decrement of three of the crystals rose slowly with strain amplitude for values of strain amplitude considerably greater than the value of the static elastic limit, while the decrement of the other crystal began to rise sharply at about the static elastic limit (curve *A*). This crystal (orientation 50°) probably was still in a strained state as crystals with orientations near 45° are much more easily strained than those with orientation angles near 0° or 90°.

When the voltage across the composite oscillator was suddenly changed from one constant value to another, the decrement took an appreciable time to change from the previous value

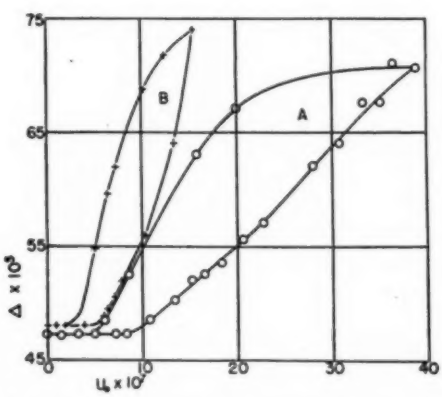

FIG. 8. Decrement *versus* maximum strain amplitude U_0. Curve *A* was for crystal No. 1 and curve *B* was for crystal No. 8.

to the final value at the new stress amplitude. The curves in Fig. 9 illustrate this effect. For curves 1 and 2 the voltage change was an increase while for the others the voltage was decreased. Usually when the voltage across the crystal was changed, a time of less than 20 seconds was required for the decrement to attain, say, 90 percent of its total change. In two of the curves of Fig. 9, however, the decrement required about a minute to attain 90 percent of its change. No attempt was made to fit these data with a mathematical function because the data were too inaccurate, particularly in the region where the decrement was changing rapidly with time. In addition there were other complicating factors. The strain amplitude is proportional to the current through the crystal and hence as the decrement (proportional to resistance, which determines the current) changed with time after the voltage across the crystal was changed to the new value, the strain amplitude was not constant during the time indicated in Fig. 9. Also, because of the low decrements involved, the time required for the strain amplitude to reach a steady state upon a change of the applied voltage from one value to another was large enough to make the effective zero of time uncertain.

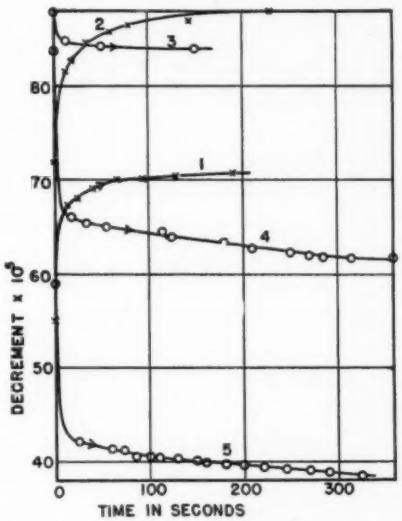

FIG. 9. Curves showing for crystal No. 7a the change in decrement with time following a sudden change of driving voltage across the composite piezoelectric oscillator. The curves were taken in the order designated by the numbers on each curve.

DISCUSSION OF DATA

A number of points should be mentioned in regard to the measurements described above. These are:

(1) The decrement measured at low amplitude decreased with time after mounting in the apparatus, approaching a constant value (Fig. 1). The final value reached was not, however, unique, in that a crystal after a second mounting would show a decline in decrement to a constant value but not necessarily to the same value found in the first experiment.

(2) The decrement was independent of strain amplitude for all maximum strain amplitudes below a critical value of the order of 10^{-5} to 10^{-6} (the bridge detector was sufficiently sensitive to balance the bridge at strain amplitudes much lower than 10^{-7}, probably 10^{-9}). The value of the low amplitude decrement was, for a given mounting in the apparatus, affected only by time (as shown in Fig. 1).

(3) The value of the low amplitude decrement was higher for all crystals measured than for Read's[1] spectroscopically pure zinc crystals. The lowest decrements found were about the same as for those of crystals made of the same zinc, as reported by Read and Tyndall.[2] It does not follow, however, that the decrement is a function only of the amount of impurities present. Other factors are much more important as is shown by the data on crystal No. 4. In Fig. 2 it had a decrement of 7×10^{-5} whereas after it had lain idle for six months and was remounted in the apparatus, the decrement at low amplitudes was 70×10^{-5} (Fig. 3).

(4) The value of strain amplitude at which the decrement started to increase became greater with elapsed time following mounting in the apparatus, i.e., increased as the value of the low amplitude decrement decreased. This effect is illustrated in Figs. 3 and 6.

(5) If a crystal had been oscillated at a sufficient amplitude momentarily to increase the decrement, then on measurements made soon after, the decrement was larger at all strain amplitudes between the value at which the decrement started to rise and the highest value obtained on the previous run. The amount that a run influenced the decrement obtained on a succeeding run decreased with elapsed time between the runs. The effect of time between runs is

illustrated particularly well by Fig. 5 but is also evident from the series of curves in Fig. 3.

(6) The decrement lagged in time behind the oscillation amplitude when the amplitude was changed suddenly. It is apparent from these curves that a finite time was required for the decrement to reach a stable value after the oscillation amplitude was changed.

The shape of the curves of decrement *versus* strain amplitude suggests that the observed decrement was composed of a constant decrement plus an amount which varied with strain amplitude. The portion of the decrement (to be designated by decrement A) which was constant with strain amplitude was measured alone at small strain amplitudes. Decrement B is that portion which was zero or negligible at zero strain amplitude and increased with increase of strain amplitude. It is possible on this basis to give a qualitative explanation of the behavior of the decrement in the experiments described above. The dislocation theory is used together with several assumptions to be listed later.

The dislocation theory[8] is based upon a certain type of local imperfection in the crystal lattice called a line dislocation. The local imperfection is concentrated about a line in a slip plane and is composed of such an arrangement of atoms that movement of the line imperfection through the crystal along a slip plane gives the same effect as if the material above the slip plane had been shifted a distance of one atomic spacing with respect to that below. The dislocations can be either positive or negative, one being complementary to the other in the sense that it is the mirror image of the other. A dislocation experiences a force in a shear stress field which reverses in sign with change in sign of the dislocation. Hence since a dislocation sets up a shear stress field of its own, dislocations of unlike sign are attracted to each other and those of like sign are repelled. Also a dislocation is attracted to the crystal surface by the force which would be given by an image dislocation of opposite sign outside of the surface. Dislocations can be formed in pairs in the interior of a crystal or singly at the surface as the result of shear stress.

In addition to the properties of dislocations summarized briefly above, the following assumptions will be used in the interpretation to be given for the results:

(a) The dislocations present as a result of previous low frequency, or "static" strains tend to form a stable lattice-like array within the crystal specimen.[8]

(b) The low amplitude decrement (A) is a function only of the total number of dislocations present at a given time in the specimen.

(c) The number of dislocations, if any, that are formed in the specimen as a result of the oscillating stress is a negligible fraction of the total number present. Presumably the short time during which stress was applied did not allow much opportunity for dislocations to form either pairwise in the interior, or at the surface.

(d) The value of decrement B is a function of the number of dislocations present which are "free" to dissipate energy. Whenever a dislocation is held within a dislocation lattice it is assumed to mean that the dislocation is prevented, or at least restricted, from participation in the energy dissipation process.

A crystal which had been recently mounted in the measuring apparatus would be expected to be in a strained state as a result of handling during mounting. Hence there would be a large number of dislocations of both signs distributed throughout the crystal. With the aid of thermal fluctuations, the forces on and between dislocations would cause them to migrate. Some dislocations, particularly those near the surface, would diffuse out of the crystal, others would disappear by cancellation of positive and negative dislocations (if the pair was originally in the same slip plane), and the remaining ones would migrate to positions such that the crystal had a minimum of potential energy, i.e. they would arrange themselves in some sort of orderly pattern. After a long time the number of dislocations in the crystal would be essentially constant, all being held in the lattice. Under assumption (b), that decrement A is a function only of the total number of dislocations present, the curves of Fig. 1 would follow. Furthermore, the final value reached by the decrement several days after

[8] A summary of the dislocation theory is given in the article by Frederick Seitz and T. A. Read, J. App. Phys. 12, 100 (1941). The forces between certain types of dislocations and other related matters are discussed in J. S. Koehler, Phys. Rev. 60, 397 (1941).

mounting would not be expected to be the same for a different mounting in the apparatus. Each mounting would entail a different kind and amount of the unavoidable strain, resulting in a different number and distribution of dislocations immediately thereafter. Hence the stable lattice reached would not be unique. This explains such data as that in Fig. 2 (crystal No. 4) where the low amplitude decrement was 7×10^{-5} and later after the crystal was remounted the decrement was 70×10^{-5}, as shown in Fig. 3. The process by which energy is dissipated in an amount proportional to the total number of dislocations and independent of amplitude is difficult to determine without more detailed information. One possibility is that irreversible heat flow occurs as the result of oscillating stress in an elastically inhomogeneous medium. In this event, the dislocations would presumably provide the elastic inhomogeneity. Quantative calculations should show whether or not this possibility is reasonable.

Decrement B, a function of strain amplitude, could be interpreted according to the following picture. The dissipation represented by decrement B would be assumed to be the result of movement of the dislocations. This movement would result in a plastic change in length of the specimen, with consequent loss of oscillation energy. The data could then be interpreted by assuming that the dislocations did not move appreciably when they were attached to the dislocation lattice and that they could be broken away from the lattice by the application of a sufficiently large stress. The amount of stress required would vary according to how tightly each dislocation was bound in the lattice. Hence as the oscillation amplitude was increased steadily from zero, more and more dislocations would be freed from the restraining influence of their neighbors and be made available to dissipate energy, with a consequent rise of the decrement. The decrement, during the subsequent decrease of amplitude would then be larger at a given amplitude than on the ascending curve because more dislocations would be free than before. Examples of this hysteresis-like effect are given in Figs. 2, 3, 5, 7, and 8. This picture, furthermore, would explain the effect shown in Figs. 3 and 5 in which an ascending branch of a curve was nearly identical to the descending branch of a curve taken soon before it. It would be due to the fact that the same number of dislocations were free to dissipate energy on both curves. The dislocations that had been freed from the dislocation lattice by the oscillating stress would, upon removal of the stress, gradually take either their old positions, or new positions in the lattice. This process would, however, take a finite time as thermal energies would be expected to be an important factor. The data given in Fig. 3 show how elapsed time after a run erases the effect of a previous run. Also, the increase of the point of rise of the decrement shown in Fig. 6 would be caused by the fact that as the crystal had more time to anneal, the dislocations which were loosely bound in the lattice would disappear from the crystal, leaving only those which were tightly bound and required a large stress to make them available to dissipate energy.

The number of dislocations that are freed from the lattice would be expected to depend somewhat on the time that the crystal was oscillated at a given amplitude, i.e., some time would be required to establish an equilibrium state. The curves of Fig. 9 show that several seconds were required for a stable value of the decrement to be reached when the oscillation amplitude was changed from one constant value to another.

In conclusion, the writers wish to express their appreciation to Professor E. P. T. Tyndall for his guidance and help during the progress of this work.

Letters to the Editor

Measurement of Surface Tension

ROBERT WEIL
South-West Essex Technical College and School of Art, Walthamstow, England
January 27, 1947

SUGDEN'S[1] method was employed for measuring the surface tension of distilled water at a temperature of 25°C in order to determine how the value would be affected by imperfections in the circularity of the capillaries. The procedure was as follows: six capillaries were drawn out from pieces of glass tubing so that the diameter at the tip was between .04 and .06 cm. While still soft the tips were squeezed to different degrees; thus the cross sections assumed elliptical shapes. It was argued that the ratio R of the minimum to the maximum diameter was a measure of the deviation from the true circularity. This ratio, as determined by means of a cathetometer, varied from .537 to .914. The diameter of the large tube was .2814 cm.

The maximum bubble pressures were determined for each specimen. A high rate of bubbling was used at first with smaller rates following it. The mean of three readings for each rate was taken: the divergences were negligible. No automatic counting device being available, it was not possible to exceed a rate of about 140 to 150 bubbles per minute. Graphs were drawn plotting pressure against rate and extrapolated to infinitely long periods of bubble formation. This extrapolation seemed justified since, after some practice, it became possible to reduce the rates to as small values as two bubbles per minute. A mean value of the measured radii was used in order to calculate the surface tension.

Two interesting results have been found: for $.9<R<1$ values for the surface tension agree very well with data as obtained by other workers with capillaries whose cross section approximates to a circle to a greater degree than those used in this investigation.

It would appear that Martin's[2] conclusions obtained from work on similar deviations in Jäger's original method do not apply here.

Secondly, when plotting the pressure p against the rate of bubbling, it was found in all cases that the values of p increased with the rate of bubbling up to about 60 bubbles per minute or more, and then definitely decreased for higher rates. It was found, as might be expected, that, on raising the rate to a greater value than could be measured visually, the pressure rose considerably. The cause for this kink in the curves is not quite obvious. It is a matter of some conjecture whether it can be accounted for by the fact that at small rates actual maxima and minima are recorded in the positions of the liquid in the gauge, while at great frequencies it is the mean positions which are observed. In some unpublished work L. B. Wood points out the necessity of extrapolating to infinitely long periods of bubble formation to obtain reliable and consistent results. It would seem that there are occasions when it is not sufficient to maintain the rate of bubbling at less than two per second, as is suggested by Adam.[3]

It was not possible to extend the measurements to capillaries with different diameters and different wall thicknesses: it is certainly desirable that this should be done.

[1] Sugden, J. Chem. Soc. p. 858 (1922); p. 27 (1924).
[2] Martin, Sitz. Akad. Wiss. Wien 123, 2491 (1914).
[3] Adam, *The Physics and Chemistry of Surfaces*, p. 375.

Letter to the Editor

FRANCIS J. MURRAY
The Institute for Advanced Study, School of Mathematics, Princeton, New Jersey
January 8, 1947

MAY I respectfully call your attention to the fact that the suggestion of Mr. Eaglesfield on linear equation solvers, on page 1125 of the current issue of the *Journal of Applied Physics* (December, 1946) duplicates a paper of mine presented to the American Mathematical Society, September 1945, and abstracted in the November issue of the *Bulletin of the American Mathematical Society*, Vol. 51 (1945), page 883.

The content of the paper appears in full in my book *The Theory of Mathematical Machines*, a current publication of the Columbia University Press.

In this paper, I prove the convergence in the case in which Σd_i^2 is used. In the case of a machine which uses $\max d_i$ as an indication, one can give examples where the machine will reach a minimum not zero.

I have constructed a number of models upon the Σd_i^2 principle and a large one is now being constructed by the Watson Scientific Computing Laboratories at Columbia University.

Here and There

Personnel

The National Bureau of Standards recently announced the retirement of two longtime employees. Harvey L. Curtis, physicist at the Bureau since 1907, had deferred his retirement in 1945 to continue direction of interior ballistics research. Frederick J. Bates, sugar physicist who had also been chief of the Optics Division since 1941, has given more than 43 years of continuous service to the Bureau.

On December 30 Carroll L. Wilson resigned as vice president and director of National Research Corporation in order to assume his duties as general manager of the Atomic Energy Commission.

Ross Gunn has resigned as superintendent of the Physics Division, Naval Research Laboratory, to act as director of physical research for the U. S. Weather Bureau.

In January three appointments to the new Department of Engineering Sciences and Applied Physics at Harvard

University were announced. Leon N. Brillouin was appointed Gordon McKay Professor of Applied Mathematics, and James B. Fisk and Ronold W. P. King were named Gordon McKay Professors of Applied Physics.

Chester Peterson has been appointed physicist in the Resistance Measurements Section of the National Bureau of Standards.

The following men have new appointments to the Department of Physics at the University of Minnesota: Charles A. Critchfield, Frank Oppenheimer, Edward J. Lofgren, Joseph Weinberg, and Otto H. Schmitt.

Division of High-Polymer Physics

The following are officers for 1947 of the Division of High-Polymer Physics of the American Physical Society: Chairman, Lawrence A. Wood; Vice Chairman, Hubert M. James; Secretary, W. James Lyons; Treasurer, Robert S. Spencer. Professor James and Dr. Spencer were also elected to the executive committee.

General Electric Fellowships at Union College

For the third year General Electric Company is offering 50 six-week, all-expense fellowships to high school science teachers in seventeen northeastern states, for summer study at Union College in Schenectady, New York.

Leonard Loeb Honored

School and Society reports that Leonard B. Loeb, professor of physics, University of California (Berkeley), has been chosen to deliver the 38th annual Kelvin lecture at the Institution of Electrical Engineers, London, England, on April 24. Professor Loeb will speak on "Electrical Discharge through Gases."

Junior Chamber Puts Physicist in Top List

The U. S. Junior Chamber of Commerce published in January its selection of the nation's ten outstanding young men of the year. Included among them was Philip Morrison of Cornell University, atomic physicist, "for his outstanding work in the development of the atomic bomb and his struggle to educate the people to the danger and promise of atomic energy."

Electronics Fellowships at MIT

A number of graduate and advanced research fellowships are being offered by the Massachusetts Institute of Technology, Cambridge, Massachusetts, for study and research in the field of electronics. They will be known as Industrial Fellowships in Electronics and are sponsored jointly by a group of industrial organizations concerned with the advancement of electronics and its applications. Applicants should communicate with the Director, Research Laboratory of Electronics. Under normal circumstances application must be made at least four months prior to the intended date of entrance.

Work to Start Soon on Schenectady Atomic Laboratory

Construction of the Knolls Atomic Power Laboratory to be built near Schenectady, New York, by the Atomic Energy Commission will start this spring. The laboratory is being erected under the supervision of the General Electric Company, which will operate it for the government when completed. It is predicted the new building will be occupied by the middle of 1948.

Acta Crystallographica

A special international organization, formed largely for this purpose, is planning the publication of a journal to perform the services formerly rendered by the *Zeitschrift für Kristallographie*. *Acta Crystallographica*, as it will be called, will be published either in England or America, and while French, German, and Russian will be permitted languages, the bulk of the journal will be in English. It is expected that there will be six issues per year totaling approximately 1000 pages. The price to individual subscribers is tentatively set at $10 a year.

The American representatives in the international organization are extremely anxious to obtain a good idea of the probable circulation of the journal in North America. Any reader of this notice who would, or who might, subscribe to *Acta Crystallographica* is urged to send a note or postcard to that effect addressed to Dr. Henry A. Barton, American Institute of Physics, 57 East 55 Street, New York 22, New York.

Reorganization of American Institute of Physics

Reorganization of the American Institute of Physics and plans for a new semi-popular journal devoted to physics and its relation to society have been announced by the Institute. Effective immediately, the 7000 members of five societies (The American Physical Society, The Optical Society of America, The Acoustical Society of America, The American Association of Physics Teachers, and The Society of Rheology) will become members of the Institute. Heretofore the Institute has been an organization of these five Member Societies without any individual memberships. Provision is also made for associate membership in the Institute, open to others interested in physics. No change is made in the organization, functions, and activities of the five societies.

The new journal, for which initial financing is now being sought, will contain news about physicists, their meetings, their work, and other activities, and about similar features in related fields; information about the action of governmental and other non-physics agencies affecting physics; articles and letters presenting the views of physicists on problems of general importance; references to current literature in physics; book reviews, etc. Technical journals in the field of physics already being published by the Institute and its Member Societies will remain unchanged.

Division of Electron and Ion Optics

The Division of Electron and Ion Optics will hold a meeting in connection with the Washington meeting of the American Physical Society on May 1–3, 1947. There will be

a program of invited papers in the general field of "The Physics of Surface Phenomena." Contributed papers will be welcomed. For further information address J. R. Pierce (secretary-treasurer), Bell Telephone Laboratories, Inc., 463 West Street, New York 14, New York.

The Bulletin of Mathematical Biophysics

The following is the table of contents for the March 1947 issue of *The Bulletin of Mathematical Biophysics:*

Suggestions for a Mathematical Biophysics of Some Psychoses—N. RASHEVSKY

A Problem in Mathematical Biophysics of Interaction of Two or More Individuals Which May Be of Interest in Mathematical Sociology—N. RASHEVSKY

Mathematical Theory of Motivation Interactions of Two Individuals: I.—ANATOL RAPOPORT

The Mechanism of the Middle Ear: I. The Two Piston Problem—MARTINUS H. M. ESSER

The University of Chicago Press, Chicago, Illinois
Volume 9 Number 1.

Symposium at Ohio State

A Symposium on Molecular Structure and Spectroscopy will be held at the Mendenhall Laboratory of Physics at The Ohio State University from Monday, June 9, through Saturday, June 14. There will be discussions of the interpretation of molecular spectroscopic data as well as methods of obtaining such data. In addition, there will be sessions devoted to microwave and Raman spectroscopy. A dormitory will be available for those who wish to reside on the campus during the meeting. For further information, or for a copy of the program when it becomes available, write to Professor Harald H. Nielsen, Mendenhall Laboratory of Physics, The Ohio State University, Columbus 10, Ohio.

International Nickel Cooperative Educational Program

A broadening of International Nickel Company's cooperation with universities and colleges in the United States and Canada in the field of engineering education through the distribution of technical literature has been announced by T. H. Wickenden, manager of the development and research division of The International Nickel Company, Inc.

The program will make available useful material for classroom instruction in training students in scientific fields. It has been offered to, and accepted by, a number of institutions in the United States and Canada which give accredited courses in mining, metallurgy, chemical engineering, and one or more other engineering courses. As rapidly as possible the program will be offered to all engineering schools.

The development and research division of the company will furnish to each institution an exhibit containing approximately 50 specimens of nickel-containing materials; a portable metals identification kit containing approximately 35 specimens of important metals and alloys for qualitative identification of metals and alloys; literature and other information concerning nickel and its alloys; and other data. Motion pictures of the company's mining, smelting, and refining operations will be made available.

New Books

Circuit Analysis by Laboratory Methods

BY CARL E. SKRODER AND M. STANLEY HELM. Pp. 288+xvi, 6×9 in. Prentice-Hall, Inc., New York, 1946. Price $5.35.

Some twenty years ago Professor Harry E. Clifford planned a system of laboratory reports which was used under his cognizance at M.I.T. and Harvard, and the form of which is still used there and in many other schools. The purpose of this system was to encourage the student to plan and think about the experiment rather than treat it as a mere manual exercise. The modus operandi was to require a preliminary report which involved the following sections: a. A statement of the problem, b. The theory involved, c. The procedure, d. The circuit diagrams, e. The results expected together with a sample calculation, and f. A proposed analysis of the results.

After having this preliminary report, together with a list of needed instruments, accepted by the instructor, the student was then free to perform the experiment and was expected to perform it with little additional guidance. The experiment was finished only when a final report, including the completion of Sections e and f, was accepted. This method was and still is in sharp contrast with the cook book method prevalent in some schools. This latter method is sometimes reduced to a point where the student is asked only to read instruments and to put the readings in appropriate squares on a data sheet provided by the instructor. There is no question as to which method does the better job of teaching.

In the book *Circuit Analysis by Laboratory Methods*, the authors attempt to follow the preliminary report system and at the same time reduce some of the drudgery involved in merely copying sections of theory from references. This they do admirably. However, by the title one is rather led to expect that the book will contain an entirely new and different set of experiments. This is not so, since many of the experiments are good old standbys, but the emphasis has very definitely been shifted from machines to circuits. Only three out of the thirty-five experiments are on rotating machine characteristics. Eight of the remainder are on series and parallel circuits including resonance, which acknowledges their importance both in engineering and as a teaching mechanism. Three are on polyphase circuits, and three on reactive power. The remainder are distributed among instruments, Kirchhoff's laws, power, resistance, etc.

Although the text explaining the philosophy of the experiments is good, it is expected that the course would be taken concurrently with a theory course in circuits. Since there should be some correlation between this and the laboratory, one would hope to find a classroom text which covers the same material in the same order. This might not be easy, although it might be accomplished by a certain amount of reorganization.

The chapter describing the report to be expected of the student is good, but it could have been rendered more vivid

by including an example of what the authors consider to be a good report on one of the experiments included in the later chapters.

It seems that the authors have lost some crispness in trying to make the book so general that it can be used in all laboratories with all kinds of equipment. Somehow the sentence, "The inductance of the coil and the capacitance of the condenser should be such that resonance will be obtained at a frequency about in the middle of the frequency range designated by the instructor," does not seem nearly as authoritative as, "Choose the inductance and capacitance so that resonance will be obtained at 2000 cps."

ERIC A. WALKER
The Pennsylvania State College

The Diffraction of X-Rays and Electrons by Free Molecules

BY M. H. PIRENNE. Pp. 160+xii, Figs. 82, 5½×8½ in. Cambridge Series of Physical Chemistry. Cambridge University Press, Cambridge, England, 1946.

The thirteen chapters cover the following topics: Coherent scattering, incoherent scattering, fluorescence radiation, experimental measurements of the scattering of x-rays by atoms, diffraction of fast electrons by atoms, diffraction of x-rays by free molecules, intermolecular interferences in gases and liquids, thermal movements in molecules, the chemical bond, use of x-ray and electron diffraction for determination of structure, Fourier analysis of interference measurements of free molecules, measurement of x-ray scattering functions of gases, and a list of molecules studied by x-ray diffraction. An excellent bibliography contains 187 references.

The book is essentially a report of the work of the Debye school in the field of x-ray scattering by free molecules. The material is well presented and the book makes easy and interesting reading. Theoretical considerations and derivations are summarized, the results and conclusions are clearly stated, and the step-by-step details omitted. The first twelve chapters could well serve as a complete coverage for twelve semi-popular lectures. Most of the work presented in the book is more than ten years old, and much of it is familiar to workers in the field. However, even the experienced x-ray diffraction worker will find that the careful authoritative presentation clears up for him a few misunderstood points. The book should serve a useful purpose as a general report and reference for this phase of the x-ray diffraction field.

B. E. WARREN
Massachusetts Institute of Technology

New Booklets

Tracerlab, Inc., 55 Oliver Street, Boston 10, Massachusetts, has published the first issue of *Tracerlog*, the purpose of which is "to publish technical information on laboratory, medical, and industrial uses of radioactivity, not to mention an occasional 'commercial' plug for Tracerlab's own products and services." It will be published monthly and mailed free of charge on request to physicists, chemists, physicians, and engineers interested in radioactivity and its applications.

Tube Department of Radio Corporation of America has announced the publication of two 16-page booklets. Form PG-101 is entitled "Power and Gas Tubes for Radio and for Industry" and Form 1275-C is named "Receiving Tubes for Television, FM, and Standard Broadcast." Either booklet may be obtained for 10 cents a copy from RCA tube distributors, or by sending 10 cents direct to Commercial Engineering, Tube Department, Radio Corporation of America, Harrison, New Jersey.

Miniature Precision Bearings, Inc., Keene, New Hampshire, offers a four-page bulletin on miniature ball bearings for precision instruments and mechanisms. It describes in detail five series: radial, super-light radial, pivot, angular contact, and thrust.

Acme Scientific Company, 1448 West Randolph Street, Chicago 7, Illinois, has issued a four-page folder describing in detail Acme's new mold polishing service. The company feels that the type of surface which it can provide on irregular contours may be useful to the readers of this journal.

Eberbach and Son Company, Ann Arbor, Michigan, publishes a 16-page house organ called *Announcer of Scientific Equipment*, of interest to research, control, and development laboratories.

Rex Rheostat Company, P. O. Box 232, Baldwin, Long Island, New York, announces its new *Catalogue No. 3*, 8 pages. The company manufactures slide-contact rheostats and resistors.

Leeds and Northrup Company, 4934 Stenton Avenue, Philadelphia 44, Pennsylvania, has published a new catalog, *ND46(1)*, which provides information about a pyrometer which supplements the Micromax line of instruments for those applications which require split-second response to temperature changes, or unusually rapid concentration on a single chart of data from many points. 16 pages.

Walker-Jimieson, Inc., 311 South Western Avenue, Chicago 12, Illinois, makers of radio and electronic supplies, have issued their 1947 *Reference Book and Buyer's Guide*. 106 pages.

Radio City Products Company, Inc., 127 West 26 Street, New York 1, New York, is announcing its new *Catalogue No. 129*, which describes a comprehensive line of radio, electrical, and electronic test instruments. 24 pages.

American Documentation Institute, 1719 N Street, N. W., Washington 6, D. C., has published its first *Catalogue*

of Auxiliary Publications in Microfilms and Photoprints. To be distributed free so long as this first edition is available. 52 pages.

Dow Corning Corporation, Midland, Michigan, has announced the third edition of its *DC Silicone Catalogue.* 12 pages.

RCA Victor Division, Camden, New Jersey, has published two new booklets for the wider dissemination of technical information about electron tubes. Each contains 16 pages, and the titles are *Receiving Tubes for Television, FM, and Standard Broadcast,* and *Power and Gas Tubes for Radio and for Industry.*

Castle Films Division of United World Films, Inc., 30 Rockefeller Plaza, New York 20, New York, is announcing a new catalog listing many new films released during the past year for school and industrial training purposes.

The Ruberoid Company, 500 Fifth Avenue, New York 18, New York, has issued a 40-page illustrated booklet by Dr. Oliver Bowles entitled *Asbestos—The Silk of the Mineral Kingdom.* Dr. Bowles is chief of the Nonmetal Economics Division of the U. S. Bureau of Mines and is a prominent authority on the subject of asbestos.

Philips Research Laboratory has published a 20-page index listing all articles which have appeared in *Philips Technical Review* during the period January 1935 (first issue) to June 1942 (last issue prior to suspension of publication during the German occupation of Holland). It is available on request from Elsevier Book Company, Inc., 215 Fourth Avenue, New York 3, New York. The index, distributed free as a service to readers, alphabetically catalogs by subject all articles which appeared during that period.

Calendar of Meetings

April

28–30 American Geophysical Union, Washington, D. C.
28–30 National Academy of Sciences, Washington, D. C.

May

1–3 American Physical Society, Washington, D. C.
8–10 Acoustical Society of America, New York, New York
17 New England Radio Engineering Meeting, Cambridge, Massachusetts
26–27 Institute of Aeronautical Sciences, Detroit, Michigan

June

1–6 Society of Automotive Engineers, French Lick, Indiana
8–10 American Society of Refrigerating Engineers, Los Angeles, California
9–13 American Institute of Electrical Engineers, Montreal, Quebec, Canada
9–14 Symposium on Molecular Structure and Microscopy, Ohio State University, Columbus, Ohio
16–19 American Society of Mechanical Engineers, Chicago, Illinois
16–20 American Society for Testing Materials, Atlantic City, New Jersey
18–21 Society for the Promotion of Engineering Education, Minneapolis, Minnesota
23–25 American Society for X-Ray and Electron Diffraction, Montreal, Quebec, Canada

July

16–19 American Society of Civil Engineers, Duluth, Minnesota